Seminar on

Navigation channels - planning, establishment and maintenance
Trends and experiences

Venue: Esbjerg Musikhus
17 September 2002

DANSK VANDBYGNINGSTEKNISK SELSKAB
DANISH SOCIETY OF HYDRAULIC ENGINEERING

v/ Helge Gravesen, Carl Bro as, Granskoven 8, 2600 Glostrup
Tlf.+45 4348 6328, Fax +45 4363 6567, email: hlg@carlbro.dk

DANSK VANDBYGNINGSTEKNISK SELSKAB
DANISH SOCIETY OF HYDRAULIC ENGINEERING

v/ Helge Gravesen, Carl Bro as, Granskoven 8, 2600 Glostrup
Tlf. +45 4348 6328, Fax +45 4363 6567, email: hlg@carlbro.dk

16.09.2002
JKJ/BHM

Seminar on

Navigation channels - planning, establishment and maintenance
Trends and experiences

Time and place: **Tuesday 17 September 2002**

Site Visit: 11.30 – 13.00 hrs, Port of Esbjerg, at the corner of 'Østre Forhavnskaj' and 'Vestkraftkaj' in 'Østerhavn'

Lunch: 13.00 – 14.00 hrs, Musikhuset Esbjerg - hovedfoyer, Havnegade18

Seminar: 14.00 – 18.00 hrs, Musikhuset Esbjerg - foredragssalen

'Dinner': 18.00 – 18.30 hrs, Musikhuset Esbjerg – take away sandwich

Language: **English**

Site Visit

11.30 – 13.00 Visit onboard " MS "Grande Europa" - one the worlds largest and fastest ro/ro-container vessels. With a lenght of 181 m, width 32.25 m, BT 53,000 and its 11 decks it is considered as a 'design ship' for the Port of Esbjerg. It accomodates 750 containers and 4650 cars. The visit is guided by Grimaldi lines shipping agent in Esbjerg, Niels Winther Co.
Visit onboard dredger from Rohde Nielsen A/S with a short introduction to the dredging activities in the port.

The site visit may be subject to modifications as vessel calls and availability may change. Present alternatives are a visit onboard 'Dana Gloria', the new ro-pax from DFDS Tor Line or a cruise in the harbour and approach channel.

Seminar

14.00- 14.15 Welcome Address by Jens Kirkegaard, DHI Water & Environment

14.15- 14.50 From tidal trench to navigation channel for modern vessels. By Erik Brenneche, Port of Esbjerg.
The approach channel in historical context (development of depth, width and alignment), navigation marks and modifications in set-up, turning basin for coal vessels (simulator), realignment of navigation channel (numerical modelling), nautical depth, maintenance dredging - focus areas and strategy.

14.50- 15.25 Deepening scenarios for the Drogden navigation channel, Denmark. By Jørgen Vesth-Hansen, Copenhagen Port.
Located at the entrance to the Baltic area Copenhagen has developed into an important cruise destination in Europe. However, limited navigable water depth combined with trends towards larger vessels and expected increase in sea transport have substantiated the need for a comprehensive feasibility study on possible deepening of the Drogden Channel. Conclusions from this study will be presented.

15.25- 15.45 Coffee break

15.45- 16.20 Risk analysis of navigation channels. By Andreas Friis-Hansen, Cowi.
Risk analysis of navigation channels is used to determine the risk level achieved with a given channel design. When comparing to target risk values, risk analysis becomes a decision support tool for the dimensions and/or alignment of the channel. An example from a recent risk analysis of navigational safety will be presented as well as the general framework and methods.

16.20- 16.55 Ship simulators as design tool for channel dimensioning. By Jakob Buus Petersen, DMI/FORCE, Copenhagen
Why using simulators and when to apply them? - examples and the use of results in the final design

16.55- 17.30 Establishment and Maintenance of Navigation Channels - A Contractors' Perspective. By Gareth Pollit, Area Manager - UK and Ireland, Rohde Nielsen A/S.
Why are Contractors interested in navigation channels? What is important for a contractor?, When to be involved? Natural and man-made channels, campaign- regular- or emergency maintenance dredging, equipment and resources, the process and types of contract, risks, satisfying the customer - understanding needs

17.30- 18.00 The consequence of water level rise on coastal morphology and navigation. By Anders Jensen, DHI Water & Environment, Hoersholm.
With estimates of future water level rises examples of types of coasts that potentially will face major changes are given and the types of impacts and consequences to coastal structures and navigation briefly described.

Seminar on
Navigation channels - planning, establishment and maintenance
Trends and experiences

Tidspunkt: Tirsdag den 17 september 2002-09-16

Deltagerliste:

	Navn	**Firma**
1	Leif Runge Schmidt	Avecon A/S
2	Niels Lykkeberg	Carl Bro A/S
3	Jørgen Andersen	Carl Bro A/S
4	Ole Alenkær Madsen	Carl Bro A/S
5	Helge Gravesen	Carl Bro A/S
6	Claus Overgård Sørensen	Cowi A/S
7	Andreas Friis-Hansen	Cowi A/S
8	Jesper Fuchs	DHI Water & Environment
9	Anders Jensen	DHI Water & Environment
10	Jens Kirkegaard	DHI Water & Environment
11	Jens Chr. Eriksen	Dredging International
12	Jakob Buus Petersen	Force technology - DMI
13	Birte Rodevang	Ingeniørhøjskolen i København
14	Per Sørensen	Kystdirektoratet
15	Bent Sandgrav	Kystdirektoratet
16	Steen Hougård	Kystdirektoratet
17	Villy Madsen	Kystdirektoratet
18	Laurits Bernitt	Kystdirektoratet
19	Jørgen Vesth-Hansen	Københavns Havn
20	Claus Iversen	Niras PortConsult
21	Jørgen Lisby	Per Aarsleff A/S
22	Erik Brenneche	Port of Esbjerg
23	Kjeld Dahl Sørensen	Port of Esbjerg
24	Torben Poulsen	Port of Esbjerg
25	Fritz Bosse	Port of Esbjerg
26	Günter Hansen	Rambøll
27	Gareth Pollit	Rohde Nielsen A/S
28	OleYding	Rohde Nielsen A/S
29	Carl Peter Thomsen	Aalborg havn A/S

1. Welcome Address by Jens Kirkegaard, DHI Water & Environment

2. From tidal trench to navigation channel for modern vessels. By Erik Brenneche, Port of Esbjerg

3. Deepening scenarios for the Drogden navigation channel, Denmark. By Jørgen Vesth-Hansen, Copenhagen Port

4. Risk analysis of navigation channels. By Andreas Friis-Hansen, COWI

5. Ship simulators as design tool for channel dimensioning. By Jakob Buus Petersen, DMI/FORCE, Copenhagen

6. Establishment and Maintenance of Navigation Channels - A Contractors' Perspective. By Gareth Pollit, Area Manager – UK and Ireland, Rohde Nielsen A/S

7. The consequence of water level rise on coastal morphology and navigation. By Anders Jensen, DHI Water & Environment, Hørsholm

8. Research papers for reference:
   Sediment Transport and Backfilling of Trenches in Oscillatory Flow, *By Jacob Hjelmager and Jørgen Fredsøe*
   Oblique Flow over Dredged Channels. I: Flow Description, II: Sediment Transport and Morphology, *By Jacob Hjelmager Jensen, Erik Østergaard Madsen and Jørgen Fredsøe*

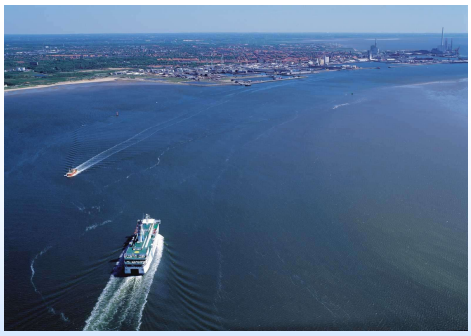

Seminar on

Navigation Channels

Planning, establishment and maintenance

Trends and experiences

Tuesday 17 September 2002

Why this seminar?

Changes in maritime transport

- **Specialisation among producers**
- **Increased international trade**
- **Larger ships**
- **New types of ships**
- **Specialisation of harbours**

Consequences:

- ***Expansion of existing harbours***
- ***New harbours***

A chance for different actors to meet

Programme:

14.00- 14.15	**Welcome** - Jens Kirkegaard, DHI
14.15- 14.50	**From tidal trench to navigation channel for modern vessels** Erik Brenneche, Port of Esbjerg.
14.50- 15.25	**Deepening scenarios for the Drogden navigation channel, Denmark** Jørgen Vesth-Hansen, Copenhagen Port.
15.25- 15.45	***Coffee break***
15.45- 16.20	**Risk analysis of navigation channels** Andreas Friis-Hansen, COWI, Lyngby
16.20- 16.55	**Ship simulators as design tool for channel dimensioning** Jakob Buus Petersen, DMI/FORCE, Copenhagen
16.55- 17.30	**Establishment and Maintenance of Navigation Channels - A Contractors' Perspective** Gareth Pollit, Area Manager - UK and Ireland, Rohde Nielsen A/S.
17.30- 18.00	**The consequence of water level rise on coastal morphology and navigation** Anders Jensen, DHI Water & Environment, Hoersholm.

Navigation Channels

Why navigation channels?

New port facilities:

- **Optimal solution for access to loading/unloading facilities**
- **Depends on local conditions**

Example: **Barge transport of Eucalyptus logs from plantations in Bahia, Brazil to Pulp Mill in Aracruz, Esperito Santo, Brazil**

Navigation Channels

Offshore port

or inlet port

Navigation Channels

Before dredging

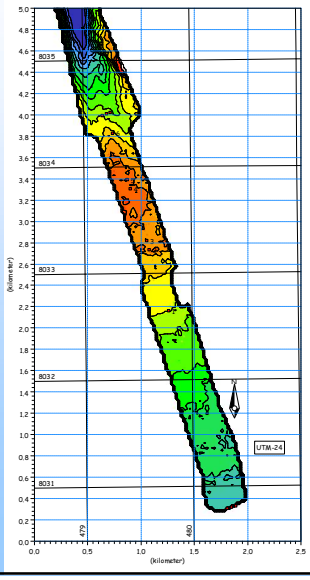

During dredging

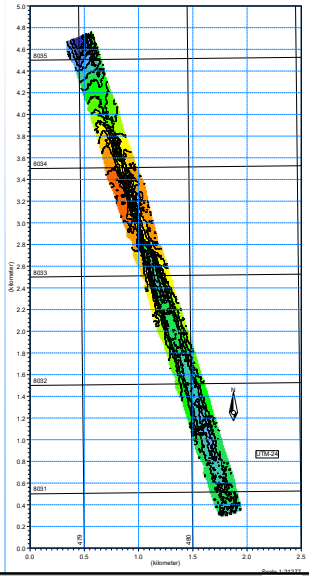

Why navigation channels?

- **Existing harbours:**
- **Access for larger vessels**
- **Increasing turnover**
- **Improvements of safety**

Example: **Port of Karachi**

Containerization - Oil imports

Navigation Channels

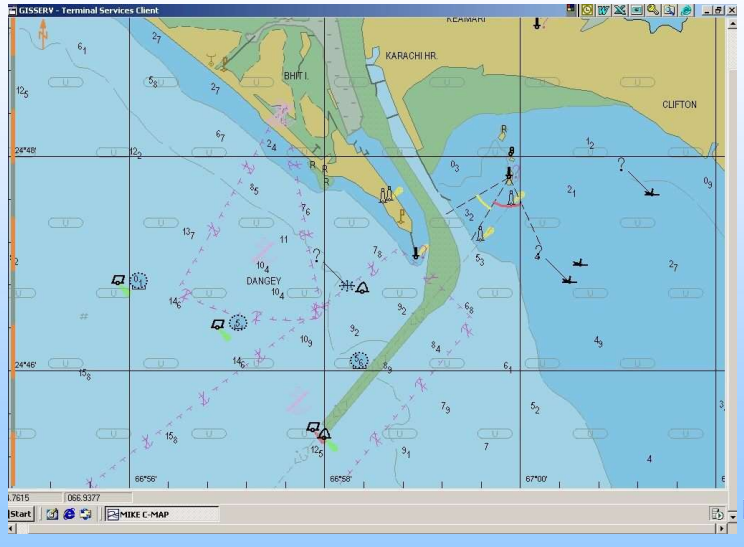

Port of Karachi

Governing factors for dredged channels

- **Products and marine transport (now and projected)**
- **Depths and bottom sediments**
- **Capital dredging, depth, width, alignment**
- **Maintenance, sediment infill, how much and how often**
- **Waves, currents, wind, water level**
- **Ship types, sizes, manoeuvrability**
- **Risk assessment**

  and environmental impact

Navigation Channels

Thank you!

Grimaldi Lines / Niels Winther Co.

Rohde Nielsen A/S

and

all Speakers

From tidal trench to navigation channel for modern vessels.

by Erik Brenneche, Port of Esbjerg

Biographi: Erik Brenneche graduated with a BSc in civil engineering from the technical highschool in Odense in 1980. Since then he has been occupied first at the State Ports Administration Esbjerg and later at the Port of Esbjerg with a variety of port related civil engineering tasks such as construction of quaywalls, boat bridges, moles, groynes, roads, sewer systems and also with surveying and dredging.

The Wadden Sea is a huge shallow water area sheltered from the North Sea by the long row of barrier islands from Fanoe in the north to Texel in the south west. The area is characterised by tidal action. The islands are separated from each other by deeps, along which the ships can access the ports in the Wadden Sea. At the North Sea end of the deeps a bar is formed.

Left to Mother Nature the sea end of a deep would move in the direction of the prevailing littoral drift. Eventually the way to sea would be too long and the watermasses would create a short cut that would swing the deep back to a straight line, whereafter this system would start all over again. This would happen regularly in a longperiodic cycle, more than 50 years has been mentioned for Graadyb, the deep that is the main item of this contribution.

In a map of 1851 Graadyb is seen situated in an almost north south going direction through the bar area with a long way to the sea. On a map of 1868 Graadyb has returned to a straight line. So the short cut mechanism has happened in the period between the two maps.

In 1868 the law of Port of Esbjerg was passed. Four years later the construction of the port began and few years after that the shipping traffic started. Thus the port by occasion started its life in a period with the shortest possible access channel from the North Sea to the port. But soon the moving channel became bothering. The bouyage task was difficult. The bouys often had to be shifted and the maps corrected. And there was difficulties with waterdepths. But only across the bar. Inside the Wadden Sea there was lots of water, between 6 and 17 meters. The natural width of the deep was also sufficient. More than 200 m mostly. But across the bar the depths varied between 4 and 6 meters at normal highwater. The width was not a constant either. So in 1909 maintenance dredging started with the steam driven 500 m^3 trailing suction dredger GRAADYB, owned by the state.

As the natural width across the bar was at least around 180 meters, the channel was maintained roughly at this width. The depth over the bar was maintained at 6 meters at normal highwater. This was fully acceptable for the shipsize of the beginning of the 20'ith century (length up to 50-60 m, breadth 10-12 m, draft up to 3-3,5 m). The average tidal amplitude at the time was 1,2 m.

Earlier in the century the entrance to Graadyb as well as Graadyb itself had been marked with occasional placed markes or preferably with occasional placed foremarks with easily recogniseable buildings (mills or Jerne church) as backmarks. With the introduction of the maintenance dredging more fixed marks could be introduced. So in the 1890'ies the Sædden Strand Fyrlinie (leading lights) was constructed as well as the first lighthouse (sector light) at Skallingen. Sædden Strand fyrlinie still exists. This is not the case with the lighthouse at the tip of Skallingen. It was destroyed after about 20 years by erosion caused by wave attack. The

same happened with the next two constructions. The place proved to be a very unstable place to construct anything. After the 2. World War further constructions of lighthouses were given up at Skallingen.

The maintenance dredging proved succesful in the attemt to maintain a stable channel across the bar. But it was a never ending job to keep up with nature. And in the 2 years 1921-23 GRAADYB needed assistance from another dredger due to a backlog from the 1. World War where the work was almost suspended. During the 1920'ies the waterdepth in the channel was increased to 6.7 m at mean low water spring due to increasing shipsize. This depth was maintained till the next war, where dredging was stopped.

After the 2. World War (plus the subsequent minesweeping period) the shoal just to the south west of the tip of Skallingen, Torre Bjaelke, had penetrated into the channel and destroyed the channel alignment. The state was short of money at the time, so it was decided to leave the channel where it was, to establish two new leading lights, one at each side of the old Sædden Strand fyrlinie, and then to maintain the channel in its new situation. Maintenance dredging was resumed in 1949.

The shipsize continued to grow. In 1960 GRAADYB was replaced by a new and more efficient dredger TAURUS. With this ship the water depth was gradually increased to 9,3 m MLWS during the late 1960'ies and beginning of the 1970'ies. In the 70'ies the width of the channel was fixed to 200 m which seemed to be a practical maintainable width and sufficient for the shipping. In 1994 another meter was added to the waterdepth by successive overdredging by a private dredging company that had just taken over from the state owned dredgers.

From the 19'th century to around 1980 Graadyb had been marked with bouys in a zig zag pattern supplied with some leading lights and sectorlights. From time to time a bouy or two have been added to improve the bouyage. About 1980 the bouys was arranged in pairs to form gates for easier recognition on the radar.A principle of cheapest possible bouyage to ensure safe navigation has always been used. This is a bit strange as the entrance to the channel is very difficult to find in bad weather what the big number of wrecks to the north and south of the channel entrance indicates. There is simply almost no distinct marks neither for the eye nor for the radar on the coastline. Since 1971 the port has had a steel tower placed 500 m to the south of the channel on the sand bank Vaade Bjaelke as a tide gauge station. This tower is loved by the shipping because it gives an extra radar mark. The expenses for the bouyage is high. Although we only pay roughly half the expenses (the state pays the other half) bouyage cost the port around 1 mio. D.Kr. a year. So how to make bouyage cheaper without harm to the safety is often a subject especially since the port started being run like a business.

Since the beginning of maintenance dredging the annually volumes dredged has been varying between ½ and 1 mio. m^3 slowly increasing concurrently with increasing waterdepths, as greater waterdepth catches more of the sand drifting along the westcoast of Skallingen and Fanoe. In the past 30 years averagely 1.2 mio. m^3 has beed dredged annually. The main problem areas are situated in the bar area (90% of the total dredging), especially Torre Bjaelke (45% of the total volume) which often protrudes into the channel, but also a sandbank at Jerg is sometimes a problem. In the long period with state owned equipment the dredging strategy was more or less continous dredging. In the past 8-9 years with a private contractor the strategy has been changed to campaign dredging. The change of method has proved almost sufficient and with some ajustment we expect to remove the "almost" in the near

future. The experienced difference is mainly that we have been in Notices to Mariners too often. Shouting out warnings of shoalings in the channel is nessessary in bad situations, but not good for the port reputation.

Dredging is expensive and this has caused several investigations of Graadyb, of the sand movement in the channel and along the coast of Skallingen, of the movement of the tip of Skallingen, of the behaviour of Hobodyb (a minor deep on the inside of Skallingen) and more. The latest of these investigations took place in 1990-92 and for the first time with comprehensive use of numerical modelling. The investigation gave answers to many questions but not all. One of the items in the investigation was the right channel alignment for minimising dredging costs. Not surprisingly the optimal alignment proved to be the straight line. It could be the original line shown by Sædden Strand Fyrlinie or a new one along Sædden Strand Nord Fyrlinie. The first suggestion showed to have negative morfological impacts. The latter was the preferable one of all investigated possibilities with 2.5-3.0 mio. m^3 of capital dredging involved. But in all cases the capital dredging work to achieve the new alignment would ruin the benefit of the investment, why we still have the post war alignment of the channel.

But what does the shipping say to this alignment? Is it acceptable?

Coming from sea a ship has to use a lot of course corrections before the basin of Sonderhavn is reached. At bouy 7 the course is altered 13E to stb., at bouy 9 18E to port. At Jerg 26E to stb. followed at 15A by another 32E to stb., at 15B another 20E to stb., at 17 another 25E to stb., at Slunden 40E to port and at Sonderhavn 45E to port. And if the navigator has not been dizzy by all these corrections he still has the chance doing all the subsequent harbour manouvres. Fortunately it sounds worse than it is. The manouvring is not any worse than at many rivers. The course alterations are experienced as a natural sequence of low degree of difficulty. And cross currents are only met at the entrances to the basins and at certain periods of the tide also in the bar area. So cross currents have not significant influence on the course alterations.

Together with the Graadyb investigation in 1990-92 the alignment, width and depth of the whole channel was briefly investigated according to the recommendations of ICORELS, and was found OK at the time according to the shipsize that normally call at Esbjerg. Before that - and also after - a pragmatic method for fixing the nessessary safe channel width, and the nessessary depth ensuring sufficient underkeel clearance, has beed used. The pragmatic method is based on known and approved practises, experienses and opinions of pilots and shipmasters with knowledge of local conditions. If the pragmatic method can still be used in the future with increasing shipsizes calling at our port, and heavily increasing environmental demands is an open question. The latest recommendations of PIANC should at least be studied thouroughly and numerical modelling and simulators be considered. Especially with the knowledge of frequent siltation problems at two bends in the channel (at Torre Bjaelke and Jerg). These have the effect that in the middle of the bends where shipping need extra width, we offer a restricted width. When the siltation problems occur they are of course announced in Notices to Mariners and the port controle controls the traffic in the channel preventing two bigger ships to meet at the critical points. But in the future we must anticipate a need to avoid critical points e.g. by moving some of the leading lights or doing some capital dredging to expand the channel or a combination.

Simulation has been used by our port in the late 80'ies where the area in front of the Sonderhavn entrance should be arranged as a turning basin for coal ships calling at a new coal quay outside the port. Simulation was used to optimize the dimensions of the turning basin and later to train the pilots in using the basin and the access to the new quay. A very impressive instrument that has developed incredably since. The port is currently involved in a project with use of the simulation instrument on ordinary PC's. This makes this advanced tool a tool for everyday use. It is at present only a tool for ship manouvres. It would be very comfortable if the tool could be extended to predict sediment movements as well. It would enable the port to estimate if greater changes in siltation inside and outside harbour entrances would occur in case of psysical changes in entrance moles, pier heads etc. Wishful thinking? 10 years ago: Yes. Today? Let's see.

Port of Copenhagen Approach Channel

1. Description of project.

The project was a feasibility study to clarify if it is financially, social and environmental sustainable to deepen the navigation channel through Drogden in the Sound between Denmark and Sweden from the present 8 meters to a maximum of 10 meters, corresponding to the clearance on top of the tunnel in Øresundsbron.

The project was co-financed by EU through the TEN-T program and by the Danish Ministry of Traffic. The project was started in July 1997 and was finished in March 2002.

2. Background

Øresund is an important international navigation route, being the entry to the ports of Copenhagen and Malmø and a link for the through traffic between Kattegat and ports in the Baltic Sea. The route through Øresund has draft limitations due to the shallow waters at the Drogden Sill located just south of the ports of Copenhagen and Malmø. The route through Øresund is some 120-140 nautical miles shorter than the deeper route through the Great Belt.

Presently, the maximum permissible draft in the Drogden navigation channel is limited to 7.7 m., thus being a hindrance for all major vessels. By excavating the permissible draft can be increased, and this will enhance the importance of Copenhagen Port for the cruise liner industry and generate additional tourist income to the Copenhagen region.

Due to expected large fuel, time and cost savings for the transit traffic between Kattegat and ports in the Baltic Sea, such an excavation will also be beneficiary for countries around the Baltic Sea and for the shipping industry as a whole. The regional importance of sea communication is expected to develop further, if or when the EU expands towards east.

3. Project outcome.

The main conclusion from the studies on the deepening include two alternative schemes:

Either deepening to –9,2 meters and widening to 325 meters
Or deepening to –10,0 meters and widening to 360 meters.

For both schemes the requirement to a 0 impact solution for the flow of water and salts to the Baltic Sea can be met as for the Øresund Link, provided, that dredging materials are deployed in a way to create flow-blocking barriers.

For both schemes, it is further concluded that:

- The profitability of the project will be extremely good
- The project will contribute to maintain and to increase cruise traffic to the Port of Copenhagen and to ensure significant revenues to metropolitan Copenhagen
- The safety of navigation locally in the Drogden channel or in general between Kattegat and the Baltic Sea shows only marginal changes.
- Implementation of the project will be possible with no major inconvenience, provided some adaptation to the environment.

The economic benefits will mainly go to international sea traffic in transit through Danish Waters.

The net present value of the project, with a horizon of 30 years, is estimated at not less than $2,9 \times 10^9$ DKK and $5,9 \times 10^9$ DKK respectively for the –9,2 and –10 meters schemes. Thus, the time for recovering the investment will be limited to a few years.

The -10 meter scheme will be best suited to prepare for a development towards larger vessels in the long term. Deployment of relatively large quantities of dredging materials at sea will be part of this scheme, and approval by environmental and planning authorities will be required.

4. The project organisation.

The project is initiated and managed by Port of Copenhagen Ltd.

Water Consult APS has been technical advisor to Port of Copenhagen. An advisory committee from public authorities, companies, business organisations and interest groups and organisations have supervised the study. Technical reports are made by HLD Joint Venture, headed by NIRAS A/S, LICengineering A/S and DHI.

9 English summary

9.0 Introduction

Port of Copenhagen is located at the entrance to the Baltic area with a total population of more than 30 million. At the same time Copenhagen is the most important cruise destination in North Europe with 215 cals and 215 000 passengers annually. However, the navigable water depth south of Copenhagen is limited to 8.0 m through Drogden channel, being 10 km long and 300 m wide.

Earlier reviews of the market situation, the expected increase in sea transport to the Baltic and a trend towards larger vessels, have substantiated the need for a comprehensive feasibility study to be carried out. With financial support from the Danish Ministry of Traffic and EU's program for Trans-European Transport Network the present study was initiated in year 2000.

The conclusions of the Feasibility Study for a possible deepening of Drogden channel and the relevant studies are briefly summarized in this section.

9.1 Works and Costs

The location and course of the existing navigation channel is found appropriate and should be maintained.

Due to the cover of the intersecting Øresund Tunnel the scope for deepening is limited to a nominal depth of 10.0 m from the present 8.0 m, and widening of the channel is only possible towards east, also due to the Tunnel.

Channel deepening is recommended to be combined with a general widening of the channel and improvement of the approach from south. The latter includes the introduction of a wedge shaped approach, partly by removing the Quartus shoal, and by relocating the existing Drogden Lighthouse.

It is demonstrated that for the following two alternative schemes a safety level for navigation similar to that of the existing channel will be achieved:

Depth/Width

- Present configuration: 8.0 m/ 300 m
- Scheme 1: 9.2 m/ 325 m
- Scheme 2: 10.0 m/ 350 m

However, the Danish Maritime Authority (Søfartsstyrelsen) has resolved that a substantial widening of the channel in excess of the indications above should be part of any scheme.

The overall costs are estimated at:

- Scheme 1: 340 mill. DKK (excl VAT)
- Scheme 2: 580 - 790 mill. DKK (excl VAT)

With regard to deployment of dredging materials priority is given in both schemes to collision protection of the Tunnel and to achievement of a 0-impact solution for the water flow, cf. subsections 9.5 and 9.6.

In scheme 1 all other dredging materials are assumed to be disposed of to external reclamation projects.

In scheme 2 it is conservatively assumed that all materials shall be disposed of to project related disposals, established for the purpose. The indicated cost interval is due to differences in relation to haulage distance and dredging methods.

Included above are cost elements totalling approximately 60 mill. DKK pertaining to the introduction and running on a temporary basis of a VTS system as well as to permanent improvements of the navigation aids of the channel.

9.2 Cruise Traffic

In general terms the market for cruise traffic in Scandinavia and in the Baltic area shows a potential for considerable growth. Located at the center of the region Copenhagen traditionally holds a strong position as cruise destination, a position that is best safeguarded through unhindered navigation in the approaches.

The southern approach through Drogden is presently only navigable for draughts of less than approximately 7.7 m, and the most recent cruise vessels constructed or ordered show typical draughts of 8.0 – 8.5 m. As a prerequisite for safeguarding the market position of Copenhagen towards 2030 it is therefore recommended to deepen Drogden Channel to –9.2 m, or better to –10 m as a long term provision. With this improve-

ment access will be possible from south for virtually all cruise vessels. However, for a positive development also berthing logistics at Langelinie and elsewhere in the harbour as well as the general power of attraction of Copenhagen are important factors.

9.3 Sea Traffic in Transit

In the event that deepening and widening of Drogden Channel are implemented, part of the sea traffic in transit through Danish waters are likely to choose the faster route through Øresund instead of Storebælt. The saving in distance amounts to approximately 130 nautical miles or 8 - 10 hours of sailing time.

This new opportunity is obviously most important for vessels that are just able to pass through the deepened channel.

The total sea traffic in transit through Danish waters has been studied and analysed. Forecasts have been prepared for different growth scenarios, and in 2030 the total increase is found to be 60 – 100 pct as compared to todays figures of approximately 60 000 transits.

The number of vessels transferred from Storebælt to Øresund will depend on the actually selected depth in Drogden, but is in no case expected to exceed 5 pct of the total transit traffic. The resulting effect of this transfer for the turnover of cargo in the Port of Copenhagen will not be significant. The cargo volume depends first of all on demands and production in the ports hinterland.

9.4 Safety of Navigation

Deepening the Drogden Channel will increase the transit traffic in Øresund.

Considering first Danish waters as a whole, the study has shown that there will be virtually no change to the frequency of marine collisions or grounding due to deepening of Drogden. The effect of a concentration of vessels in Øresund is offset by the shortened navigation route and reduced concentration elsewhere in Danish waters. Considering only Øresund, the frequency of marine casualties will be marginally increased, mainly in the north part (Helsingør/Helsingborg).

Improved supervision of this water may be appropriate.

The safety of the Øresund Tunnel can be kept at the existing level by carrying out small protective works whereas the occurrence of mastheads in the formal flight corridors to and from Copenhagen Airport will be slightly increased.

The potential increase in risk of oil spill as a result of increased traffic is offset by a current development towards double hull tankers.

Detailed studies have been carried out of Drogden channel proper to determine the necessary increase of the channel width. Under the assumption that the level of safety shall be maintained as for the existing channel, the following widths have resulted from alternative calculation methods:

- For 9 m depth a width of at least 320 m is required.
- For 10 m depth a width of 320 - 370 m is required, depending on the extent of additional navigation improvement.

On this basis the schemes set out in section 9.1 are recommended. Alternative schemes involving a substantial increase of the channel width, as requested by the Danish Maritime Authority in order to achieve a significant improvement of risk levels, have not been considered in the feasibility study.

9.5 Water Flow and Penetration of Drogden Sill

The Drogden sill constitutes a natural barrier to the inflow from Kattegat to Øresund of the lower saline part of stratified water. The sill is consequently a critical factor for the salinity in the Baltic Sea.

It is demonstrated in the study that the frequency of so-called 'sill penetrations', deep stratified saline water traversing the barrier, remains unchanged.

In order to maintain the overall flow of water through Øresund at its present level it will be necessary to provide some compensation for the increased flow through a deeper and wider channel. It is found that

this requirement can be met by creation of flow-blocking, artificial barriers cf. subsection 9.6. It is shown in the study that all requirements to maintaining the present flow of water and salt between Kattegat and the Baltic Sea can be met by installation of such barriers for channel widths up to 400 m. Larger channel sections have not been considered.

In the navigation channel an increase by up to 10 –20 pct of the peak flow velocity will result as compared to the present conditions, almost exclusively in the direction of the channel and of no real concern for the navigation through the channel. The present conditions in the nearby Flinterenden and off Dragør will not be affected.

9.6 Use of Dredging Materials

The quantities to be dredged amount to 2.5 mill m³ for the 9.2 m scheme and 6.3 mill m³ for the 10 m scheme. Dredging materials will be unpolluted, mixed sand, gravel, clay till and Copenhagen limestone. If handled with some care the materials can be extensively used in new reclamation works to create flow-blocking barriers and for construction or recreational purposes.

A survey carried out as part of the study on up-coming reclamation schemes in the greater Copenhagen area seems to indicate that potentially some 3 mill m³ can be disposed of in this context.

For the 10 m scheme two alternative deployments are proposed in order to comply with the requirement to a 0-impact solution:

- Perimeter dike at Middelgrund
- Reclamation / submerged barriers at Peberholm

A perimeter dike at Middelgrund opens up the prospect of a long-term development of a possible new part of the city with several interesting fields of application. Reclamation at Peberholm can furthermore be designed with features, submerged stone reefs etc, for improved fish and bird life.

9.7 Environmental and Economic Account

The aggregate benefits of transferring part of the sea traffic in transit through Danish waters from Storebælt to Øresund will be considerable.

In the study the accumulated savings of time and fuel have been established together with the reduction of harmful emission from the vessels of noxious gazes and particle.

Assuming average economic growth, the following aggregate savings are found for the 10 m dredging scheme in year 2030 compared to the non-dredging alternative:

- reduction of navigation time 63 000 hours
- saving of fuel 52 000 tons
- reduction of CO_2 emission 165 000 tons

In the economic analysis the costs and benefits of the project are established as compared to the non-dredging situation.

The overall profitableness of the project is extremely good. The calculated net present value of both schemes is in the order of 10 times the initial investment. In other words, the time for recovering the investment is only 2 years and the sensitivity is low. Disregarding all savings of time for both vessels and cargo (on the safe side), it is found that the profitableness of the project is still good, but the time for recovery will then be 5 – 6 years.

Deepening of Drogden channel is by nature a transgressing infrastructure project. It is not possible to couple the initial costs and the returns that largely go to vessels registered outside Denmark. Slightly less than 50 % of the returns are estimated to go to vessels registered in EU-member states.

Secondary effects are not included in the economic analysis of which particularly the turnover related to increased cruise traffic will be of importance to the Port and to metropolitan Copenhagen.

9.8 Overall Conclusions

Two alternative schemes have been considered in the feasibility study:

- either deepening to -9.2 m and widening to 325 m
- or, deepening to -10.0 m and widening to 360 m

For both schemes the requirement to a 0-impact solution for the flow of water and salts to the Baltic Sea can be met as for the Øresund link, provided that dredging materials are deployed in a way to create flow-blocking barriers.

For both schemes it is further concluded that:

- the profitableness of the project will be extremely good
- the project will contribute to maintain and to increase cruise traffic to the Port of Copenhagen and to ensure significant revenues to metropolitan Copenhagen
- nothing but marginal changes to the safety of navigation will result, neither locally in Drogden channel nor in general between Kattegat and the Baltic Sea
- implementation of the project will be possible with no major inconvenience, provided some adaptation to the environment
- the economic benefits will mainly go to international sea traffic in transit through Danish waters

The net present value of the project, with a horizon of 30 years, is estimated at not less than 2.9×10^9 DKK and 5.9×10^9 DKK respectively for the 9.2 m and 10 m schemes. Thus, the time for recovering the investment will be limited to a few years.

The 10 m scheme will be best suited to prepare for a development towards larger vessels in the long term. Deployment of relatively large quantities of dredging materials at sea will be part of this scheme, and approval by environmental and planning authorities will be required.

	Antal skibs-passager i Øresund			Antal skibs-passager i Storebælt		
	Uændret	9 m	10 m	Uændret	9m	10 m
Tankskib	6.600	7.100	7.900	7.200	6.700	5.900
Bulk	2.100	2.300	3.200	4.600	4.400	3.500
General cargo	38.300	40.200	41.200	13.500	11.600	10.600
Container	6.500	6.500	6.800	4.000	3.800	3.500
RORO	8.900	9.000	9.100	2.100	2.000	1.900
Andet	4.800	4.800	4.800	6.600	6.600	6.600
I alt	67.000	69.900	73.000	38.000	35.100	32.000

Trafik gennem Øresund og Storebælt i 2030, ved hhv. 9m og 10 m vanddybde i Drogden, middelscenarie.

		Nødvendig rendebredde (m)					
Tid		År 2000			År 2030		
Nominel dybde		8m	9m	10m	8m	9m	10m
Absolut	PIANC	503	538	562	503	538	562
	Ellipse	728	738	753	749	769	814
	Interview	373	392	446	373	392	446
Relativ	PIANC	300*	321	335	300*	321	335
	Ellipse	300*	304	310	308	317	335
					300*	309	326
	Interview	300*	319	372	300*	319	372
	GRACAT	300*	307	319	317	329	335
					300*	319	326

Lande	2000		2030 lav		2030 middel		2030 høj	
	9m	10m	9m	10m	9m	10m	9m	10
Danmark	5%	4%	9%	7%	8%	7%	8%	6
EU	39%	39%	39%	41%	39%	41%	39%	41
Polen, Rusland, Baltikum	14%	12%	15%	14%	15%	14%	16%	15
Øvrige	42%	45%	37%	38%	38%	38%	38%	38
Samlet - lav (mll. Kr.)	-209,6	-446,8	-339,4	-666,9	-440,5	-857,3	-629,2	-126
Samlet - høj (mll. Kr.)	-216,2	-463,1	-352,0	-694,8	-457,1	-892,8	-653,1	-131

Procentuel fordeling af benefits på lande.

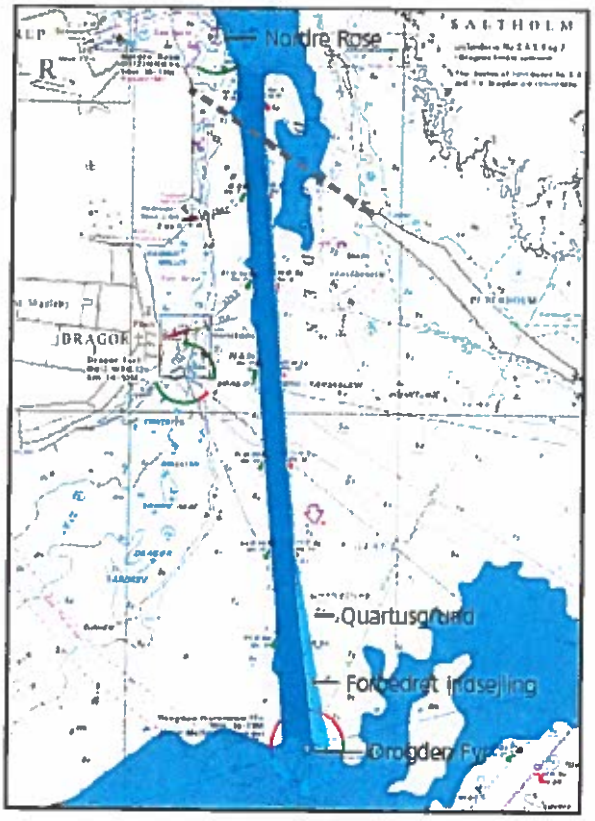
Nordre Rose
SALTHOLM
DRAGØR
Quartusgrund
Forbedret indsejling
Drogden Fyr

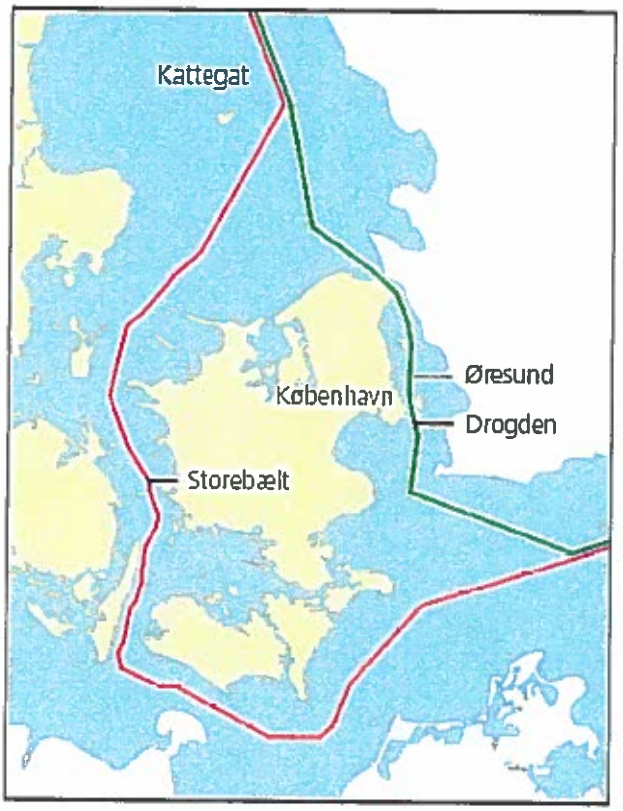
Kattegat
Øresund
København
Drogden
Storebælt

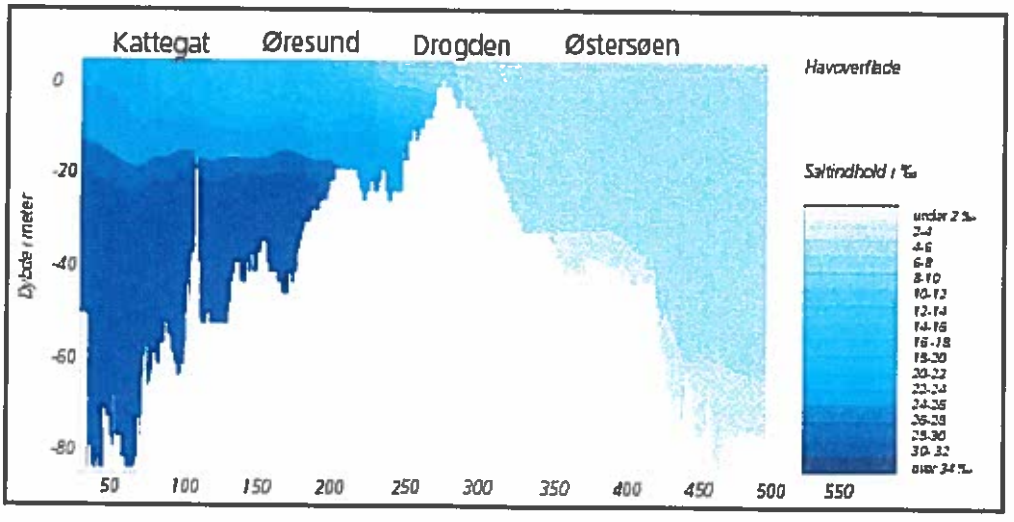
Kattegat
Øresund
Drogden
Østersøen
Havoverflade
Saltindhold i ‰
Dybde i meter
0
-20
-40
-60
-80
50
100
150
200
250
300
350
400
450
500
550

Risk Analysis of Navigation Channels

Dansk Vandbygningsteknisk Selskab
Andreas Friis-Hansen
COWI A/S
17. September 2002

Overview

- Risk Analysis of Navigational Safety in Danish Waters
  - Example of a risk analysis
  - Focus on dredging alternatives for risk reduction
- Comments on risk analysis in general
- Methods for initial design of navigation channels
- Fehmarn belt feasibility study

Objective

- Decision support: Best allocation of resources
  - If the navigational safety shall be improved:
    - What should be done and where?
    - What are the costs?
    - Which is the better option?
- Existing risk
  - Expected annual number of spills (Oil, Gas, Chemicals)
- Identification and analysis of measures to improve navigational safety (Risk Control Options)
  - Cost effectiveness: What are the costs of averting a spill?
- Risk Acceptance criteria
  - How much is reasonable to spend in order to avoid a spill?

Steps of a risk analysis (FSA)

- Hazard identification
  - what can go wrong, scenarios
- Risk assessment (in present situation)
  - Frequency
  - Consequence
- Risk Control Options (RCOs)
  - Risk reduction
  - Costs (initial and operational)
- Cost-benefit assessment
  - Ranking of RCOs
- Acceptance criteria

Project overview

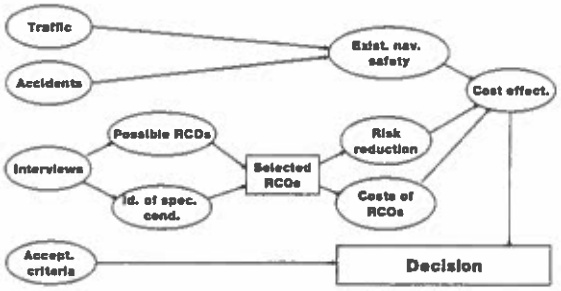

Accidents in Danish waters

- Selected locations
  - Drogden
  - Langelandsbit
  - Hatter area
  - Kadetrenden
  - The Sound North
- Represent 73 of 206 accidents in the period 1997-2001

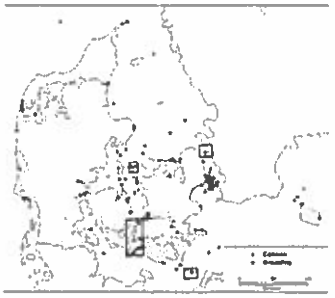

Drogden

- Analysed RCOs
  - VTS Drogden
  - AIS-surveillance
  - Wider channel
- Traffic
  - approx. 40 000 annual passages
- Accidents
  - 29 groundings (5 years)
  - 9 collisions (5 years)

Hatter area (Samso)

- Analysed RCOs
  - VTS Hatter
  - Hatter included in VTS Great Belt
  - AIS-surveillance from VTS Great Belt operator room
  - Deepening of Hatter main route
  - Partial removal of Hatter Bern
- Traffic
  - Approx. 22 000 annual passages
- Accidents
  - 11 groundings (5 years)
  - 3 collisions (15 years)

Hatter dredging alternatives

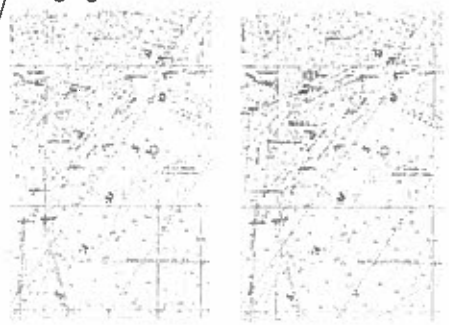

Existing navigational safety (1)

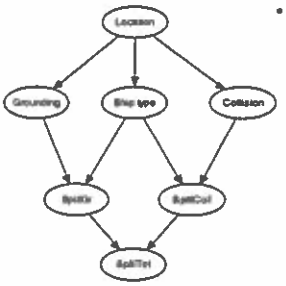

- Probability of spill per ship passage
  - Accident frequency estimated for each location
  - Traffic distribution on ship type estimated for each location
  - Spill probability estimated for each ship type and accident type
  - The total spill probability per ship passage is computed

Existing navigational safety (2)

	Drogden South	Drogden North	Langeland s- bast	Hatter DW-route	Hatter main route	Kadet-renden	The Sound northern part
Spill frequency per ship passage	4.7E-06	2.3E-06	5.3E-06	1.7E-04	2.7E-06	7.8E-07	1.3E-06
Traffic, annual	40074	40074	21967	460	21967	63000	38747
Expected annual number of spills	0.19	0.09	0.12	0.08	0.06	0.05	0.05
Index, spill	5.6		2.3	2.7		1.0	1.0

Project overview

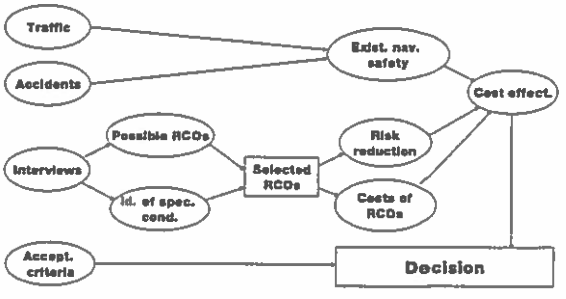

Risk Reduction

- The risk can be reduced by
  - Reducing the frequency of occurrence
    - Wider/deeper channel (passive)
    - Surveillance (active)
    - Electronic aids
    - Buoying
  - Reducing the consequences
    - Double hull
- Basis
  - Statistics and observations from present study
  - Interviews
  - Statistics and observations from other studies
    - Journals, conference proceedings, reports
  - Models and assumptions for behaviour in the new situation
    - collision and grounding frequency models

Cost estimation: Dredging at Hatter

- Estimated amounts to remove
- Costs per m3 for each sediment type

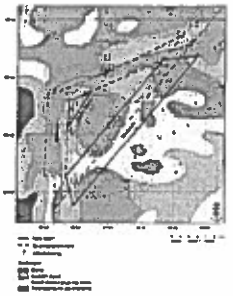

Costs

RCO	Initial costs [mill. DKK]	Operational costs, annually [mill. DKK]	Lifetime of the investment [years]	Total costs in the lifetime of the investment [mill. DKK]
VTS Drogden	1.0	0.3	10	80.0
AIS surveillance, Drogden	4.0	0.5	10	89.0
Wider Langelin channel	350.0	0.0	50	350.0
Langelinie/Saltholm incorporated into VTS Great Belt	4.0	2.5	10	29.0
AIS surveillance, Langelinie/Saltholm incorporated into VTS Great Belt	2.0	2.5	10	27.0
VTS for the Hatter area	9.0	9.0	10	99.0
Hatter area incorporated into VTS Great Belt	8.0	2.5	10	40.0
AIS surveillance, Hatter incorporated into VTS Great Belt	2.0	2.5	10	27.0
Dredging in Hatter main route	200.0	0.0	50	200.0
Partial removal of Hatter Barn	140.0	0.2	50	142.0
VTS + optimation	8.0	9.0	10	98.0
Repeated temporary surveillance of the replacements	1.5	1.3	10	14.5
VTS the Sound north	20.0	10.0	10	120.0
Racon on M1 (the Sound northern part)	0.5	0.05	5	0.8

Cost effectiveness

$$Cost\ per\ averted\ spill = \frac{Cost\ of\ RCO}{No.of\ averted\ spills}$$

Ranking of RCOs

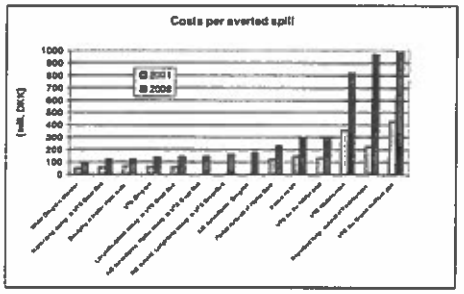

Risk Acceptance Criteria

RCOs should be implemented if

Costs of averting a spill < F* Costs of an occurred spill

- Direct costs of a spill (400 t)
  - Clean-up costs
  - Repair of ship/loss of ship
  - Loss of cargo
  - Lost revenue
  - Loss of life
- Total approx. 50 mill. kr.
- Indirect costs (not assessed)
  - Environmental costs
    - Damage to wildlife
    - Damage to natural resources
    - Damage to recreational areas
    - Impact on tourism, fishing industry, sea farming
  - Political impact
    - Loss of goodwill
    - Administrative burden

Conclusion

- The analysis has given
  - A picture of the existing navigational safety in Danish waters
  - An identification and prioritisation of risk reducing measures
  - Basis for determining reasonable expenditure to avert a spill
- If the navigational safety shall be improved, the following RCOs are the most cost effective:

1. Widening of the Drogden channel (to 600 m)
2a. Deepening of the main route at Hatter (to 19 m)
2b. Hatter area incorporated in VTS Great Belts surveillance area
3. VTS at Drogden

Risk Management

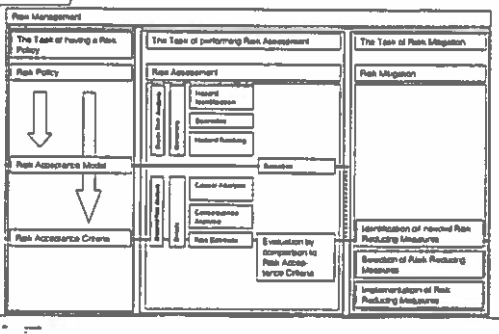

Steps of a risk analysis (FSA)

- Hazard identification
  - what can go wrong, scenarios
- Risk assessment (in present situation)
  - Frequency
  - Consequence
- Risk Control Options (RCOs)
  - Risk reduction
  - Costs (initial and operational)
- Cost-benefit
  - Ranking of RCOs
- Acceptance criteria

Acceptance criteria

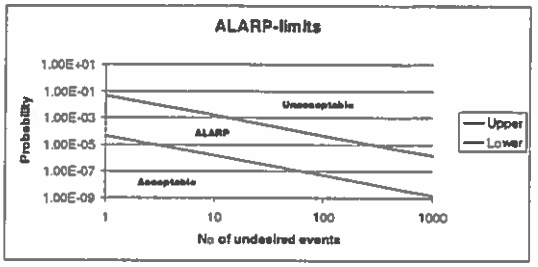

Design of navigation channels

- To determine necessary width of a channel
  - Real-time simulation
  - Fast-time simulation
  - PIANC
  - Ship Domain models
  - Risk models: Collision and grounding

PIANC

- Initial estimates of channel width
- Design ship, breadth B
- Necessary width of channel W= C*B
  - C is determined by consideration of
    - Ship speed
    - Wind
    - Current (transverse and longitudinal)
    - Waves
    - Water depth
    - Sea bed roughness
    - Cargo
    - Traffic intensity
- The method does not quantify the risk level

Ship domain theory

- Design ship
  - L_s = 95%fractile of the ship length
- Elliptic domain around the ship
  - $L_{ellipse} = 8 * L_{ship}$
  - $B_{ellipse} = 3.2 * L_{ship}$
- Channel dimensions
  - W = 7.4 *L (meeting traffic, service speed)
  - W = 4.2 *L (harbour speed, restricted waters)
- The method does not quantify the risk level

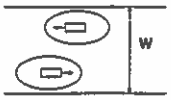

COWI

Collision model Drogden

- Observed distributions of transverse location of ships
  - Combined uniform and normal distribution
- Formulas for estimation of mean and standard deviation
  - Based on channel width, traffic intensity and separation scheme
- Geometric collision frequency
- Causation factor
  - Accounts for human intervention

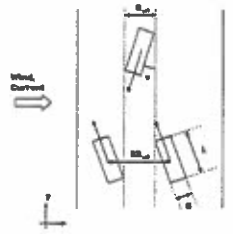

COWI

Survey of Ship Tracks in Fehmarn Belt

Henrik Gluver
Ben C. Gerwick., Inc. San Fransico, USA

Dan Olsen
COWI Consultant Engineers and Planners, Denmark

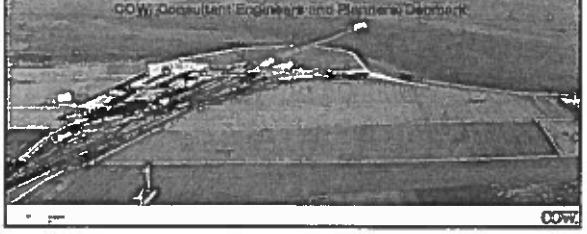

COWI

Survey of Ship Tracks in Fehmarn Belt

- Civil Engineering - Ship collision with bridges
- Bridge arrangement and design criteria for ship impact
- Dimensioning accidental ship impact requirements
- Deterministic approach - probabilistic approach

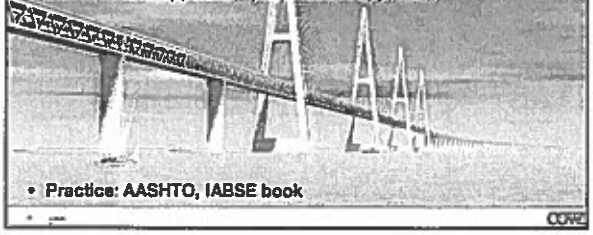

- Practice: AASHTO, IABSE book

COWI

Survey of Ship Tracks in Fehmarn Belt

- Radar tracks of 1900 westbound passages
- Deutche Marine Marienleuchte
- Aug 1998 till Jan 1999
- Call sign
- Hull number
- Picture
- DWT
- Length and
- Direction

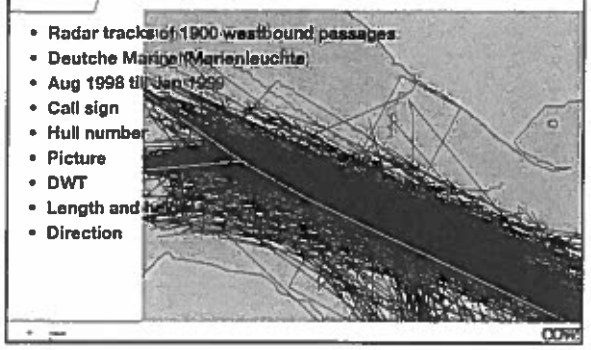

Survey of Ship Tracks in Fehmarn Belt

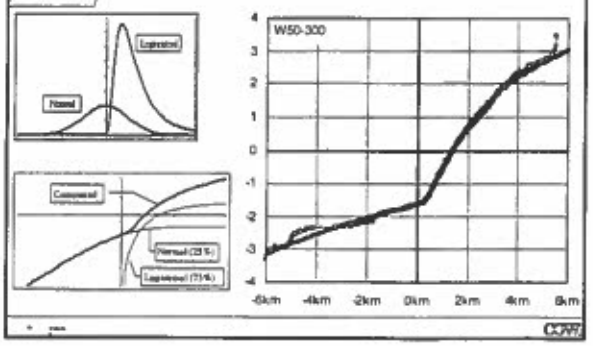

Survey of Ship Tracks in Fehmarn Belt

- Normal distribution st. dev. 350 m
- Approach span piers exposed to ship collision
- Ship traffic to be reformed
- Early marking of future navigation route
- VTS system to be established early

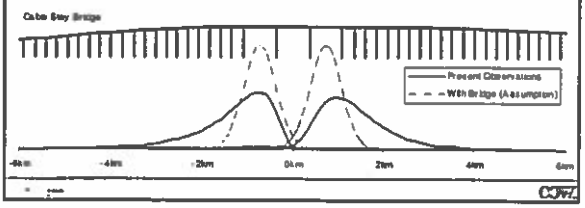

Ship simulators as a design tool for channel dimensioning.

by
Jakob Buus Petersen

DVS, Esbjerg 17. September 2002

Overview

- Introduction Force – DMI
- Why use simulation?
- Steps in port development studies
- Methods
  - Empirical
  - Simulation
- Data
  - Ships (PMM, Ocean)
  - Environment
- Examples

Introduction

- FORCE-DMI: Private consulting company
- No shareholders - Self-owned
- Maritime department:
- Works in more than 40 countries
- Offices in U.K. and Malaysia
- 120 employees

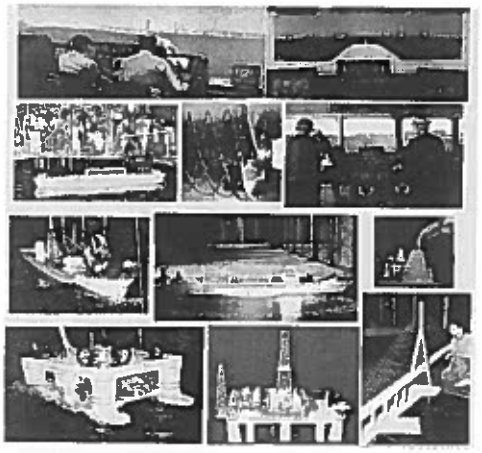

Why simulation?

- Design of approach channels, navigational aids, one way, two way traffic
- Design of harbour entrances
- Design of turning basins
- Determining environmental limits
- Berthing manoeuvres, thrusters, tug capacity
- Risk of grounding, wave and manoeuvre induced motions, squat
- Bottom up models, detailed modelling

Steps in port development studies

- Ship model development (OCEAN, PMM)
- Fast time simulations
- Desktop Simulations (QuickSim)
- Full Mission Simulations (Validation)

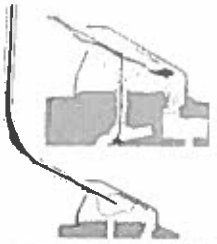

Force – Danish Maritime Institute

Purpose

Channel design using simulations techniques.
Parameters:

- Water depth (squat)
- Channel beam
- Manoeuvring space

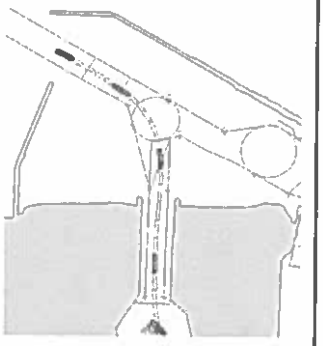

Methods

- Empirical (desk-top) Method
  - Using PIANC calculations.
  - General considerations.
- Simulation "direct method"
  - Detailed modelling.
  - Fast-time simulations.
  - Quicksim.
  - Full mission simulations.

Empirical methods

- Study general PIANC recommendations
- Calculate channel width and depth
- Used at initial design stage, but .....

Simulation "direct method"

Includes detailed models of:

- Actual channel and harbour layout
- Relevant ships
- Environmental conditions
  (current, wind, waves, banks)

Ship models

- Manoeuvring in deep and (unrestricted) shallow water
- Current effects
- Wind effects
- Bank effects
- Ship-ship interaction
- Modelling of tugs
- Wave effects (1st and 2nd order)

Wave response OCEAN

- Frequency domain 3D code
- Response amplitude operators (1st and 2nd order)
- Estimation of grounding probablity (speed, depth, Hs, Tp, θ)
- Time domain by convolution integrals
- Time domain simulations include combined wind, current, wave and manoeuvre induced motions

Environment data

- Bathymetry (depths)
- Current (Mike 21)
- Wind
- Waves
- Banks

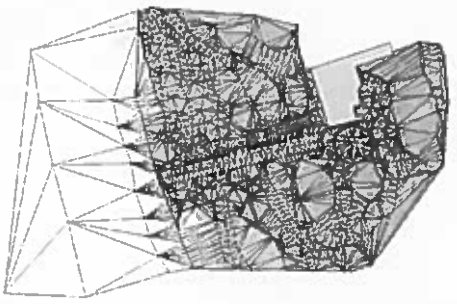

Fast-time simulations (1)

- Set-up of simulations
  - Data requirement
  - Numerical navigator
  - Plan
  - Environment set-up
  - Execution of runs
  - Results

Quicksim concept (2)

The Quicksim concept:

- simple 3D database
- full 2D database
- run on a single PC
- man in the loop.

Full mission simulation (3)

- Full bridge mock-up
- Man in the loop
- Confirmation of final design
- Debriefing including all involved parties

Examples

- Manzanillo
- Dos Bocas
- Frederikshavn
- Channel example 1
- Channel example 2
- LNG terminal

Manzanillo

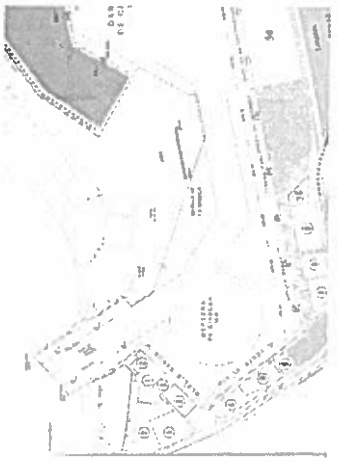

Original suggestion

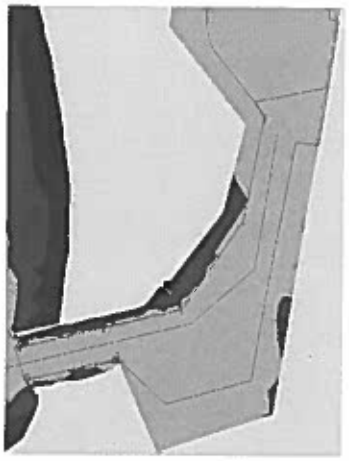

Final solution

Dos Bocas

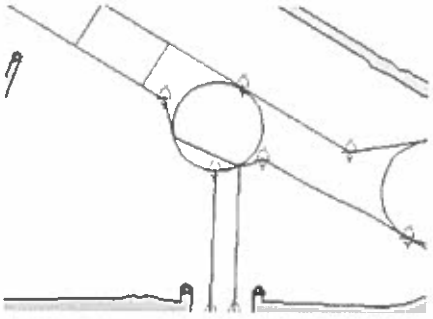

Dos Bocas before

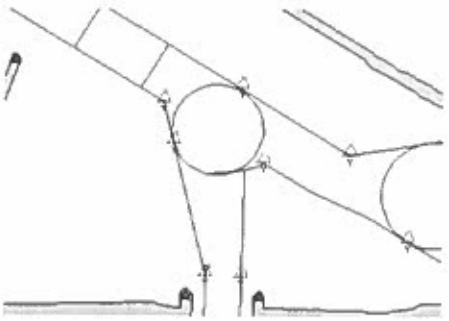

Dos Bocas after

Dos Bocas

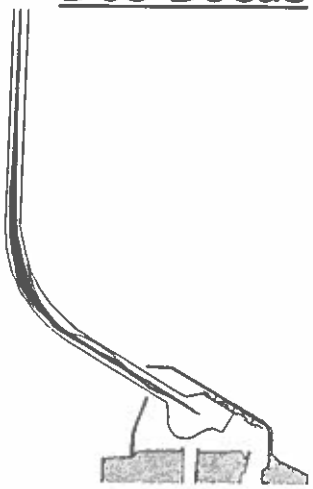

Frederikshavn

Test of 3 different channels between breakwaters, the original was 90 m

110 m btw. breakwaters

130 m btw. breakwaters

150 m btw. breakwaters

Channel example 1

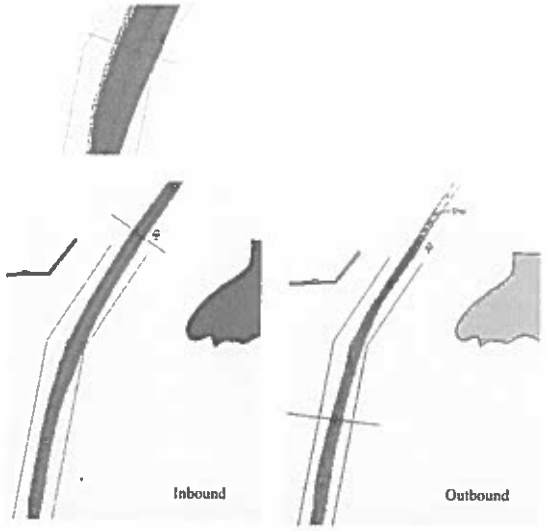

Channel example 2

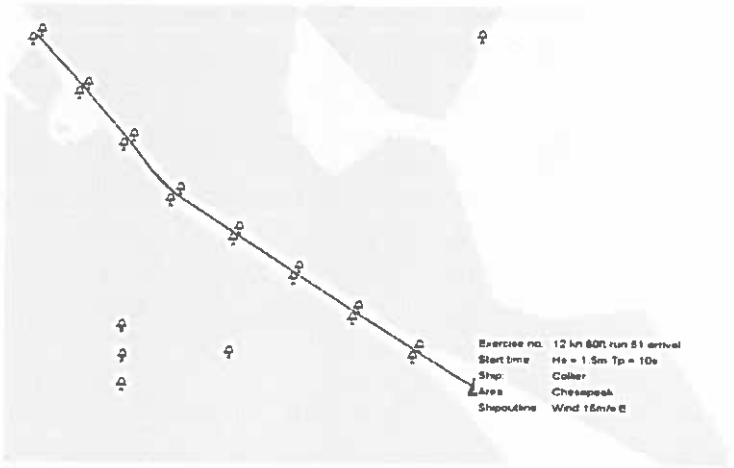

LNG terminal

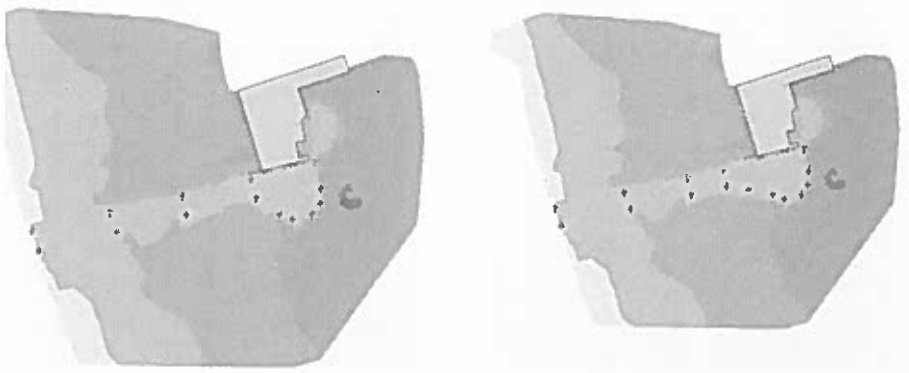

Before

After

Conclusions:

Simulation tools can be used for:

- Reduction of risk of collisions and groundings
- Tool during the design process of approach channels and harbour layouts
- Final validation of channel or harbour design
- The simulation scene (scenario) is an excellent dicussion forum which involves pilots, captains, naval architects and civil engineers

Establishment and Maintenance of Navigation Channels (A Contractors' Perspective)

(By Gareth Pollit and Ole Yding)

ESTABLISHMENT AND MAINTENANCE OF NAVIGATION CHANNELS (A CONTRACTORS' PERSPECTIVE) (Slide 1)

No Notes.

SYNOPSIS (Slide 2)

The establishment and maintenance of channels sets challenges for many disciplines from promoter clients to harbour masters, from marine pilots to the green lobby. The short talk this afternoon will generally only address the Industry from a Contractors' perspective. I hope it will give an insight into the Contractor´s involvement in the process and the challenges that he has to address. The presentation will include some anecdotal notes on my personal experience whilst managing a Port Operators Fleet in a contracting environment.

After a short overview of the industry I shall look at specific aspects of the establishment and maintenance of channels, the equipment and resources available, the process of contracting and some final opinion on where all parties can be involved in a win win situation.

INTRODUCTION (Slide 3)

Dredging, unfortunately, is expensive based on capital intensive equipment and sometimes it is difficult to wonder what the Contractor or Client gets for his money.

It is here that I wish to highlight some subtle differences in perception from both parties perspective in relation to the ESTABLISHMENT of channels and the MAINTENANCE of channels.

The Establishment of Channels is nearly always related to Capital schemes and the cost of dredging new approach channels is part and parcel of the Capital Cost. Accounts departments then take over and balance the figures over a number of years so that the Profit and Loss accounts are satisfactory and that the return on Capital Employed by the Client is adequate. In turn the cost of dredging is factored into the whole and contractors and Clients know where they are from the start.

The Maintenance of channels is on the other hand a necessary evil. I do not know of a single client who likes to spend money on dredging. The money spent immediately affects the bottom line, nothing is produced and if you are lucky the status quo is maintained. If you get your assessment of siltation wrong and in the wrong direction dredging can wipe away profits in days. Contractors and Clients are always under severe pressures therefore when considering maintenance works. Generally the money is not there to do sufficient dredging.

We are continually fighting nature, people cannot see what we do and ultimately you do not feel you have anything for your investment. Whats worse is that as soon as we have finished nature endeavours to fill in what we have done.

However, someone has to do the job. Why do we elect to do it?

INTRODUCTION (Slide 4)

Contractors must make a profit. Sometimes I think this is overlooked by promoters. But it is a competitive world and thats OK. What is difficult is when margins are slashed due to risks borne by the Contractor over which he has no control. I will come back to that later.

Dredging is about long term investment. Typically 20 to 25 years for a dredger. We are unable to predict the market so far in advance. We therefore have much to do in the way of ensuring the business remains stable through the quite periods. This fact will influence the Contractors frame of mind when planning and pricing works. It is no good having under capacity in the summer months in good sea conditions and then having overcapacity in the winter. Contractors have to pay for the equipment all year round.

Most contractors seek to grow and expand. However, this must be done cautiously. Equipment cannot be purchased for a single project. Some degree of forward use expectation must be present.

I think that many of us feel the need to contribute to society and its well being. Work should be carried out professionally and with fun. How to demonstrate that is sometimes difficult. Dredging is not a black art. Forums like this are especially useful in ensuring that all parties to a dredging contract understand and are sympathetic to each others business in an effort to get to the WIN WIN Scenario.

INTRODUCTION (Slide 5)

The world of the Contractor is one of many conflicting elements.

We can be seen to be destroyers of the environment. I have even had phone calls from airlines saying we are polluting the sea with oil when in fact all that was happening was the visibility of the disposal plume from the air. Dredging reduces oxygen levels and habitats of sealife. We burn tons of bunker fuel each day.

Our operations are expensive.

We have to protect ourselves against onerous contract and payment conditions. This can sometimes cause difficulties in the Client Contractor relationship.

We are legally bound by a raft of legislation. Some of which is common with Clients as the various conventions are applied. Others are specific to our business. The ISM code of practice, ships certification etc.

We are always bound by the demands of our owners and shareholders seeking to maximise their investment. Ours is a long term business. Shareholders always seem to want the jam now.

ESTABLISHMENT OF CHANNELS (Slide 6)

The establishment of channels are generally considered as capital schemes. As discussed earlier this has an impact on its funding but it also is treated differently by the licensing authorities. The promoter has often to deal with many disparate quasi legislative bodies. All with their own agenda. Many of you will be aware of the Dibden scheme in Southampton which is now under Government Review. A substantial part of the public enquiry relates to dredging.

Here the chart shows the upper portions of Southampton Water where the channel was established some 7 years ago around an existing watercourse. The deepening was carried under a conventional contract. The scale and scope of the job was known, the site investigation considered sufficient and all parties entered the contract satisfactorily. I can only presume all parties concluded the contract satisfactorily. The Client knew his end cost and the Contractor knew his utilisation and subsequent dredging costs. All very organised!

The input from the contractor at early stages also merits comment.

It ensures that the promoter is designing and detailing the works with a mind on the possible construction methods. The support from contractors is often asked to be given free of charge on the basis that you might be invited to tender. This is in my opinion is unfair on the contractor who can dedicate considerable resources to the project. The alternative is to decline to assist which can be construed as one of lack interest.

From the Contractors viewpoint it can though be of use in his understanding of the project and his pricing will be more accurate. It will also assist the Client in forecasting correctly his final out turn costs. On balance early contractor involvement should be encouraged. Whether he should get paid for this out of the Consultants fees is probably not for discussion here.

In the case of Southampton Water consideration was given to reducing future maintenance costs. The dredge pockets were left higher than the channel allowing ploughing techniques to be used for pulling material away from the berth faces. This is especially important for three reasons.

A plough can be mobilised quickly and manoeuvre easily in confined spaces.
A buffer always exists within the channel allowing consideration to campaign dredging.
A TSHD can operate more efficiently on long runs with limited manoeuvring.

ESTABLISHMENT OF CHANNELS - RESOURCES (Slide 7)
The equipment required for the establishment of Channels is varied. The principle equipment is the:

Backhoe or Dipper Dredger.

The Trailer Suction Hopper Dredger.

The Bucket Ladder Dredger.

The Cutter Suction Dredger.

The Grab Dredger.

MAINTENANCE OF CHANNELS (Slide 8)

In respect of maintenance of channels there are three main descriptions of the process all requiring a different philosophy of approach by the Contractor.

Campaign Dredging .....Visiting at pre-planned times. Generally used where the dredging requirements in terms of siltation rates are well known.

Regular Dredging .....Where depths vary rapidly and consistently. Where buffer zones would be of limited use. Resources need to be readily available. Matching vessel size to workload is important.

Emergency Dredging ..... due to rapid influx, new traffic requirements or shift in shape of natural channels. This is where Contractors will start scurrying around, ripping up pre-planned schedules and juggling with the logistics of securing a vessel for their Client.

The method adopted will be determined either from research in the case of new channels, or by experience,or a combination of both. For contractors new to an area it is extraordinarily difficult to obtain pre existing dredge records. Contractors will naturally try to retain this information so as to give them an edge over the competition. If Clients and contractors are to work better together it is essential that dredge information is provided in a complete a manner as possible. Otherwise each contractor ends up reinventing the wheel which cannot be conducive to best practice and economic dredging.

MAINTENANCE OF CHANNELS (Slide 9)

An example of a maintained Channel is the Sunk Dredge Channel in the Humber Estuary. This channel demonstrates many of the difficulties for Client and Contractor.

Some 1.2m m3 of sand was dredged last year involving some 70 days of dredger time. The previous year some 1.8m m3 was dredged in 102 days. How can both budget for this uncertainty.

Being a natural channel it suffers from movements and rapid depth changes. The Client's approach has been influenced by the Contractor´s ability to economically plan his resources. The Client also determines the navigation depth 6 weeks in advance so that vessels arriving from the Far East and Australia can be loaded correctly and discharged at the appropriate ports.

This channel is surveyed fortnightly and dredging triggered by critical depths being reached or by slack time in the dredgers programme to enable buffer zones to be established. Various materials can be found ranging from sands to silts and subsequently the unit cost of dredging changes. However, the Contractors rate is fixed.

In this case, because of the variability in material, timing and quantity a dayrate has been agreed with the Client. This can cause difficulties with the Contractor as he must respond to a call to dredge and he must be prepared to deal with different materials. Mobilisation is included within the dayrate, i.e. the Client will not be penalised if the dredger is a long sailing distance away.

However, one benefit to the Contractor is that it can provide some long term core business provided flexibility can be maintained in programming the vessels use. The more flexible approach provided by the Client the sharper a price can be given.

Slopes can become unstable requiring emergency dredging and the shape needs to be maintained to allow safe passage of vessels.

MAINTENANCE OF CHANNELS (Slide 10)

The Client maintains regular survey and research to try and predict dredging requirements. This is done hand in hand with the dredging organisation in an effort to reduce dredging costs. The contractor must continually look at material type and adjust his dredging methodology to suit.

Liaison with the Harbour Masters and predicted traffic requirements may also dispel or increase the need for dredging.

Do not just leave the dredgers to it. Regular discussion and agreement between all parties is essential for economic dredging.

VOLUMETRIC DATA NEWPORT (Slide 11)
UNDERSTANDING THE TASK - VOLUMETRIC CHARTS

One problem facing the Contractor is to understand in a practical way what the channel is doing and what impact his efforts have. Examination of a survey chart do not in my mind show information that is useful to the planning of dredging campaigns. Survey has two aims. To direct the dredger to the particular areas that require dredging and to inform ships captains and pilots where not to sail.
It does not tell when you should dredge, how much you should dredge or how much time it will take you to dredge.

We produced volumetric charts for all of ABP ports.

For each channel we define the plan encompassing the area that historically has been dredged. The navigation depth is known. The volume within the fixed dredge area ABOVE navigation depth is computed. The volume BENEATH the navigation depth is computed. The DIFFERENCE is calculated.

It can then be determined when the next campaign is likely, how much will be required, and how much time we need to do the job.

VOLUMETRIC DATA PORT TALBOT (Slide 12)

In this chart of Port Talbot the channel is stable in terms of its routing. It is a man made channel, straight and not subject to morphology changes.

The dredging is carried out in two Major campaigns over the year with minor intermediate dredging at other times. In this way, over a period of time a good understanding of requirements can be achieved.

THE FUTURE (Slide 13)
FUTURE GROWTH

I would like to add just a few words about the future and pose some open ended questions.

Promoters of schemes must look at the forward costs of maintaining new developments. How many times have new installations been built with financial viability stricken by high dredge maintenance costs.

Is dredging plant and equipment local or does it have to be brought in from afar?
Some promoters are so dependent on dredging that they have their own fleet e.g. ABP(UK), Dragages Ports (France), NPA (South Africa), Brisbane (Austrailia).

More alarmingly:

Will new regulation impose new dredging restrictions?

I am increasingly seeing signs and demands from Clients about the ability to cater for contaminated soils. Threshold levels are decreasing and there may soon be a presumption against dredging at sea. Where will we take the material?

Is there a beneficial use?

Will technology advance quickly enough to satisfy the regulators?

Who is prepared to invest in the research and development to find the right solution?

These are not unique challenges for one group. We all have a stake.

TRAILING SUCTION HOPPER DREDGER(TSHD) (Slide 14)

This is THE prime tool used for the dredging maintenance market.

Its description perfectly describes its operation.

Advantages: Relative immunity to weather, independent operation, can work in congested waterways, transports material over long distances, mobilisation costs are comparatively small. High production rates achievable.

Disadvantages: Inability to dredge strong materials, can be restricted by small areas, sensitive to debris, can carry more water than solids.

TSHD SECTIONAL VIEW (Slide 15)

Main Components are:

Accommodation Unit housing the Bridge and Dredge Controls.
The Hopper.
The Suction Pipe.
The Dredge Pump.
The Dragheads.
The Overflow- (ALMO system).
Discharge Mechanism via Bottom Doors, Valves, Split Hull, Pumping and Rainbowing.

TSHD SCHEMATIC (Slide 16)
TYPICAL DREDGE FLOW

Draghead (with or without jetwater), Suction Pipe, Dredge Pump (with or without Degassing), Discharge Pipe To Hopper, Bottom Dumping, Pump Ashore or Rainbow.

Problems for Contractors:

Significant Wear and Tear variations dependent on material.
Damage to dragheads.
Loss of Suction Pipe (Wires from Gantries).
Loss of Suction due to gas content.
Pump damage.
Water inundation.(Separate Pump Rooms on some dredgers)
Debris trapped in pump or bottom doors.
When Pumping-blocked pipeline.
Shallow working causes damage to propellers, cavitation in pumps and grounding possibilities.

CUTTER SUCTION (Slide 17)
CUTTER SUCTION DREDGER

Can be used for maintenance dredging but usually only the smaller models where access is difficult for other equipment.

As the name implies the principle involves cutting by the means of a rotating head combined with suction power. The cutting head pivots around the pontoon in sweeping arcs. The dredger moves by ”walking” on its spuds or is laid to anchor.

Advantages are:
Can dredge a wide variety of materials and then carry by means of solids in suspension in a pipeline to a disposal site.
Can operate in shallow waters, can cut to required profiles easily.

Disadvantages are:
Very sensitive to sea conditions, limited distances for discharge, limited dredging depths.
High mobilisation (usually no self propulsion unit).

Main Components:
Spuds (Walking and Working).
Control Room.

Main Engine and Pump room.
Ladder.
Cutting Head.
Swing Wires.
Service Platform.

TYPICAL CUTTER SUCTION SITE (Slide 18)

Typical site consists of the cutter unit, floating pipeline and spread unit.

May involve additional booster pump if discharge point long distance away. Problems for contractors are very similar to that of the TSHD with the added wear and tear on the cutter head and the need to keep the discharge lines unblocked at all times. Floating pipeline needs regular attendance in poor sea states.

BACKHOE DREDGER (Slide 19)

Mechanism of Working Similar to that of the cutter in that it is a pontoon mounted dredger with spuds. The excavating effort in this case however is the hydraulic excavator and the spread is incapable of moving the dredge material under its own power.

Advantages are:
Ability to dredge a wide range of materials, incl. boulders or debris, can work in confined areas, does not require anchors or wires.

Disadvantages are:
Slower output than TSHD or cutter. Requires separate spread to transport material.

Usually has very high mobilisation costs (Usually it has no propulsive power of its own). Can impart severe shock loads to the pontoon and spuds increasing maintenance costs.

BACKHOE SECTIONAL VIEW (Slide 20)

Main Components are:

Pontoon.
Spuds.
Hydraulic Excavator.

Attendant craft needed to transport material.

GRAB DREDGER (Slide 21)

One of the oldest types of dredger that has fallen from grace in recent years.

Advantages are:
Loads with minimum dilution of solids. Can accommodate boulders and debris, Carries its own cargo to dump. Can work in confined areas.

Disadvantages are:
Slow production, Poor Level control, damage and stoppages due to bottom door wire problems.

Liked by Harbour Masters because it can reach and do work that other dredgers cannot do.

TYPICAL GRAB OPERATION (Slide 22)

No notes.

NOT TYPICAL!! (Slide 23)

No notes.

TYPICAL BUCKET DREDGER SITE (Slide 24)
BUCKET DREDGER

Out of favour in some quarters much of it related to the perception that it is the noisiest of dredgers. This perception is generally misplaced and can offer economic alternatives to other equipment.

It is unique in that of the bucket dredger variety its action is continuous. Pontoon mounted like the cutter it operates by a continuous chain of buckets that scoop material from the seabed and discharge into hoppers.

Advantages are:
Its continuous and relatively high production rates, its ability to deal with clays, gravels boulders and debris. High dredge accuracies can be achieved. As it is anchored and manoeuvred by anchors and winches it is not as susceptible to poor sea conditions. It is efficient in providing high solids content during dredging.

Disadvantages are:
That wires can introduce restrictions in navigable waterways, requires ancillary equipment to transport material and is not efficient in shallow bands of dredging. Sticky clays can also be difficult as the material is not readily discharged from the buckets.

BUCKET DREDGER (Slide 25)

Main Components:
Control Room.
Engine Room.
Ladder and Hoist Wires.
Bottom Tumbler.
Side Chutes.
Bucket Chain.
Anchor system (Generally 6 wires).

ANCILLARY EQUIPMENT (Slide 26)
PLOUGH BED LEVELLER

Most works with TSHD in channels will involve the plough for a number of purposes.

To pull material away from restricted areas.
To level the seabed after trailing.
To act as a general support vessel (also for survey).
Can also be used if of this design for buoy handling and dredge pipe handling.

ANCILLARY EQUIPMENT (Slide 27)
HOPPER BARGE

Either of self propelled or dump barge construction.

Can be split or bottom door dumping.

Can be susceptible to weather conditions at disposal ground.

ANCILLARY EQUIPMENT (Slide 28)
SURVEY VESSEL

No notes.

ANCILLARY EQUIPMENT (Slide 29)

Market intelligence, trade press and word of mouth all play a part in the Contractor´s ability to source dredging opportunities. His next step is to make sure he is selected for inclusion on the tender list with one caveat and one plea.

The Caveat ....The process of tendering is a very costly one for Contractors. Obviously success rates for winning contracts is critical to the survival of Contractors. A success rate (or failure rate if you are a pessimist) is maybe 1:10 or worse. The costs of this effort eventually gets passed on in overhead contributions from those works successfully tendered. We do not like large tender lists as the chances of success are limited. This cannot always be in the Client's best interests. Clients should carefully consider the size of the tender list.

The Plea .... Prequalification process also has not moved with the times. The information required prior to tender is becoming extensive. Numerous copies are required and the information requested is similar between many Clients. I make a plea to standardise the base information required. Collect it electronically if you can. The purpose of prequalification is to identify those contractors capable and willing to carry out the scope of works not to create paper.

PROCESS (Slide 30)

When requesting tenders consideration should be given to the time allowed for tendering. If too short the Contractor will either decline or raise his intended margins as he has not had enough time to properly consider the bid. Contractors do not start on the tender immediately. They are probably in the middle of something else.

Information should be as complete as possible especially site investigation. The contractor will then not have to spend time searching out information readily known to the Client.

The contractor will fairly soon after receipt of the documents plan his tender programme. Dependent on size and complexity this may involve preliminary discussions with his suppliers, seeking out joint venture partners, if not done at prequalification stage.

A period of collection and evaluation proceeds with site visits and sub contract prices requested.
It is also the time to seek clarification of the documents from the Client. Unless of a confidential nature these are generally circulated to all tenderers. We are very cautious with our questions, therefore, if it is likely the question or answer will disadvantage our bid.

Pricing is carried out. It is unlikely that the final price will be known until minutes before the envelope is sealed and dispatched to the Client. This is for many reasons such as making sure the latest information is reflected in the bids, sub contract prices come in at the last minute and the bid director decides to make that last minute commercial adjustment.

Together with the price will usually come a list of qualifications or clarifications. This will be in direct proportion to how onerous the tender document has been written. Non standard conditions, risk that rightly should belong to the Client will all incur a comment from the Contractor. Adjudication is then extremely difficult.

PROCESS (Slide 31)
PRICING

The following factors go into making up the price:

The base cost of supplying the equipment must be determined. This will take into consideration the anticipated utilisation, depreciation and finance of the asset, the maintenance costs, fuel and crew costs.

PRODUCTION CALCULATION (Slide 32)
KEY FACTOR
CYCLE TIME

Loading of Cargo (Material, Overflowing, Gases etc.).
Sailing Time (Speed Restrictions, Low water obstructions, Tide, Locks, etc.).
Disposal (Sea state, Tidal accessibility, Hook up, Pumping, Material Clearance from Hopper).
Return to Site.
Manoeuvring (Traffic, Restricted working areas etc.).

PRODUCTION (Slide 33)
TYPICAL LOADING CURVES

Aim is to stop dredging at the most economic point bearing in mind loading and sailing time.
Long Haul will require as high a load as practical.
Short Haul may require a lesser load per trip but more trips.
Material type will impact.
Sands will settle quickly and it will be worth extending the loading period to maximise the cargoes.
Silts will settle slowly with little benefit in extended loading. Here it is critical that during the loading process the mixture is as dense as possible so that the dredger does not end up carrying water. Typically solids will represent 35% of hopper volume. In the case of sands it could be possible to overload.

All recorded electronically and the crew can establish the best timings. This is the time to check if the estimator got it right or the crew got it wrong. The first few trips are therefore critical in a new dredge area to ensure everything and everyone is achieving optimal performance.

PROCESS (Slide 34)
RISK ANALYSIS

Ground Data ..... Contractor needs to have confidence in the ground data in order not only to choose the right equipment but also to calculate dredging production rates.
Dredge profile .... especially on slopes can be difficult to calculate as if too steep natural slippage will occur.
Slippage from beneath open jetties can also occur.
Weather .... Likelihood of stoppages due to weather. My experience is that in maintenance dredging less than 1% is lost on average. This is generally achieved by ensuring alternative dredge areas are available.

Capital works can be more susceptible as the plant, as previously described, is more prone to weather. In these cases historic anecdotal evidence must be used to calculate the risk of weather overrun.

Similarly traffic delays are usually quite small and in the case of capital works is usually not taking place in existing traffic routes.

The Contractor should be well versed with his plant capability. However, he must take account of the condition of the vessel and the amount of routine or legal maintenance that is required. Damages due to debris cause delays and this risk is one that Clients should carry, especially those who are responsible for good housekeeping adjacent to quay walls, jetties and the like.

Plant availability is always a balancing act. From the time of tender to job award there can be a considerable time lag. During this period other works can be awarded. It then becomes first ask becomes first served. With good dialogue, however, between the parties these programming restraints should be overcome. If the contractor realises his plant will not be available whilst in the tender period it is only reasonable that he informs the Client and returns the document or agrees with the Client that an alternative programme can be arranged.

PROCESS (Slide 35)
OTHER FACTORS

Insurances etc;
Marine.
Employers and Third Parties.
Contractors All Risk.

Bonds, Project Finance Costs (Work carried out well in advance of payments).

Site Overheads:
Supervision.
Accommodation.
Crew Changes.
Travel and Transport.
Water, Skips and Waste Disposal.
Pilotage and Port Charges.

Survey:
Survey Vessel.
Surveyors.

COMMERCIAL ADJUSTMENTS

General Risk.
HO Overhead.
Contribution.
Late Adjustments.

CUSTOMER AND CONTRACTOR SATISFACTION (Slide 36)

My first thoughts were to put this on separate slides. But the slides would have been the same.

Ultimately I do not think either party will be satisfied unless a high percentage of the following has been achieved:

- The works have been carried out without harm to people or the environment.
- The works are completed on time and to specification. This means the contractor has carried out the works as expected and the customer has his scheme on time.
- The works are completed to budget. An obvious statement. Not only the project budget but also the contractors estimate.

CUSTOMER AND CONTRACTOR SATISFACTION (Slide 37)

Best ways to Achieve these aims:

- A high degree of trust and respect for both organisations. We all have a job to do.
- As much openness as possible. A problem shared is a problem halved.
- Recognition of the pressures both sides can be working under by understanding each others business.

DHI WATER & ENVIRONMENT

DHI work

Elbe plume

- ✓ High precipitation, maximum discharge
- ✓ Change in erosion pattern of sediment
- ✓ Changed fluxes of sediment and nutrients
- ✓ Increased deposition
- ✓ Morphology changes in estuary

11

DHI WATER & ENVIRONMENT

Yearly mean sea level in Esbjerg

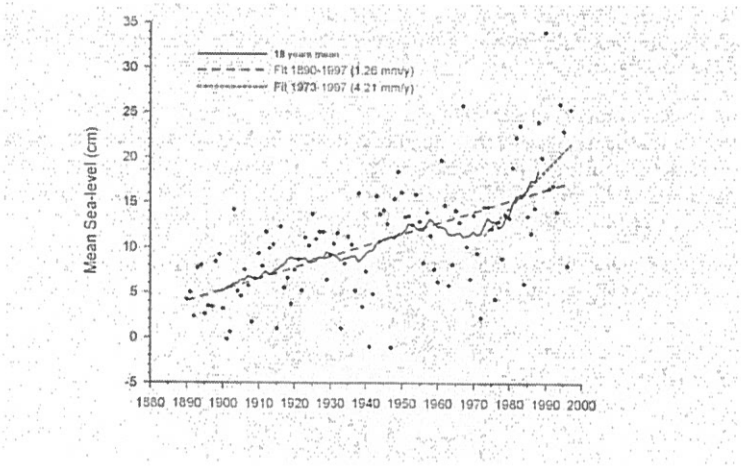

Source: Christiansen et al in Climate Change Research DMI 2001.

Effect on sea level rise on return period of design water level

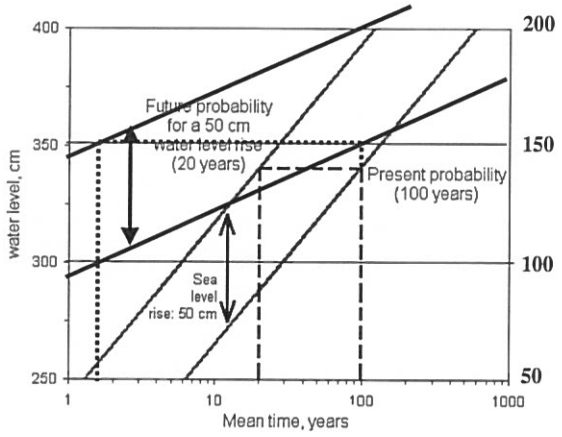

Red and blue example from an exposed coast
Green example from a sheltered coast

Karsten Mangor 2002

Storm surge occurrence at Esbjerg

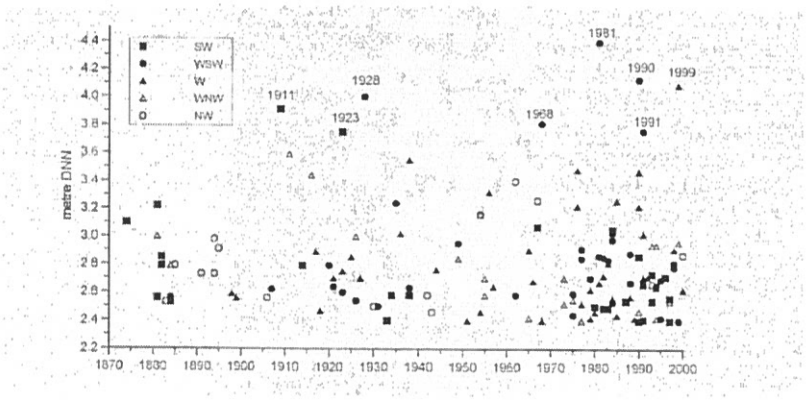

Source: Christiansen et al in Climate Change Research DMI 2001.

Maintenance dredging in Grådyb

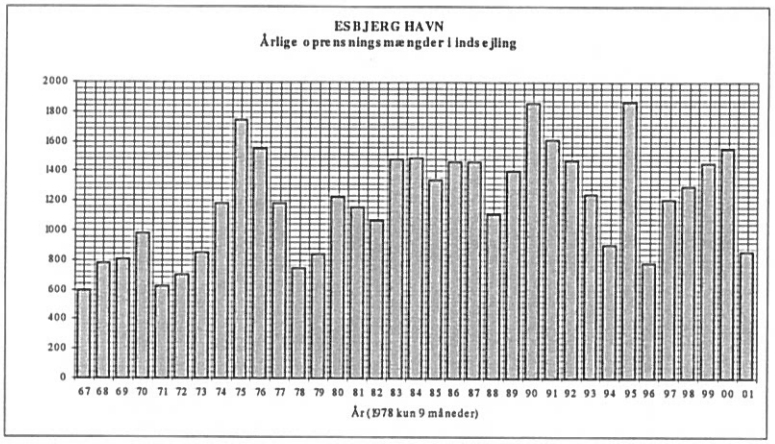

Beach nourishment

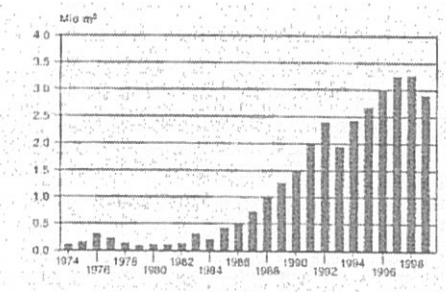

Future need 6 mill m^3

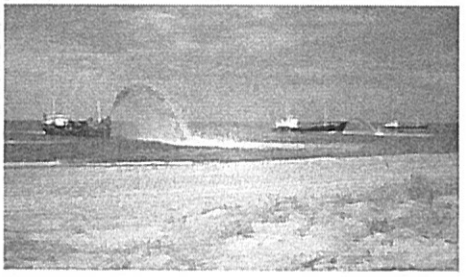

Sediment Transport and Backfilling of Trenches in Oscillatory Flow

By Jacob Hjelmager Jensen[1] and Jørgen Fredsøe[2]

Abstract: By means of detailed mathematical modeling the processes responsible for the morphological evolution of small-scale excavations exposed to wave-induced flow are investigated. The problem is relevant when assessing rates of sedimentation of trenches dredged for the purpose of laying out pipelines or cables in the marine environment. A flow and sediment transport model formulated in curvilinear coordinates is applied. The unsteady Reynolds-averaged Navier-Stokes equations along with a standard k-ε turbulence model and the equation of continuity constitute the flow model. The action of waves is simulated by an oscillating pressure gradient imposed on the horizontal momentum equation. The sediment transport is composed of bed and suspended load taking into account the effect of gravity on the former. The convection-diffusion concept is applied to calculate the distribution of suspended sediment concentration. Intraperiod flow and sediment transport processes are resolved, and the effect of these on the backfilling is quantified by a parameter defined by the ratio between the amplitude of oscillation of the flow and the width of the trench. The role of this parameter is twofold. It indicates the extent of flow separation developing over the lee-side slope of the trench. The energetic turbulence associated with the presence of a separation zone impedes sedimentation; it indicates the relative-to-the-trench-width distance covered by advected suspended sediment. For small values of the parameter, sediment will only be exchanged over relatively small distances as opposed to large values where sediment from the undredged regions will encounter the deepest sections of the trench thus enhancing sedimentation. Consequently, with respect to backfilling, the parameter in question governs two counteracting processes. For large values, the separation bubble is the prevailing mechanism for the distribution of the period-averaged transport of sediment and, in turn, for the evolution, of the trench morphology. The flow model is validated against measurements from a U-tube experiment.

INTRODUCTION

In a marine environment the impact of waves is a typical concern in backfilling assessments. Backfilling of artificially dredged trenches is not preferential in the preparation phase prior to laying out pipelines. If backfilling rates are too high, the actual laying may be hindered and reexcavation may be required. On the other hand, if rates are too low, then forces exerted by the flow on the pipe may inflict severe damage on it.

In recent years a number of investigations concerned with steady flow and sediment transport processes—sometimes including wave-stirring effects—over trenches and dredged channels have been published. In these studies two backfilling mechanisms recur. First, backfilling takes place when the carrying capacity of the flow is less within the excavated region than outside (Fredsøe 1979). A decrease in the carrying capacity of the flow across an excavated bed is caused by a reduction in flow properties (velocities and turbulence intensity) and by a reduced action of waves. Second, backfilling takes place on the slopes of the excavation as bed load sediment gravitates toward the bottom of it [e.g., Fredsøe (1978) and Bijker (1980)]. Analytical treatment of the backfilling process is given by Mayor-Mora et al. (1976), Fredsøe (1979), and Bijker (1980) focusing on the modeling of the adaptation length of suspended sediment. The hydrodynamics of these models are simplified using a depth-averaged flow description. The sediment transport descriptions are simplified as well, relying on parametric models for erosion and deposition conditions at the bed. Although conceptual, the models capture the fundamental behavior of sedimentation in steady flow. Alfrink and van Rijn (1983) provided a more sophisticated description of steady flow across a channel by resolving the properties of the flow over the depth and using a k-ε turbulence model. van Rijn (1986) improved the sediment transport description by solving the diffusion-convection equation of suspended sediment. The description of waves was obtained by a conservation law of energy flux taking into account the wave field transformation across the channel. When waves are present, the reduction in capacity of the flow is influenced by additional phenomena. If the excavated-width-to-wavelength ratio is large (e.g., navigation channels), then the transformation of surface waves will become important for sedimentation as pointed out by Fredsøe and Deigaard (1986). In this case wave-induced velocities and therefore the carrying capacity of the flow change across the channel as a consequence of shoaling, reflection, wave-breaking, and refraction.

The common approach when modeling the impact of waves is to regard them as a mechanism for stirring sediment by adding wave-related turbulence to that of the coexisting current [e.g., Fredsøe (1979) and van Rijn (1986)]. The enhanced (time-independent) turbulence is assumed to be responsible for the diffusion, while the current alone is assumed to be responsible for transporting sediment. If, however, the amplitude of oscillation is significant compared to the excavated width, sediment transport and backfilling processes will be strongly influenced by intraperiod advection and diffusion of sediment. Kobayashi (1982) proposed an intraperiod approach for the morphology of trenches in pure wave-induced flow. In this work sediment in suspension was ignored, and sedimentation was caused solely by the action of gravity on bed load particles as in Fredsøe (1978), making the model well suited for cases where the flow direction is parallel with the alignment of the trench.

PURPOSE OF PRESENT STUDY

The purpose of this paper is to describe the backfilling of trenches through relevant nondimensional parameters by using

[1]Coast. Res. Engr., Inst. of Hydrodyn. and Water Resour., Tech. Univ. of Denmark, DK-2800 Lyngby, Denmark; currently, Danish Hydr. Inst., Agern Alle 5, DK-2970 Hørsholm, Denmark. E-mail: jhj@dhi.dk

[2]Prof., Inst. of Hydrodyn. and Water Resour., Tech. Univ. of Denmark, DK-2800 Lyngby, Denmark. E-mail: fredsoe@isva.dtu.dk

Note. Discussion open until March 1, 2002. To extend the closing date one month, a written request must be filed with the ASCE Manager of Journals. The manuscript for this paper was submitted for review and possible publication on May 31, 2000; revised March 1, 2001. This paper is part of the *Journal of Waterway, Port, Coastal, and Ocean Engineering*, Vol. 127, No. 5, September/October, 2001. ©ASCE, ISSN 0733-950X/01/0005-0272–0281/$8.00 + $.50 per page. Paper No. 22182.

detailed mathematical modeling of phase-resolved oscillatory flow and associated sediment transport processes. The direction of the flow is assumed to be perpendicular to the trench alignment. The trench is characterized by a small width-to-water-depth ratio, such that spatial variations in wave motion are small across the trench. Backfilling is studied in the critical phase before the pipeline is implemented. Since the morphological trench evolution can become quite different after the pipeline is implemented, this case, although being of great engineering importance as well, is not considered. By solving equations of the model on a boundary-fitted coordinate system, an accurate description of the near-bed flow is obtained (which is a prerequisite to a reliable sediment transport prediction) as bed load, and the main part of suspended sediment transport take place here. Owing to nonlinearities between forces of the flow and the sediment transport, a sediment transport model based on period-averaged flow will produce erroneous results. For this reason phase-resolving processes are necessary.

MATHEMATICAL MODEL

Governing Flow Equations

In a Cartesian coordinate system, the equations of motion and the continuity equation read

$$\frac{\partial u}{\partial t} + u\frac{\partial u}{\partial x} + v\frac{\partial u}{\partial y} = -\frac{1}{\rho}\frac{\partial p}{\partial x} + \frac{\partial}{\partial x}\left(\nu_T \frac{\partial u}{\partial x}\right) + \frac{\partial}{\partial y}\left(\nu_T \frac{\partial u}{\partial y}\right) + \frac{f_x}{\rho} \tag{1}$$

$$\frac{\partial v}{\partial t} + u\frac{\partial v}{\partial x} + v\frac{\partial v}{\partial y} = -\frac{1}{\rho}\frac{\partial p}{\partial y} + \frac{\partial}{\partial x}\left(\nu_T \frac{\partial v}{\partial x}\right) + \frac{\partial}{\partial y}\left(\nu_T \frac{\partial v}{\partial y}\right) \tag{2}$$

$$\frac{\partial u}{\partial x} + \frac{\partial v}{\partial y} = 0 \tag{3}$$

where u and v = velocity components in the x- and y-directions, respectively; t = time; ρ = density of water; p = pressure; and ν_T = eddy viscosity.

The action of waves is obtained by employing a uniformly distributed oscillating force f_x [see (1)] to drive the horizontal flow

$$f_x = \rho\frac{\partial U}{\partial t}, \quad U = U_{max}\sin\left(2\pi\frac{t}{T}\right) \tag{4}$$

where U = potential free-stream velocity at a location undisturbed by the trench and, for the sake of simplicity, is taken to vary sinusoidally [see (4)]. Furthermore, U_{max} = amplitude of velocity, and T = wave period.

The unsteady k-ε turbulence model described in Launder and Spalding (1974) is used to calculate the distribution of ν_T. The model consists of differential equations for the turbulent kinetic energy k and the dissipation rate ε.

Boundary Conditions

The rigid lid assumption is applied at the water surface. Hence, the symmetry condition ($\partial/\partial y = 0$) is imposed for u, k, and ε, whereas v equals zero. At the bed a no-slip condition for the velocities is imposed. The equation of turbulent kinetic energy uses a zero flux condition. For the dissipation of turbulent kinetic energy, a standard equilibrium condition—between production and dissipation of turbulent kinetic energy—is utilized. On the lateral boundaries periodicity is applied. The lateral boundaries are located sufficiently far away from the excavation—typically five amplitudes of oscillation—ensuring that the flow field at these locations is uniform at all times.

Sediment Transport Description

The bed is assumed to consist of noncohesive sediment with a mean grain diameter corresponding to sand and a geometric standard deviation equal to 1.4. The transport of bed load q_b and suspended sediment q_s constitute the sediment transport q.

The bed load transport is calculated by using the Meyer-Peter and Müller formula

$$\frac{q_b}{\sqrt{(s-1)gd^3}} = 8(\theta - \theta_c)^{3/2}, \quad \theta = \frac{\tau_b}{\rho(s-1)gd} \tag{5}$$

where s (=2.65) = relative density of the sand; g = acceleration of gravity; d = mean grain diameter of sand; θ = Shields parameter; τ_b = bed-shear stress; and θ_c = critical Shields parameter for the mobilization of sediment. Taking gravitation into account and assuming the flow direction to be perpendicular to the slope alignment, θ_c is—according to Engelund and Fredsøe (1982)—given by

$$\theta_c = \theta_{co}\left(\frac{1}{\mu_s}\tan\left(\frac{\partial z}{\partial x_s}\right) + 1\right)\cos\left(\frac{\partial z}{\partial x_s}\right) \simeq \theta_{co} + \mu\frac{\partial z}{\partial x_s} \tag{6}$$

where θ_{co} (≃0.05) = critical Shields parameter on flat bed; μ_s (≃0.5) = static friction coefficient; z = bed elevation measured vertically from $y = 0$, $\partial z/\partial x_s$ = bed slope in direction of flow; and $\mu = \theta_{co}/\mu_s$ (≃0.1).

The convection-diffusion equation is applied to calculate the distribution of concentration of suspended sediment c assuming the diffusivity is equal to the eddy viscosity ν_T

$$\frac{\partial c}{\partial t} + u\frac{\partial c}{\partial x} + v\frac{\partial c}{\partial y} = w_s\frac{\partial c}{\partial y} + \frac{\partial}{\partial x}\left(\nu_T\frac{\partial c}{\partial x}\right) + \frac{\partial}{\partial y}\left(\nu_T\frac{\partial c}{\partial y}\right) \tag{7}$$

where w_s = fall velocity of mean grain diameter in suspension.

The no-flux condition ($w_s c + \nu_T \partial c/\partial y = 0$) is imposed at the water surface, whereas the bed boundary condition proposed by Engelund and Fredsøe (1976) is utilized. Here, the concentration is specified directly at $y = 2d$. The suspended sediment transport q_s is obtained by depth-integrating the product of concentration and horizontal velocity.

Model for Morphological Evolution

The evolution of the trench morphology is assumed to be quasi-steady. Under quasi-steady conditions the shape of the trench is retained on a timescale larger than that of the wave period. The period-averaged transport field can therefore be used in the equation of conservation of sediment

$$\frac{\partial z}{\partial t} + \frac{1}{1-n}\frac{\partial \bar{q}}{\partial x} = 0, \quad \bar{q} = \frac{1}{T}\int_0^T q\,dt \tag{8}$$

where n (=0.4) = porosity of sand. The overbar signify a period-averaged quantity. In (8) the term accounting for sediment stored in suspension becomes zero when period-averaging and is therefore omitted. The numerical treatment of (8) is identical to that reported in Jensen et al. (1999).

Computational Features

Equations presented above are solved on a curvilinear coordinate system by using the finite-volume method (Patankar 1980). The equation of continuity is converted into an equation for the pressure, which is solved using the PISO-algorithm [velocity-pressure coupled solution algorithm, see e.g., Patankar (1980)]. The Quick scheme (Leonard 1979) is employed for a third-order representation of convective terms in the momentum equations. A backward-difference is used to represent the dynamic term. An in-depth model description is given by Tjerry (1995). Results insensitive to mesh refinement were achieved when using not less than 45 grid points in the vertical and 50 in the horizontal (the latter for the trenched part).

ASSESSMENT OF PROBLEM

In Fig. 1 a definition sketch is given. A long straight sine-shaped trench excavated in an otherwise plane seabed is con-

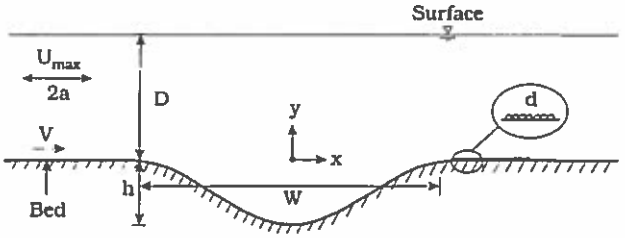

FIG. 1. Definition Sketch

sidered. The water depth outside the trench is denoted D, whereas W and h are symbols for excavated width and depth.

Nondimensional Parameters

By grouping the quantities defined in Fig. 1, the trapping of sediment can be associated with the following relevant nondimensional parameters:

$$\Delta = \Delta\left(\frac{h}{W}, \frac{h}{D}, \theta_{max}, KC, \frac{w_s}{U_{max}}, \frac{k_N}{D}, \frac{U_{max}}{U_{max} + V}\right) \tag{9}$$

where h/W = steepness parameter; h/D = expansion parameter; θ_{max} = maximum Shields parameter encountered during a wave period at a location far from the trench; and KC = Keulegan-Carpenter number well-known from offshore engineering practice, defined here by

$$KC = 2\pi \frac{a}{W} \tag{10}$$

where a [$=U_{max}T/2\pi$—from right of (4)] = amplitude of oscillation. Furthermore, w_s/U_{max} = characteristic parameter for the adaptation of suspended sediment; $U_{max}/(U_{max} + V)$ = wave-current strength parameter; V = superimposed depth-integrated velocity; and k_N = Nikuradse equivalent bed roughness related to the grain diameter ($k_N = 2.5d$) (Engelund and Hansen 1972). This is assumed to be valid under sheet flow conditions where the bed is flat (i.e., when values of θ_{max} exceeds 0.5–0.8). If ripples are present, a larger bed roughness must be introduced unless these are resolved by the numerical model.

Strictly speaking, (4) is restricted to shallow waters where the pressure distribution can be assumed to be nondispersed, such that wave-induced vertical velocities are negligible, Eq. (4) may, however, be used with reasonable accuracy outside the range of shallow water wave theory as the pressure inside the boundary layer, where all sediment is located, does not differ from that just outside of it. By limiting the study to cases where the excavated-width-to-wave-length ratio is small (e.g., pipeline trenches), this method becomes quite a good approximation for describing the wave-induced pressure field in the trench vicinity since (1) the transformation of the wave across the trench will be negligible; and (2) the wave forcing across the trench will be nearly uniform. The ratio has been excluded from (9) assuming it to be small enough that these conditions are met.

Since the mathematical model has confirmed that the timescale of backfilling does not depend strongly on the initial shape of the trench, a parameter characterizing this has been omitted from (9).

Parameter Significance

The significance of KC may to a certain extent be perceived intuitively: If the amplitude of oscillation is small compared to the width of the trench, then sediment will encounter only very local parts of the trench as opposed to relatively large excursion lengths. In the latter case deeper parts of the trench are fed continuously with sediment from outside the trench by the incoming flow. All other things being equal, sedimentation is enhanced when values of KC are relatively large since the exchange of sediment takes place over greater distances.

This enhancement in sedimentation with KC is to some extent counteracted by another KC-related mechanism. When exposed to oscillatory motion, the two slopes of the trench will take turns in being the lee-side and the flow-facing slope. Separation of the flow will thus be initiated once every half-period. The maximum size of the separation bubble depends on the magnitude of the excursion length. If large, compared to the width of the trench, the separation bubble will have time to expand and may eventually occupy a comparatively large part of it. Conversely, if a is relatively small, the separation bubble is limited by the time available for growth. High levels of turbulence are often associated with zones of separated flow and the extension of the region of energetic turbulence is related to the size of it. This implies that sedimentation is obstructed when values of KC are relatively large.

Usually the role of h/D in sedimentation studies is linked with changes in flow properties. In the case of a navigation channel where $W >> D$, the velocities across it is reduced over the depth corresponding to the water depth (i.e., $1 + h/D$). The validity of depth-averaged flow models used [e.g., by Fredsøe (1979) and Bijker (1980)] is therefore good for channels. Such models are, however, questionable when applied to the trench case where the excavated width and depth is often only a fraction of the water depth, implying that the sediment transport is only being slightly modified. The presence of the trench will disturb the flow field only in its vicinity.

If potential solution of flow over a trench is considered, the term "vicinity" can be made specific. In such a solution the curvature of streamlines is known to decay in the vertical direction by a factor of exp $(-2\pi y/W)$ (very similar to the vertical variation beneath gravity water waves). The vertical length scale of the disturbance in the pressure field caused by the presence of the trench is therefore of the order W implying that the flow above $y \sim W$ is only slightly affected by the trench. Hence, the part of the water depth that is active for changes in the carrying capacity of the flow confines itself entirely to $y < W$. In the case of pipeline trenches where $W < D$, the relevant parameter to describe the reduction in velocities is h/W (i.e., the steepness parameter).

From the discussion above, the steepness parameter and the Keulegan-Carpenter number are expected, at least with respect to the flow description, to be the most significant of those appearing in (9). The two parameters related directly to sediment transport are not given the same attention.

EXPERIMENTS

In this section flow measurements are described. In a later section some supplementary experiments with sediment are reported.

Experimental Setup

The experimental investigation was conducted in an oscillatory U-tube facility. The U-tube (illustrated in Fig. 2) has the following dimensions: length of 10 m, height of 29 cm, and width of 39 cm. The period of oscillation was $T = 10.0$ s. Flow measurements were conducted using a one-component laser Doppler anemometer.

Two nearly sinusoidally shaped concrete trench models were installed in the working section located in the middle of the tunnel. In both cases the depth of the trench was equal to 9 cm (Fig. 2). The smaller of the trenches was 50 cm wide, whereas the larger was 100 cm wide. The sidewalls of the U-

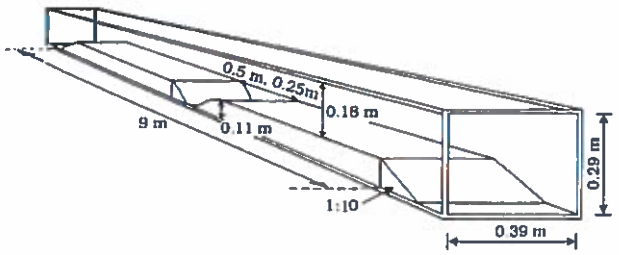

FIG. 2. Working Section of U-Tube

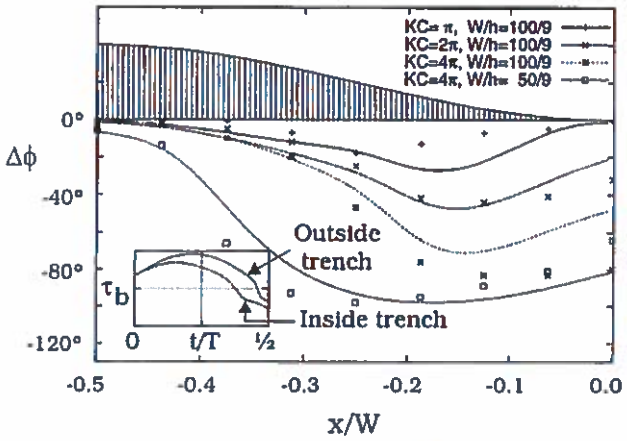

FIG. 3. Comparison between Theoretically and Experimentally Obtained Phase Lags between Flow Separation Far Outside and within Trench for Three Keulegan-Carpenter Numbers and Two Steepness Parameters; Trench Profile Shown in Upper Part of Figure Is Distorted

tube were hydraulically smooth, whereas the bed was covered with sandpaper with a characteristic roughness height of 0.35 mm. The experimental investigation comprises measurements of (1) horizontal velocity profiles at three different cross sections; and (2) horizontal velocity along the bed 1.5 mm above it. The latter was used to obtain the phase lag between the onset of flow separation far outside and at a given position within the trench $\Delta\phi$. In laminar oscillatory flow over a flat bed, the bed-shear stress is 45° in advance of the free-stream velocity, whereas in the turbulent case it reduces to approximately 10°–15° [e.g., Jensen et al. (1989)]. This value will change over nonuniform topography (e.g., it will increase when the flow is confronted with the wave-related adverse pressure gradient in addition to the pressure gradient induced by an expansion in depth).

Experimental Results

In Fig. 3, results of the mathematical model are compared with that of the experimental investigation. The variation in bed-shear stress during the time of positive flow is shown in the inset displayed in the lower left corner of the figure. Curves in the inset are the theoretical ones, obtained partly at an undisturbed flat bed location (full-drawn line) and partly at a position within the trench (dashed line). $\Delta\phi$ is the difference between the zero-crossings. The variation of this value across the trench is shown for three Keulegan-Carpenter numbers and two steepness parameters.

In both experimental and theoretical results, flow separation is initiated within the trench at a location somewhere between the steepest and the deepest parts of it. [The location of the point of separation in an accelerating flow is treated theoretically in Schlichting (1968, p. 401).] For increasing values of both KC and h/W the onset of separation occurs earlier in the wave-phase. Taking into consideration that separation can be

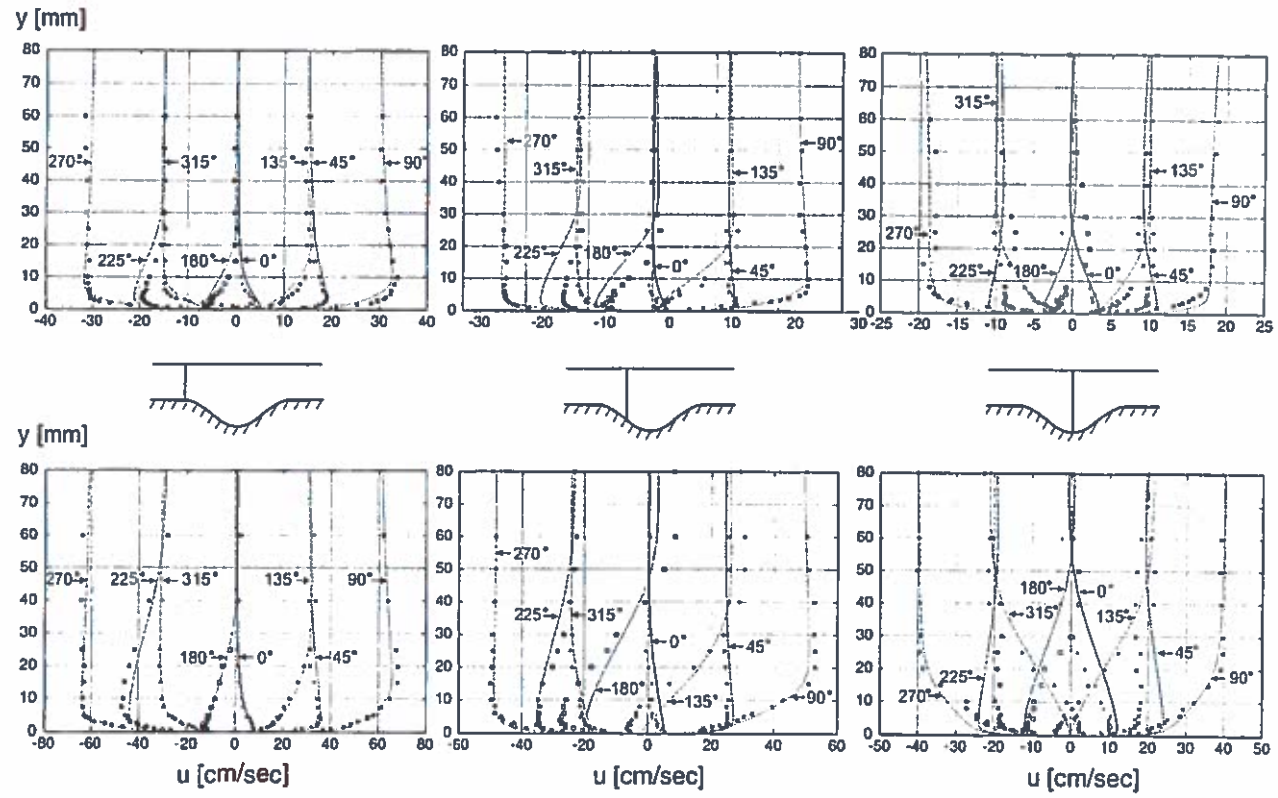

FIG. 4. Profiles of Horizontal Velocity at Three Cross Sections for $KC = \pi$ (Left) and $KC = 2\pi$ (Right). Theoretical Results Are Indicated by Lines Whereas Symbols Are Experimental Results

triggered or delayed by even small local imperfections in the bed, it is reasonable to say that the model is capable of predicting increasing phase differences for increasing values of KC and h/W satisfactorily.

In Fig. 4, profiles of horizontal velocity are shown at three vertical cross sections sited over the bottom of trench, over the steepest section, and where the trench adjoin the flat bed. Both theoretical and experimental results are shown for $KC = \pi$ (upper part of figure) and 2π (lower part of figure).

In conclusion, it can be said that the mathematical model performs well in predicting general flow field properties.

THEORETICAL RESULTS

Intraperiod Processes

A description of backfilling processes is made difficult by temporal and spatial changes in the flow. In the accelerating part of the wave-phase the flow over the lee-side slope of the trench is capable of overcoming the adverse pressure gradient associated with an expansion in depth. Hence, the upgrowth of the separation bubble can be suppressed during this stage. This implies that sediment traveling with the flow may continue to accelerate although larger depths are encountered. The reduction in the carrying capacity of the flow therefore awaits the decelerating wave-phase. All other things being equal, sedimentation will take place mainly during this stage. However, this happens synchronously with the upgrowth of the separation bubble. As separation zones are characterized by high levels of turbulence, sediment is accumulated within it. This is seen in Fig. 5 where snapshots of turbulent kinetic energy and concentration distributions are shown for $KC = 2\pi$ for a short time span just around flow reversal. The corresponding wave-phases are indicated in insets by dots on the sine curve defined in (4).

When the flow reverses, the separation bubble is ejected. The ejected separation bubble is able to retain rotation, such that the energetic turbulence is maintained. In this way, sediment is kept in suspension and removed from the trench by the reversed flow. In the following half-period, a new separation bubble will develop on the opposite side, whereupon processes are repeated in the subsequent half-period.

In Fig. 6, the Shields parameter is depicted as a contour plot in the (x, t)-plane displaying characteristic features of the near-bed flow. The trench is located at $-0.5 \leq x/W \leq 0.5$ and the time axis covers a full wave period. Results are obtained with $KC = 0.4\pi$ (upper part of figure) and 2.5π (lower part of figure) using $W/h = 5$, $h/D = 0.05$, $\theta_{max} = 1$, and $k_N/D = 5 \times 10^{-5}$.

In accordance with (4), the outer free-stream flow approaches the trench from the left and right in the time interval $0 < t/T < 0.5$ and $0.5 < t/T < 1$, respectively. Local maxima in the Shields parameter are seen to be located where the flat bed adjoins the trench (i.e., at $x/W = \pm 0.5$). The cause of their existence is explained in the following.

The local maximum found just upstream and downstream of the trench is caused by the response of the flow to the pressure perturbation induced by the trench itself. As the extent of the pressure perturbation exceeds the extent of the trench—a property that even potential flow possess—the streamlines on both sides of the trench will bend before the actual bed starts to curve, literally cutting a corner. As a consequence, streamlines converge here, and the bed-shear stress is amplified. This is most easily recognized in the upper part of Fig. 6. Due to this phenomenon, values nearly twice as large as θ_{max} are seen. The increase in θ by a factor of 2 corresponds to an amplification in the friction velocity by 1.4 being of the same magnitude as that obtained in potential flow for the bed velocity (slip condition). The convergence of streamlines and the associated bed-shear stress amplification in front of the trench entails enhanced sedimentation owing to a burst of sediment that accompanies the amplification.

This increase in near-bed velocities was identified in the experiments described previously.

For $KC = 2.5\pi$ the pattern becomes more complex [where nonlinearities of (1) and (2) comes into play] than for $KC = 0.4\pi$ owing to a more pronounced flow separation and an enlarged maximum on the flow-facing slope. The enlargement is due to flow being accelerated over the contracting part of the trench. The flow acceleration is a mechanism for rapid sus-

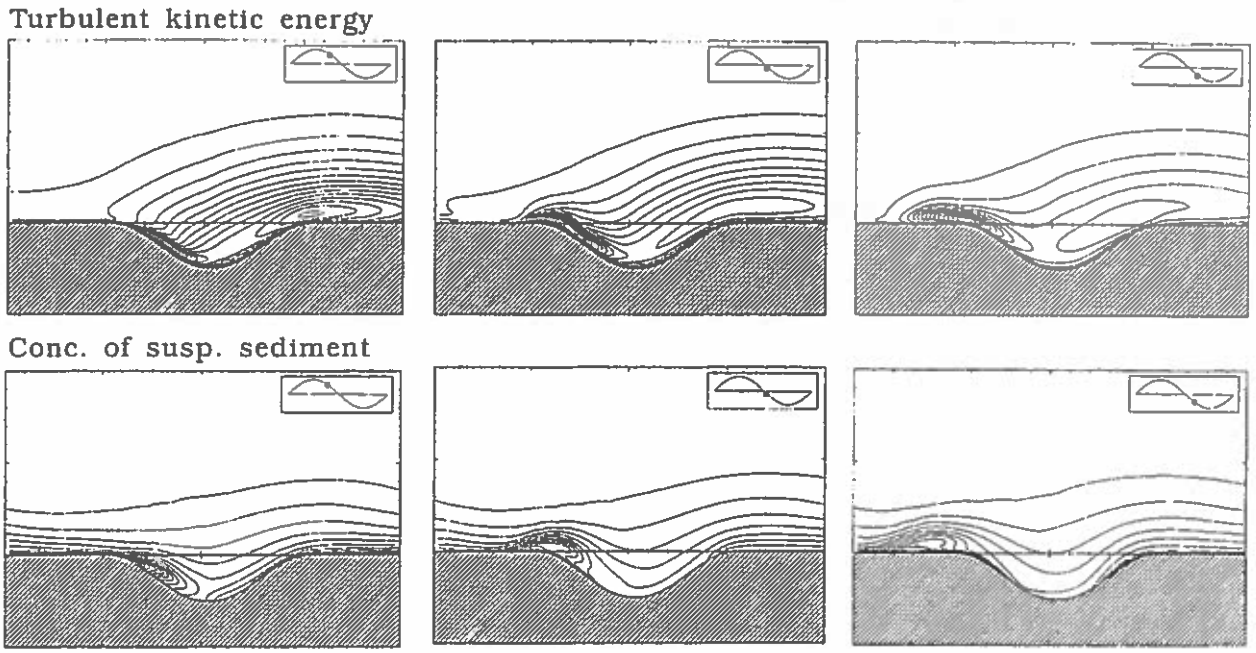

FIG. 5. Snapshots of Turbulent Kinetic Energy (Upper) and Contours of Concentration (Lower) Just around Flow Reversal with $KC = 2\pi$, $W/h = 5$, $\theta_{max} = 1$, $h/D = 0.05$, $k_N/D = 5 \times 10^{-5}$, and $w_s/U_{max} = 0.01$

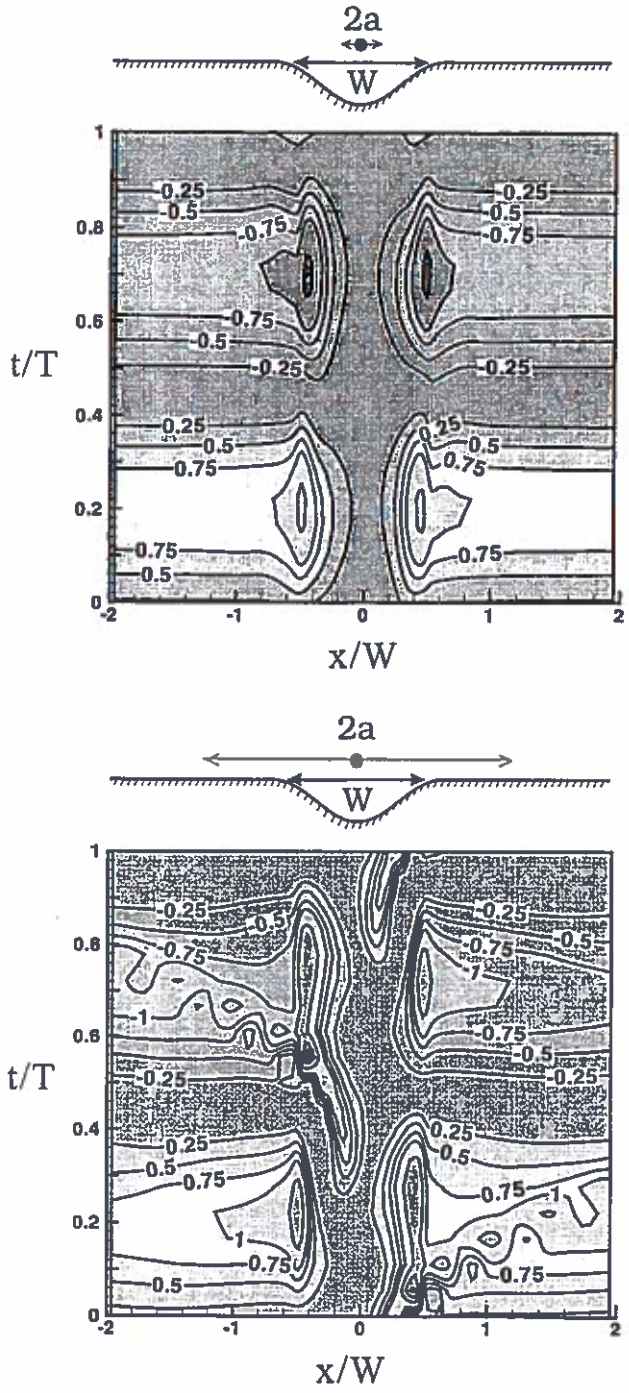

FIG. 6. Contours of Shields Parameter during Wave Period for $KC = 0.4\pi$ (Upper) and 2.5π (Lower); Remaining Parameters as in Fig. 5

pension on the slopes and, in turn, for the reshaping of the trench morphology. If, as a consequence of this maximum, the amount of suspended sediment at flow reversal is greater just downstream the trench compared to that far from it, then this process will act to enhance sedimentation.

The Shields parameter beneath the developing separation bubble ($KC = 2.5\pi$) will reach values larger than θ_{max} at the end of each half-period. The wave-related adverse pressure gradient is both decelerating water over the flat bed and accelerating reversed water within the trench. The separation bubble gains momentum to such an extent that the Shields parameter beneath it compares with θ_{max} and is therefore of a magnitude that enables it to pick up sediment. The acceleration of the excessive flux of reversed water within the trench continues until the boundary layer flow on the adjacent flat bed reverses after which the ejection process takes place.

Also, narrow maxima bands are seen over the adjacent flat bed region. These are tracks of detached separation bubbles that still cause the Shields parameter to reach values larger than θ_{max}.

Period-Averaged Flow Pattern—Streaming

The alternating sequence of flow separation and flow acceleration taking turns over the slopes of the trench will in the period-averaged sense create a departing near-bed flow within it (i.e., a flow directed outward toward the flat bed). Due to the constraint of continuity, a return flow is directed toward the center of the trench at higher levels in the water column. This is confirmed in Fig. 7 where period-averaged velocity profiles obtained from the results presented in the upper part of Fig. 4 are shown at the three cross sections defined previously.

The measured peak value of this period-averaged flow reaches approximately up to 17% of the free-stream velocity amplitude, whereas the mathematical model predicts some 12%. Streamlines of the period-averaged flow obtained with the mathematical model for $KC = \pi$ are depicted in Fig. 8 revealing a pair of counterrotating vortices. These rotate clockwise and anticlockwise on the left- and right-side slope of the trench, respectively. This period-averaged flow is referred to as streaming with reference to Longuet-Higgins (1953). Here, a similar problem is treated, and it is shown that surface waves progressing over a plane bed induce a steady boundary layer flow. The flow induced by an oscillating cylinder in fluid at rest was treated by Schlichting (1968). He found that a steady

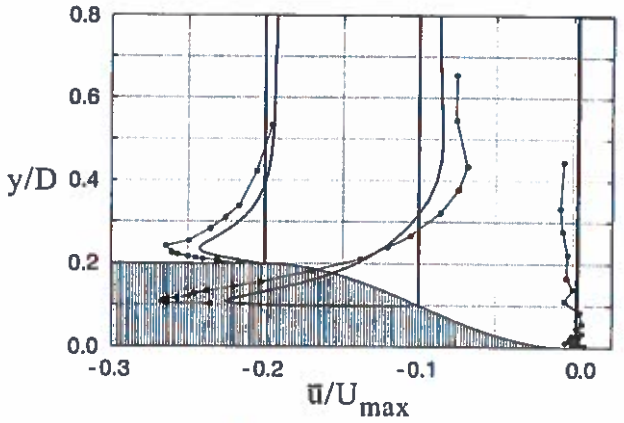

FIG. 7. Period-Averaged Profiles of Horizontal Velocity; Experimental and Theoretical Results Are Indicated Respectively by Lines with and without Dots

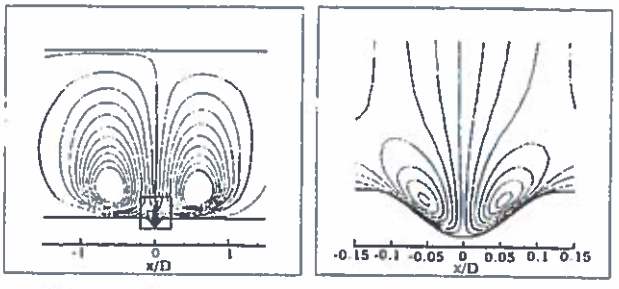

FIG. 8. Streamlines of Period-Averaged Flow for $KC = \pi$, $W/h = 5$, $h/D = 0.05$, and $k_N/D = 5 \times 10^{-5}$

flow—of a mathematical form similar to that found by Longuet-Higgins (1953)—was imparted on the flow obtained from the linearized equations of motion and concluded that this steady flow "has its origin in the convective terms and is caused by the interaction between inertia and viscosity."

In the present case, streaming is induced outside the trench (Fig. 8). The excursion length of the detached separation bubbles determines how far from the trench streaming is induced. For sufficiently small values of KC, the outer cells vanish, and the streaming pattern confines itself entirely within the trench.

In addition to the streaming pattern resolved in Fig. 8, counterrotating cells develop just outside the trench. These, as opposed to the cells within the trench, are very thin and rotate anticlockwise and clockwise on the left and right side of the trench, respectively, and are attributed mainly to the phenomenon causing the bed-shear stress amplification (described in the previous section).

The streaming pattern seen in Fig. 8 is obtained only if a detailed phase-resolved flow description is applied. Its correlation with the period-averaged sediment transport is elaborated in the following.

Period-Averaged Sediment Transport

Keeping the streaming pattern described above in mind, the time-averaged sediment transport pattern can be interpreted. In Fig. 9, the variation of the suspended (right side of figure) and the bed load (left side of figure) part of the period-averaged sediment transport is shown for different values of KC. The period-averaged transports $\overline{q}_b$ and $\overline{q}_s$ are normalized with q_{bmax} and q_{smax}, respectively (i.e., by maximum values of sediment transport found far from the trench).

The upper part of the figure shows results from a trench with steep slopes ($W/h = 5$), whereas results of the lower part of the figure are obtained with a more gently sloping trench ($W/h = 20$). Other parameters are $h/D = 0.05$, $\theta_{max} = 1$, $k_N/D = 5 \times 10^{-5}$, and $w_s/U_{max} = 0.01$.

The corresponding variation in averaged bed-shear stress is displayed in insets in Fig. 9 indicating the direction of streaming at the bed. If the forces of the flow at a given location were perfectly sinusoidal during a wave period (i.e., no streaming), then the action of gravity on the submerged weight would produce a net drift toward the bottom of the trench (Fredsøe 1978, 1979). If, on the other hand, the effect of gravity were disregarded in (6), then the streaming would cause erosion of bed load sediment. The direction of the bed load transport on the slopes is an outcome of a battle between the effect of gravity and the streaming. A sediment transport field that, in the period-averaged sense, is directed inward toward the center of the trench (i.e., opposing the direction of the period-averaged bed-shear stress) is a requisite for backfilling. If gradients in sediment transport, $d\overline{q}/dx$, are positive, then the bed is eroding; if they are negative, then sedimentation will take place [see (8)]. In the left side of Fig. 9 it is seen that gradients in the bed load transport are positive at the center of the trench for large values of KC, implying that sand in the bed load layer is removed from here (sediment is moving outward). The bed load is in phase with the bed-shear stress indicating that the gravitational force is overwhelmed by the force that the streaming exerts. While the latter is scaled with θ_{max} [see right of (5)]

$$\overline{\theta} = \theta_{max} \frac{\overline{\tau}_b}{\tau_{bmax}} \tag{11}$$

the gravity correction term is not [see (6)]. It is not surprising that streaming dictates the sediment transport considering the magnitude of θ_{max}.

For small values of KC, however, bed load sediment is attracted toward the bottom of the trench, because in this case the convective terms in (1) and (2) are small, and as a consequence streaming vanishes.

A more gently sloping trench will weaken both the streaming and the gravitational forces. Relatively speaking, the former will be reduced more than the latter, which becomes evident when lower left part of Fig. 9 is compared with upper left part. Here the period-averaged peak value on the gentle

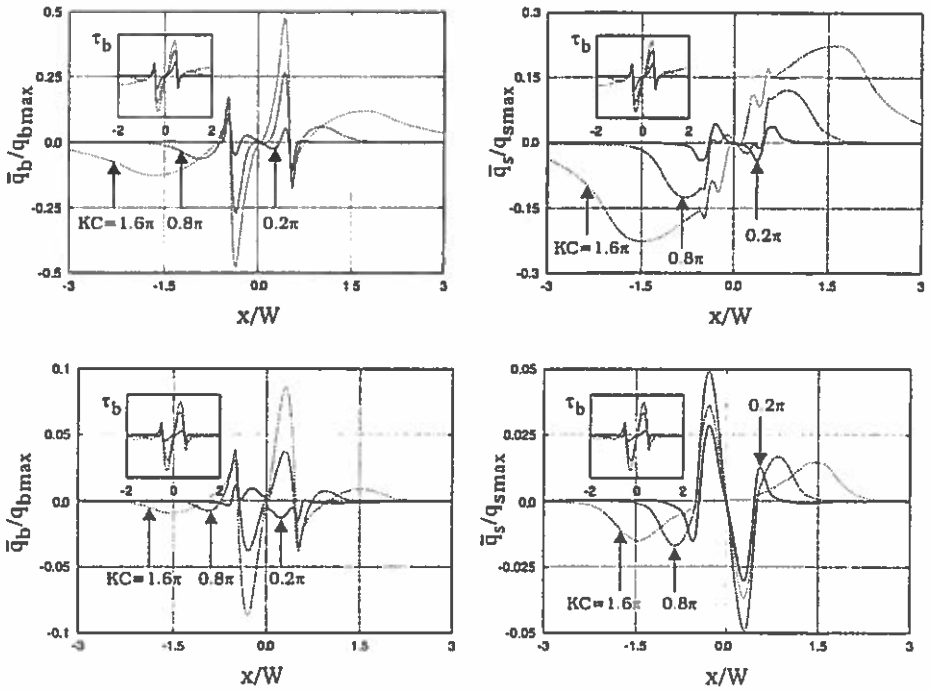

FIG. 9. Period-Averaged Bed Load and Suspended Sediment Transport over Trench for $W/h = 5$ (Upper) and $W/h = 20$ (Lower) for Three Different Keulegan-Carpenter Numbers; Insets Show Period-Averaged Bed-Shear Stress for Corresponding Values of KC; Remaining Parameters as in Fig. 5

slopes is seen to be reduced by a factor of 6 compared to that on the steep for the same value of KC.

Moreover, the effect of the bed-shear stress amplification appears as peaks in the bed load transport.

On the flat bed within a distance of an excursion length from the trenched region, the time-averaged sediment transports $\bar{q}_b$ and $\bar{q}_s$ attain values different from zero in contradiction to the case of no trenching. This is the effect of a force in addition to that of the regular oscillatory motion. It is caused by the sweeping action of the detached separation bubbles. As these rotate clockwise and anticlockwise on the left and right side, respectively, sediment will on average be departing the trench. When h/W or KC increases, $\bar{q}$ is amplified since the magnitude of $\bar{q}$ depends on the strength of the detached separation bubbles.

At deeper regions of the steep-sided trench the suspended sediment transport, $\bar{q}_s$, is directed toward the center (see the right side of Fig. 9). Hence, suspended sediment will deposit here (opposite to erosion of the slope region). For the gently sloping trench, deposition of suspended sediment is seen within the entire excavated region for all values of KC—the transport being 180° out of phase with the bed-shear stress. On the other hand, the bed load in the trench with gentle slopes is in phase. There is a tendency, however, that the force of gravity retards that of the streaming at the center, and deposition is found for small values of KC.

To sum up, sediment is attracted toward the bottom of the trench when values of KC and h/W are small, but depart the trench when large. This is worth stressing when the initial evolution of the trench morphology is to be studied. In fact, steep trenches tend to widen before actual backfilling occurs. A widening effectively reduces both the Keulegan-Carpenter number and the steepness of the trench.

Experimental Verification of Sediment Transport Pattern

Supplementary tests were conducted at the experimental facility previously described. A handful of fine sand with d = 0.20 mm was distributed on the bottom of the trench creating a starving bed situation. Initially, the trench was exposed to $KC = 0.05\pi$. The Keulegan-Carpenter number was then regularly increased with 0.05π and the layer of sand was closely observed. Each test lasted 100 periods. These observations revealed that loose sand did in fact escape the solid trench qualitatively supporting the theoretical findings concerning the tendency for trench erosion at large values of KC. For W = 100 cm this condition occurred at $KC \sim 0.9\pi$–1.1π, whereas for W = 50 cm $KC \sim 0.8\pi$–0.9π. When values of KC exceeded 1.5π the trench was self-cleansing, and particles were seen to move about more or less conjointly, while slowly drifting away from the trench indicating that streaming was present over the flat bed. Eventually, an equilibrium position was established (i.e., a position where particles would oscillate without drifting). The distance between the location of equilibrium and the trench was clearly related to the Keulegan-Carpenter number as increasing it made particles drift further away.

Initial Trapping of Sediment

For engineering purposes one of the most important outputs of the foregoing analysis is to predict how much sediment is trapped within the trench. The trapping Δ is defined here by

$$\Delta = \Delta_b + \Delta_s, \quad \Delta_b = \frac{\bar{q}_{b0} - \bar{q}_{b1}}{q_{max}}, \quad \Delta_s = \frac{\bar{q}_{s0} - \bar{q}_{s1}}{q_{max}} \qquad (12)$$

where positive values signify deposition and subscripts 0 and 1 refer to control box boundaries. In the following, sedimentation within two different control boxes is presented. The boundaries of the first box are sited at the two steepest locations of the trench, whereas boundaries of the second are sited at the two locations where the trench and flat bed adjoin.

Fig. 10(a) shows the amount of trapped suspended sediment with the Keulegan-Carpenter number for the outer control box (CB). Fig. 10(b) shows the equivalent for the inner CB. These results are obtained with $w_s/U_{max} = 0.01$ and W/h = 5, 10, and 20. In Fig. 10(c), deposition of suspended sediment with the wave-current parameter is shown for four values of KC with $W/h = 5$ and $w_s/(U_{max} + V) = 0.01$. In all three cases, h/D = 0.05, $\theta_{max} = 1$, and $k_N/D = 5 \times 10^{-5}$.

With respect to the inner control box, a maximum in deposition is found at $KC \sim 1.5$–2.5 depending on the steepness of the slopes. A maximum can occur only when two coexisting factors govern the backfilling. For small values of KC, a larger fraction of the incoming sediment can deposit due to a relatively weak separation zone. For large values, however, the separation zone and the associated level of turbulence prevails the sediment transport processes to such a degree that the amount of incoming sediment in a half-period is fully counteracted by that washed out of the trench in the preceding half-

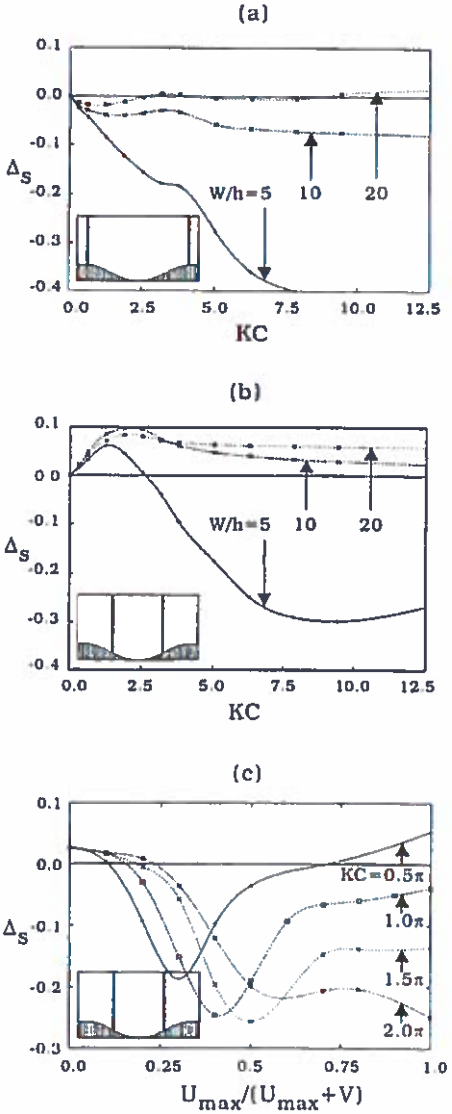

FIG. 10. Trapped Suspended Sediment with KC within: (a) Outer CB; (b) Inner CB for Three Values of W/h; and with $U_{max}/(U_{max} + V)$ within (c) Inner CB for Four Values of KC; Remaining Parameters as in Fig. 5

period. An increase in Δ_s for large values of KC is, nevertheless, observed for $W/h = 5$ [Fig. 10(b)]. This happens when the separation bubble has sufficient time during a half-period to attain a fully developed size before being ejected. For $W/h = 5$ the bubble will occupy the trench completely at the end of each half-period when $KC \sim 8-10$. As a consequence, the zone of energetic turbulence is not extended, and the flow becomes saturated with sediment causing deposition in the remainder of the half-period.

The results shown in Fig. 10(c) (wave-current case) are obtained by adding a steady pressure gradient to the driving force f_x in (4). The value of the wave-current parameter indicates the relative strength between the two components of f_x.

The relatively large negative sedimentation values found for intermediate values of the wave-current parameter are caused by a particularly strong separation bubble.

Compared with the wave-alone case, the reversal of the outer flow is postponed until very late in the wave-phase owing to the copresence of the current. As a consequence, the lee-side separation bubble in the combined wave-current flow is detained within the trench and therefore accelerated for a prolonged time. If the value of the wave-current parameter is small, the wave-related pressure gradient is correspondingly small and the acceleration of the recirculating water is weaker. Eventually, the current-alone case is attained where the separation bubble is attached to the trench acquiring a fully developed size. As a consequence of a stationary separation bubble, deposition increases and becomes positive.

If the amount of trapped suspended sediment from the two control boxes in Figs. 10(a and b) is subtracted, then the sedimentation budget of the upper part of the trench slopes is obtained. In all calculations performed, the subtraction gave negative values implying that the width of the trench increases with time. The dislodgment of sand from the inner CB (see, e.g., $W/h = 5$ in Fig. 10) therefore happens simultaneously with the self-widening. This is important since a widening involves a decrease in h/W and in KC. According to Fig. 10, these modulations will dampen the erosional processes responsible for the negative sedimentation budget. In the initial stage, the morphology may therefore, under certain conditions, undergo a period of transition after which the actual deterioration of the trench commences.

By splitting up the instantaneous velocity [i.e., $u(x, y, t)$] into a period-averaged [$\overline{U}(x, y)$] and an unsteady [$u'(x, y, t)$] component the flow can be regarded as being composed of steady flow (i.e., the streaming) and pure wave motion. The same splitting procedure can be applied to the concentration field [$c(x, y, t) = \overline{C}(x, y) + c'(x, y, t)$]. Hereby, the period-averaged suspended sediment transport that is found from the depth-integrated value of $\overline{uc}$ is composed by two terms; namely, the depth-integrated values of $\overline{UC}$ *and* $\overline{u'c'}$. If the backfilling definition [see (12)] is utilized on each of these components

$$\Delta_s = \Delta_{\overline{UC}} + \Delta_{\overline{u'c'}} \tag{13}$$

the contribution to backfilling from streaming and pure wave motion can be estimated separately. The latter resembles the solution obtained from solving the linearized equations of motion. If this decomposition is applied on results presented in Fig. 10(b), the curves shown in Fig. 11 are obtained. For comparison, results obtained by actually omitting the convective terms of (1) and (2) and keeping all other things equal have been included.

Even for mildly sloping trenches, the effect of streaming is appreciable. On the other hand, $\Delta_{\overline{u'c'}}$ is seen to be positive and constant when a is larger than $\sim W/2$, which is in agreement with the results of the impaired flow model. This is to be expected since suspended sediment encounters the maximum

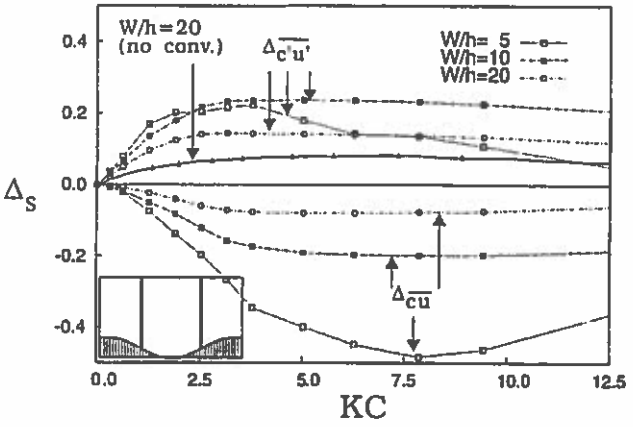

FIG. 11. Backfilling Results Shown in Fig. 10(b) Decomposed into Contributions from Steady Part (Streaming) and Unsteady Part (Pure Wave Motion)

change in depth and therefore in carrying capacity when $KC > \pi$. The difference in magnitude is attributed to the amplification effect. Consequently, models that neglect streaming (i.e., convective terms of the equations of motion) underestimate the timescale of backfilling for smaller values of KC and, more seriously, overestimate for larger values of it.

Morphology of Trenches Exposed to Waves

From a phenomenological point of view $\Delta_{\overline{UC}}$ cannot continue to be greater than $\Delta_{\overline{u'c'}}$ if the trench morphology is able to adjust to the forces of the flow. The widening of the trench explained why $\Delta_{\overline{u'c'}}$ eventually becomes the larger term. To support this explanation a simulation of the evolution of the trench morphology is made using the following parameters: $W/h = 5$, $h/D = 0.05$, $\theta_{max} = 1$, $KC = 2\pi$, $k_N/D = 5 \times 10^{-5}$, and $w_s/U_{max} = 0.01$. In Fig. 12 the evolution is shown with a time-space surface plot with projected bed elevations on the base plate.

In the initial stage, the trench widens rapidly, and eroded sand from within it is deposited on the flat bed forming two distinctive shoals. For a while the trench is self-deepening causing a 10% increase in excavated depth. Only at a later stage (i.e., $tU_{max}/D > 150$) is the actual deterioration of the trench initiated. A rough estimate of the timescale of backfilling is ~500 based on the assumption that the distance between

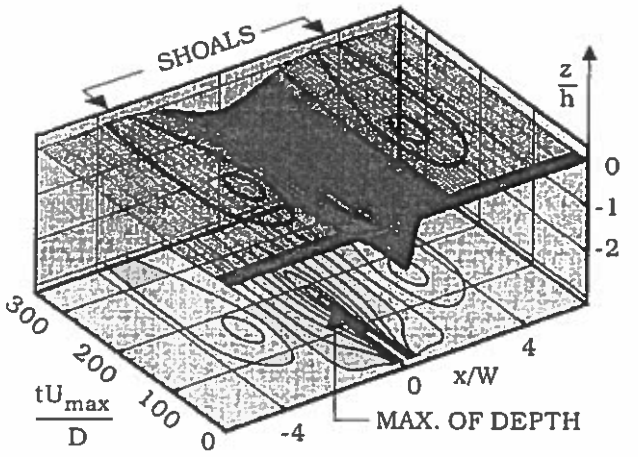

FIG. 12. Morphological Evolution of Trench Exposed to Waves with $KC = 2\pi$, Remaining Parameters (Based on Initial Profile of Trench) as in Fig. 5

the center of gravity of the trench and the bed level outside the excavated region decays exponentially after $tU_{max}/D > 150$.

CONCLUSIONS

A detailed description of oscillatory flow resembling that induced by waves has been applied to study the sediment transport pattern and the evolution of trench morphology. The dynamical flow field is marked by coherent vortices originally born as separation bubbles. Resolving these is a requisite for reliable predictions of backfilling rates of small-scale excavations (e.g., pipeline trenches). The flow model has been validated against experiments conducted in a U-tube facility, and good agreement was found. The intraperiod description showed that sediment, carried by the flow toward the trench from shifting sides of it every half-period, is trapped by the energetic turbulence associated with regions of separated flow. It has been shown that the separation bubble, which is washed away when the flow reverses, is capable of accumulating sediment to such a degree that sedimentation is delayed and prevented in the initial stage of steep slopes. The outcome of a detailed flow description is that streaming comes into existence when period-averaging the flow field. The streaming acts upon the bed in a manner that obstructs sedimentation. Before the actual filling mechanisms can dominate, a modulation of the trench morphology involving both self-widening and self-deepening can take place due to the overwhelming impact of streaming. The strength of streaming in which the Keulegan-Carpenter number and the steepness parameter are decisive explains associated negative sedimentation budgets. As a consequence of self-widening, a gradual decrease in the strength of streaming and therefore in erosional processes takes place. This was made evident not only by curves of initial trapping but also by a full morphological simulation.

ACKNOWLEDGMENTS

Assistance in the execution of experimental work provided by Sanne Niemann and valuable comments by Erik Østergaard Madsen are highly appreciated. This work is supported by "Numerical and Experimental Fluid Mechanics" funded by the Danish Technical Research Council (STVF).

REFERENCES

Alfrink, B. J., and van Rijn, L. C. (1983). "Two-equation turbulence model for flow over trenches." *J. Hydr. Engrg.*, ASCE, 109(7), 941–958.

Bijker, E. W. (1980). "Sedimentation in channels and trenches." *Proc., 17th Coast. Engrg. Conf.*, Vol. II, ASCE, New York, 1708–1718.

Engelund, F., and Fredsøe, J. (1976). "A sediment transport model for straight alluvial channels." *Nordic Hydrology*, Copenhagen, 7, 293–306.

Engelund, F., and Fredsøe, J. (1982). "Hydraulic theory of alluvial rivers." *Adv. in Hydrosci.*, 13, 187–215.

Engelund, F., and Hansen, E. (1972). *A monograph on sediment transport in alluvial streams*, 3rd Ed., Technical Press, Copenhagen.

Fredsøe, J. (1978). "Sedimentation of river navigation channels." *J. Hydr. Div.*, ASCE, 104(2), 223–236.

Fredsøe, J. (1979). "Natural backfilling of pipeline trenches." *J. Petr. Technol.*, 31, 1223–1230.

Fredsøe, J., and Deigaard, R. (1986). "The state of the art of predicting natural backfilling of sand in navigation channels." *Proc., 11th World Dredging Conf.*, CEDA, Delft, The Netherlands, 49–68.

Jensen, B. L., Sumer, B. M., and Fredsøe, J. (1989). "Turbulent oscillatory boundary layers at high Reynolds numbers." *J. Fluid Mech.*, Cambridge, U.K., 206, 265–297.

Jensen, J. H., Madsen, E. Ø., and Fredsøe, J. (1999). "Oblique flow over dredged channels. II: Sediment transport and morphology." *J. Hydr. Engrg.*, ASCE, 125(11), 1190–1198.

Kobayashi, N. (1982). "Sediment transport on a gentle slope due to waves." *J. Wtrwy., Port, Coast., and Oc. Div.*, ASCE, 108(3), 254–271.

Launder, B. E., and Spalding, D. B. (1974). "The numerical computation of turbulent flows." *Comp. Methods Appl. Mech. Engrg.*, 3, 269–289.

Leonard, B. P. (1979). "A stable and accurate convective modelling procedure based on quadratic upstream interpolation." *Comp. Methods Appl. Mech. Engrg.*, 19, 59–98.

Longuet-Higgins, M. S. (1953). "Mass transport in water waves." *Philosophical Trans. Royal Soc.*, London, 245, 535–581.

Mayor-Mora, R., Mortensen, P., and Fredsøe, J. (1976). "Sedimentation studies of the Niger River delta." *Proc., 15th Coast. Engrg. Conf.*, Vol. II, ASCE, New York, 2151–2169.

Patankar, S. V. (1980). *Numerical heat transfer and fluid flows*, Hemisphere, New York.

Schlichting, H. (1968). *Boundary layer theory*, 6th Ed., McGraw-Hill, New York.

Tjerry, S. (1995). "Morphological calculation of dunes in alluvial rivers." PhD thesis, Inst. of Hydrodyn. and Water Resour. (ISVA), Technical University of Denmark, Lyngby, Denmark.

van Rijn, L. C. (1986). "Sedimentation of dredged channels by currents and waves." *J. Wtrwy., Port, Coast., and Oc. Engrg.*, ASCE, 112(5), 541–559.

NOTATION

The following symbols are used in this paper:

a = amplitude of oscillation;
c = concentration of suspended sediment;
D = water depth outside trench;
d = grain diameter;
f_x = volume force;
g = acceleration of gravity;
h = excavated depth;
KC = Keulegan-Carpenter number;
k = turbulent kinetic energy;
k_N = Nikuradse roughness;
n = porosity of sand;
p = pressure;
q = sediment transport;
q_b = bed load transport;
q_s = suspended sediment transport;
s = relative density of sand;
T = wave period;
t = time;
U = potential flow velocity;
u = horizontal velocity;
v = vertical velocity;
x = horizontal coordinate;
y = vertical coordinate;
W = width of trench;
w_s = fall velocity of mean grain diameter in suspension;
z = bed elevation;
Δ = sedimentation;
$\Delta\phi$ = difference between time of onset of separation within and outside trench;
ε = dissipation rate of turbulent kinetic energy;
θ = Shields parameter;
θ_c = critical Shields parameter;
θ_{co} = critical Shields parameter on plane bed;
μ_s = static friction coefficient;
ν_T = eddy viscosity;
ρ = density of water; and
τ_b = bed-shear stress.

Subscripts

max = maximum of quantity outside excavated region.

OBLIQUE FLOW OVER DREDGED CHANNELS. I: FLOW DESCRIPTION

By Jacob Hjelmager Jensen,[1] Erik Østergaard Madsen,[2] and Jørgen Fredsøe[3]

ABSTRACT: A 3D investigation of flow across long, straight channels aligned obliquely to the flow direction has been conducted. The applied mathematical model solves the Reynolds-averaged Navier-Stokes equations using a k-ε model for turbulence closure in a curvilinear coordinate system. The uniformity along the channel alignment allows the three momentum equations to be solved in a 2D computational domain. With respect to a steady current entering a channel obliquely, two important flow features arise: (1) The flow will be refracted in the direction of the channel alignment, which may be described by depth-averaged models; and (2) a secondary flow will be introduced due to shear in the velocity profile. This can only be described using a 3D approach. The secondary flow will cause a horizontal deflection of streamlines over the vertical. Only by capturing the 3D flow behavior can the direction and magnitude of the bed shear stress be well modeled. When crossing a channel obliquely, the flow is gradually accelerated in the direction of the channel alignment. Results of the numerical flow model are compared with existing experimental data and good agreement is found.

INTRODUCTION

Predicting the natural backfilling of dredged channels is a problem often encountered in engineering practice. Backfilling occurs both when the sediment transport capacity is less within the channel than outside (Fredsøe 1979; Alfrink and van Rijn 1983) and when bed load particles move on a sloping bed affected by the action of gravity (Fredsøe 1978). The backfilling of dredged channels is predicted successfully only if a detailed description of the flow and sediment transport processes is applied. This paper will focus on the detailed flow behavior, whereas Part II (Jensen et al. 1999)—a continuation of the present investigation—will focus on the sediment transport processes.

Over the last decades several investigations concerned with the steady flow and sediment transport processes across dredged channels have been reported including the work by Fredsøe (1978, 1979), Bijker (1980), Koutitas and O'Connor (1981), Alfrink and van Rijn (1983), van Rijn (1986, 1987), and Basara and Younis (1995). Koutitas and O'Connor (1981) used a simple one-equation turbulence model and the assumption of hydrostatic pressure distribution to investigate the flow over channels aligned perpendicularly to the flow direction. The flow direction was improved significantly by Alfrink and van Rijn (1983) who introduced a k-ε turbulence model to solve the full 2D problem. Basara and Younis (1995) used second-order schemes for the turbulence closure. Basara and Younis (1995) concluded that the second-order closure improved the flow description to some extent as compared with the k-ε model (first-order closure) but not to the extent that would justify a practical application.

Boer (1985) studied flow over oblique channels extensively both experimentally and numerically by applying various 2DH (horizontal, depth-averaged) flow models of increasing complexity. van Rijn (1987) used a quasi-3D flow model, assuming hydrostatic pressure distribution and logarithmic velocity profiles of horizontal flow. The profile of vertical velocity was obtained through the equation of continuity. The purpose of the present paper is to study a steady current crossing a long, straight channel obliquely by the use of a detailed 3D mathematical model. An experimental investigation of flow over oblique channels was conducted at the Hydraulics Research Station (HRS Wallingford 1973) and will serve as a test for model verification in this paper. As the current enters the channel obliquely it will refract in the direction of the channel alignment. The current refraction is caused by the positive pressure gradient confronting the flow as it enters the channel. The current refraction varies over the depth, and the flow field, which is unidirectional far upstream and downstream of the channel, becomes 3D. The majority of numerical flow models applied in studies concerned with navigation channels has, however, been 2DH models. To predict the detailed flow behavior and the direction and magnitude of the bed-shear stress in particular, a 3D flow description is necessary. The 3D model presented in this paper is built on the assumption of uniformity in one of the three directions—for the present application the alignment of the dredged channel. In flow problems with the above-mentioned characteristic the velocity vectors are generally 3D; however, the solution may be obtained on a 2D grid due to the uniformity. Consequently, the number of computational grid points are heavily reduced compared with the number required in 3D models based on a 3D grid.

DEPTH-AVERAGED FLOW DESCRIPTION

Based on depth-averaged considerations, the following section briefly discusses the physics behind the steady-state flow pattern of a current obliquely crossing a long, straight channel.

In a Cartesian coordinate system the depth-averaged steady-state equations of motion and the depth-averaged equation of continuity read

$$\rho D\frac{du}{dt}=\rho D\left(u\frac{\partial u}{\partial x}+w\frac{\partial u}{\partial z}\right)=-D\frac{\partial p}{\partial x}-\tau_{bx}+\frac{\partial T_{xx}}{\partial x}+\frac{\partial T_{xz}}{\partial z} \quad (1)$$

$$\rho D\frac{dw}{dt}=\rho D\left(u\frac{\partial w}{\partial x}+w\frac{\partial w}{\partial z}\right)=-D\frac{\partial p}{\partial z}-\tau_{bz}+\frac{\partial T_{zz}}{\partial z}+\frac{\partial T_{xz}}{\partial x} \quad (2)$$

$$\frac{\partial(Du)}{\partial x}+\frac{\partial(Dw)}{\partial z}=0 \quad (3)$$

where u and w = horizontal depth-averaged velocity components in the x- and z-directions, respectively; ρ = water density; D = water depth; t = time; p = pressure; τ_{bx} and τ_{bz} = bed-shear stress in the x- and z-directions, respectively; and T_{xx}, T_{xz}, T_{zz} = stress components responding to gradients in the horizontal depth-averaged velocity field.

The topography of long, straight channels is uniform in the

[1]PhD, Inst. of Hydrodynamics and Water Resour., Tech. Univ. of Denmark, DK-2800 Lyngby, Denmark; currently, Danish Hydr. Inst., Agern Allé 5, DK-2970 Hørsholm, Denmark.

[2]PhD student, Inst. of Hydrodynamics and Water Resour., Tech. Univ. of Denmark, DK-2800 Lyngby, Denmark.

[3]Prof., Inst. of Hydrodynamics and Water Resour., Tech. Univ. of Denmark, DK-2800 Lyngby, Denmark.

Note. Discussion open until April 1, 2000. Separate discussions should be submitted for the individual papers in this symposium. To extend the closing date one month, a written request must be filed with the ASCE Manager of Journals. The manuscript for this paper was submitted for review and possible publication on September 9, 1998. This paper is part of the *Journal of Hydraulic Engineering*, Vol. 125, No. 11, November, 1999. ©ASCE, ISSN 0733-9429/99/0011-1181–1189/$8.00 + $.50 per page. Paper No. 19192.

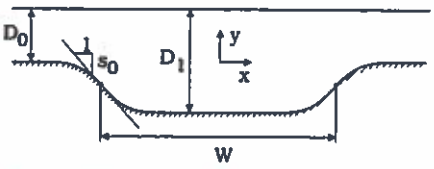

FIG. 1. Definition Sketch of Channel Parameters

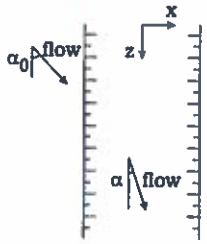

FIG. 2. Definition of Flow Angles

direction of the channel alignment; thus the z-dependency of (1–3) [except for the driving force term $\partial p/\partial z$ in (2)] can be eliminated if the z-axis is chosen parallel to this direction. This direction is termed the longitudinal direction.

In Fig. 1, a definition sketch of the parameters is shown. The geometry of the channel, excavated in an otherwise plane bed, is simply described by sinusoidally shaped slopes, which are adjoined by a plane part of the channel as shown in Fig. 1. The channel width W is defined as the distance between the center of the upstream slope and the center of the downstream slope. Moreover, s_0 is the symbol for the maximum steepness of the slope. The water depth upstream of the channel is denoted D_0, whereas D_1 is the water depth within the channel. The angle of attack of the flow, also referred to as the inlet angle, is denoted α_0, whereas α is the local depth-averaged angle of the flow within the channel (Fig. 2).

The flow attacking a channel obliquely may be divided into the following three distinctive cases characterized by the inlet angle α_0:

1. The current direction is parallel to the channel alignment, $\alpha_0 = 0°$.
2. The current direction is perpendicular to the channel alignment, $\alpha_0 = 90°$.
3. The current attacks the channel at an angle within the interval $0° < \alpha_0 < 90°$.

To give an explanation of the underlying physics, Cases 1 and 2 are considered in terms of the depth-averaged velocities u (the cross-channel component) and w (the longitudinal component). The combination of these two 2D cases can partly explain the refraction pattern in the general case (i.e., Case 3). The development of flow attacking an infinitely wide channel obliquely (Case 4) is treated subsequently.

Case 1: Current Parallel to Channel Alignment

When the current is parallel to the channel alignment (Fig. 3), the depth-averaged velocity within the channel w_1 exceeds the depth-averaged velocity outside the channel w_0, which can be explained in the following.

From geometrical considerations, the longitudinal pressure gradient $\partial p/\partial z$ can be shown to be constant across the channel. Therefore, as the driving force equals the local water depth times the longitudinal pressure gradient, a larger flux of water will be driven in the deeper sections. An estimate of the relative increase in the longitudinal depth-averaged velocity in the center of the channel w_1/w_0 is obtained assuming that the bed-shear stress τ_{bz} balances the driving force

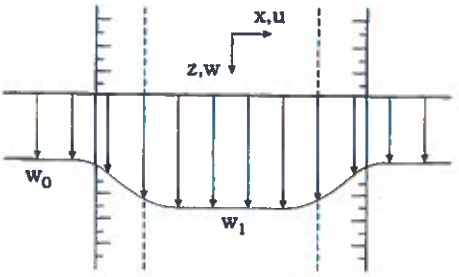

FIG. 3. Depth-Averaged Velocity Profile for Flow Parallel to Channel

$$\tau_{bz} = -D\frac{\partial p}{\partial z} \tag{4}$$

Applying (4) on the outside and within the channel, the following relation is found:

$$\frac{\tau_{bz0}}{\tau_{bz1}} = \frac{D_0}{D_1} \tag{5}$$

where subscript 0 refers to the value of a variable upstream of the channel; and subscript 1 refers to the maximum value of a variable within the channel. By further adopting the Colebrook-White friction formula

$$\frac{1}{C_f} = \frac{V_f}{V} = \frac{1}{6.1 - 2.5\ln\left(\frac{k_N}{D}\right)} \tag{6}$$

where V = depth-averaged total velocity, the following relation is obtained:

$$\frac{w_1}{w_0} = \frac{C_{f1}}{C_{f0}}\sqrt{\frac{D_1}{D_0}} \tag{7}$$

noting that $V\ (=\sqrt{u^2 + w^2})$ reduces to $V = w$ in the case of a current being parallel to the channel alignment. In (6) C_f = friction formula coefficient; k_N = Nikuradse bed roughness; and V_f = friction velocity found from $V_f = \sqrt{|\tau_b|/\rho}$, where τ_b = bed-shear stress. This shows that the inside channel velocities increase proportionally to the square root of the expansion in depth, neglecting small variations in C_f with depth.

Case 2: Current Perpendicular to Channel Alignment

In this case, the depth-averaged continuity constraint leads to

$$\frac{u_1}{u_0} = \frac{D_0}{D_1} \tag{8}$$

from which it is easily seen that the cross-channel depth-averaged velocity within the channel is inversely proportional to the expansion in depth. The bed-shear stress in the channel is therefore always reduced compared with that in the undisturbed flow.

Case 3: Obliquely Attacking Current

In this case, an interaction of the above described effects of a depth expansion will occur. With the z-axis aligned along the trace of the channel, then $\partial(Dw)/\partial z = 0$ [see (3)] implying that (8) remains valid for a current attacking obliquely as well as perpendicularly.

The refraction of the depth-averaged velocity is caused partly by the decrease in the u-component and partly by increase in the w-component. When the flow crosses the upstream slope, it will turn corresponding to the decrease in the u-component. In contrast, the acceleration of the w-component

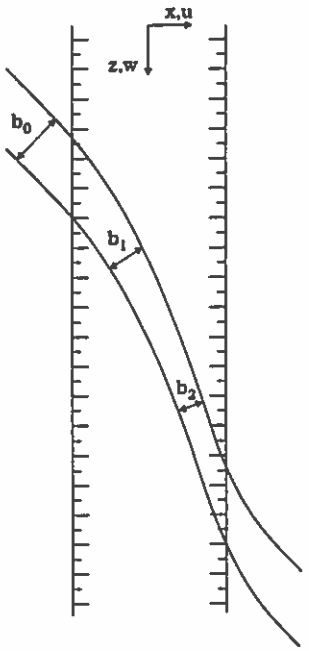

FIG. 4. Depth-Averaged Refraction Pattern

is a slow process that gradually refracts the current further toward the channel alignment.

The depth-averaged streamlines will behave as sketched in Fig. 4. As seen from Fig. 4 the horizontal distance between two streamlines of the depth-averaged flow decreases within the channel as a consequence of the refraction. If the equation of continuity is applied between two streamlines upstream of the channel and between the same two streamlines at a point within the channel, the following relation is obtained:

$$\frac{V_1}{V_0} = \frac{b_0}{b_1}\frac{D_0}{D_1} \tag{9}$$

where b_0 and b_1 = widths between streamlines outside and within the channel, respectively. Note that if b_0/b_1 is larger than the depth ratio D_1/D_0, the total velocity within the channel exceeds the upstream total velocity.

Case 4: Obliquely Attacking Current over Channels of Infinite Width

The total velocity V_{eq} and the corresponding flow angle α_{eq} for the fully developed flow inside a channel of infinite width are evaluated in the following. At the end of this section the development of the longitudinal velocity component w in an infinitely wide channel is studied. This is done because the development in w is a rather slow process. As a result, only channels that are very wide will experience flow that become fully developed prior to its arrival at the downstream slope. If (2) is applied upstream of and within the channel, the following is obtained:

$$\tau_{bz0} = \tau_{b0}\cos(\alpha_0) = -D_0\frac{\partial p}{\partial z} \tag{10a}$$

$$\tau_{bzeq} = \tau_{beq}\cos(\alpha_{eq}) = -D_1\frac{\partial p}{\partial z} \tag{10b}$$

where τ_{b0} and τ_{beq} = total bed-shear stresses upstream of and within the channel, respectively—the latter being valid when the bed-shear stress attains its value for the fully developed flow at some point downstream. By dividing (10*b*) by (10*a*) the following relation is found:

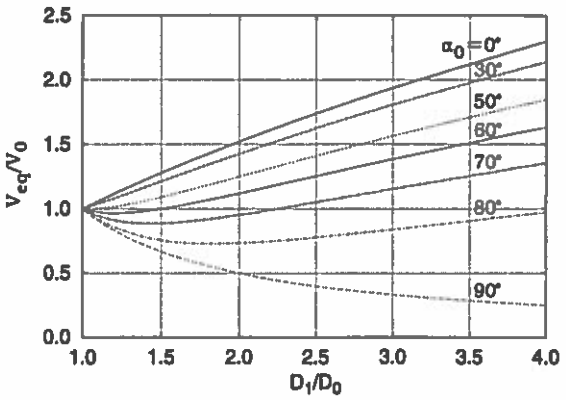

FIG. 5. Fully Developed Depth-Averaged Velocity Inside Channel Relative to Corresponding Inlet Value [Eq. (12)]. k_N/D_0 = 0.0001

$$\frac{\tau_{beq}\cos(\alpha_{eq})}{\tau_{b0}\cos(\alpha_0)} = \frac{D_1}{D_0} \tag{10c}$$

Combining (10*c*) with (6) and (8) gives an analytical expression for the total velocity inside the channel and the corresponding flow angle

$$\cos(\alpha_{eq}) = \sqrt{\left(\frac{1}{2}\left(\frac{C_{f0}}{C_{f1}}\right)^2\left(\frac{D_0}{D_1}\right)^3\frac{\sin^2(\alpha_0)}{\cos(\alpha_0)}\right)^2 + 1} - \frac{1}{2}\left(\frac{C_{f0}}{C_{f1}}\right)^2\left(\frac{D_0}{D_1}\right)^3\frac{\sin^2(\alpha_0)}{\cos(\alpha_0)} \tag{11}$$

$$\frac{V_{eq}}{V_0} = \frac{D_0}{D_1}\frac{\sin(\alpha_0)}{\sin(\alpha_{eq})} \tag{12}$$

In Boer (1985), a set of equations resembling (11) and (12) is presented. However, in the present case (11) and (12) are derived with only the mathematical assumption that the Colebrook-White friction formula [(6)] is valid. Eq. (12) is depicted in Fig. 5.

The fully developed depth-averaged velocity within the channel most likely exceeds the corresponding inlet value if the expansion in depth is large and the inlet angle is small. For $\alpha_0 = 90°$ and 0° the total velocity decreases and increases, respectively, regardless of the expansion in depth. For an intermediate inlet angle, the total velocity is seen first to decrease whereupon it increases with the expansion in depth. This is caused by an interaction of the two limiting cases demonstrated in preceding sections. The continuity constraint on the cross-channel velocity will dominate the total velocity for relatively small expansions and large inlet angles, whereas the accelerated longitudinal velocity will dominate for relatively large expansions and small inlet angles.

To emphasize how slow the development of the longitudinal velocity component is, the timescale for the process is evaluated in the following. The nondimensional depth-averaged momentum equation for w [see (2)] can be written as follows:

$$\tilde{D}\frac{d\tilde{w}}{d\tilde{t}} = -\tilde{\tau}_{bz} - \tilde{D}\frac{d\tilde{p}}{d\tilde{z}} \tag{13}$$

using D_0 and V_0 as dimensional scales such that $\tilde{D} = D/D_0$, $\tilde{w} = w/V_0$, $\tilde{t} = tV_0/D_0$, $\tilde{\tau}_{bz} = \tau_{bz}/(\rho V_0^2)$, $\tilde{p} = p/(\rho V_0^2)$, and $\tilde{z} = z/D_0$. If V/V_f is taken to be constant (and equal to C_{f1}) $\tilde{\tau}_{bz}$ reads

$$\tilde{\tau}_{bz} = \frac{\tau_{bz}}{\rho V_0^2} = \frac{\tilde{w}\tilde{V}}{C_{f1}^2} = \frac{\tilde{w}\sqrt{\tilde{w}^2 + \tilde{u}^2}}{C_{f1}^2} = \frac{\tilde{w}^2\sqrt{1 + \tan^2(\alpha)}}{C_{f1}^2} \tag{14}$$

whereas $d\tilde{p}/d\tilde{z}$ can be found upstream

$$\frac{d\tilde{p}}{d\tilde{z}} = -\tilde{\tau}_{bz0}\cos(\alpha_0) = -\frac{\cos(\alpha_0)}{C_{f0}^2} \tag{15}$$

Eq. (13) can be solved analytically if the variation in $\tan(\alpha)$ across the channel as an approximation is neglected. Later, it will be shown that this approximation gives very good results compared with the full numerical solution. The analytical solution of (13) now becomes

$$\tilde{t} = \frac{1}{2\sqrt{ae}} \ln\left(\frac{\sqrt{\frac{a}{e}} + \tilde{w}}{\sqrt{\frac{a}{e}} - \tilde{w}}\right) \tag{16}$$

where $a = \cos(\alpha_0)/C_{f0}^2$; and $e = D_0/(D_1 C_{f1}^2)\sqrt{1 + \tan^2(\alpha)}$.

An upper estimate of $\tan(\alpha)$ in (16) is obtained as follows. Just inside the channel u is reduced from u_0 to u_1 due to continuity, whereas w equals w_0 as it takes a while to accelerate the longitudinal flow. Hereby

$$\tan(\alpha) = \frac{u_1}{w_0} = \frac{u_1}{u_0}\frac{u_0}{w_0} = \frac{u_1}{u_0}\tan(\alpha_0) \tag{17}$$

By inserting the upper estimate of $\tan(\alpha)$ given in (17) into (14) it is seen that the timescale is being overestimated because the friction is overestimated. On the other hand, if $\tan(\alpha) = \tan(\alpha_{eq})$ is taken as a lower estimate, the friction is estimated too small and the timescale becomes underestimated. Therefore, the correct solution to (13) lies in the interval between the two estimates.

In its given form, (16) gives the nondimensional time it takes to accelerate the nondimensional longitudinal velocity from 0 to $\tilde{w}$. Consequently, the time ΔT required to accelerate $\tilde{w}$ from the upstream value to, say, 95% of the inside channel equilibrium value for uniform flow is found as $\Delta T = \tilde{t}(0.95\tilde{w}_{eq}) - \tilde{t}(\tilde{w}_0)$. If a central estimate for $\tan(\alpha)$ is used in (16), then $\Delta T \approx 1{,}500$ for the situation where $k_N/D_0 = 0.001$, $\alpha_0 = 45°$, and $D_1/D_0 = 2$. This corresponds to a distance in the cross-channel direction of $L = \Delta T D_0^2/D_1 \sin(\alpha_0) = 530 D_0$. The above findings show that the oblique flow crossing channels of dimensions typical for navigation channels will continue to accelerate over the entire channel stretch unless the upstream flow angle is very small.

The solution to (13) in terms of $\tilde{w}(\tilde{x})$ can be found by introducing $\tilde{x}(=x/D_0)$ as the nondimensional cross-channel coordinate. The cross-channel coordinate $\tilde{x}$ is measured from the lowest point on the slope, and $\tilde{x}$ and $\tilde{t}$ are related through the nondimensional depth-averaged transverse velocity

$$\tilde{t} = \frac{\tilde{x}}{\tilde{u}_1}, \quad \tilde{u}_1 = \frac{u_1}{V_0} = \frac{u_0}{V_0}\frac{D_0}{D_1} = \frac{D_0}{D_1}\sin(\alpha_0) \tag{18}$$

If (18) is inserted into (16) and $\tilde{w}$ is isolated, the acceleration of the nondimensional longitudinal depth-averaged velocity with $\tilde{x}$ is found

$$\tilde{w}(\tilde{x}) = \sqrt{\frac{a}{e}}\frac{\exp(a_2\tilde{x}) - 1}{\exp(a_2\tilde{x}) + 1} \tag{19}$$

where $a_2 = 2\sqrt{ae}D_1/(D_0 \sin(\alpha_0))$.

3D FLOW DESCRIPTION

The 2D depth-averaged flow pattern has been analyzed above. This section takes the analysis one step further and describes the full 3D flow problem, which is solved numerically assuming that the flow is uniform in the direction parallel to the alignment of the channel. The purpose of using a 3D description is to investigate the effect of the shear in the incoming flow on the near-bed flow angles. In addition to the current refraction of the depth-averaged velocity, a secondary flow pattern is induced when the flow enters the navigational channel obliquely. This is important in relation to the magnitude and direction of the bed-shear stress. A well-modeled magnitude and direction of the bed-shear stress are crucial for an accurate prediction of the sediment transport [see Part II (Jensen et al. 1999)]. The presence of a secondary flow pattern is caused by nonequilibrium between the pressure gradient and the centrifugal forces. The nonequilibrium is caused by the nonuniform distribution of the latter forces owing to the vertical variation in the incoming flow velocity. In river bends, this imbalance is known to cause the so-called helical motions [see, e.g., Rozovskii (1961) or Engelund (1974)].

In a Cartesian coordinate system the three equations of motion and the continuity equation read:

$$u\frac{\partial u}{\partial x} + v\frac{\partial u}{\partial y} + w\frac{\partial u}{\partial z} = -\frac{1}{\rho}\frac{\partial p}{\partial x} + \frac{\partial}{\partial x}\left(\nu_T\frac{\partial u}{\partial x}\right) + \frac{\partial}{\partial y}\left(\nu_T\frac{\partial u}{\partial y}\right) + \frac{\partial}{\partial z}\left(\nu_T\frac{\partial u}{\partial z}\right) \tag{20}$$

$$u\frac{\partial v}{\partial x} + v\frac{\partial v}{\partial y} + w\frac{\partial v}{\partial z} = -\frac{1}{\rho}\frac{\partial p}{\partial y} + \frac{\partial}{\partial x}\left(\nu_T\frac{\partial v}{\partial x}\right) + \frac{\partial}{\partial y}\left(\nu_T\frac{\partial v}{\partial y}\right) + \frac{\partial}{\partial z}\left(\nu_T\frac{\partial v}{\partial z}\right) \tag{21}$$

$$u\frac{\partial w}{\partial x} + v\frac{\partial w}{\partial y} + w\frac{\partial w}{\partial z} = -\frac{1}{\rho}\frac{\partial p}{\partial z} + \frac{\partial}{\partial x}\left(\nu_T\frac{\partial w}{\partial x}\right) + \frac{\partial}{\partial y}\left(\nu_T\frac{\partial w}{\partial y}\right) + \frac{\partial}{\partial z}\left(\nu_T\frac{\partial w}{\partial z}\right) \tag{22}$$

$$\frac{\partial u}{\partial x} + \frac{\partial v}{\partial y} + \frac{\partial w}{\partial z} = 0 \tag{23}$$

where v = vertical velocity component in the y-direction; and ν_T = eddy viscosity. The two horizontal velocity components, u and w, and the flowangle α, now depend on y as well as x. Although only steady-state flow problems are considered in this paper, the full time-dependent flow equations have been solved. The transient time is, however, of no interest for the present investigation; thus the dynamic term of the governing momentum equations has been omitted.

Because of the uniformity in the z-direction, (20)–(22) are reduced to

$$u\frac{\partial u}{\partial x} + v\frac{\partial u}{\partial y} = -\frac{1}{\rho}\frac{\partial p}{\partial x} + \frac{\partial}{\partial x}\left(\nu_T\frac{\partial u}{\partial x}\right) + \frac{\partial}{\partial y}\left(\nu_T\frac{\partial u}{\partial y}\right) \tag{24}$$

$$u\frac{\partial v}{\partial x} + v\frac{\partial v}{\partial y} = -\frac{1}{\rho}\frac{\partial p}{\partial y} + \frac{\partial}{\partial x}\left(\nu_T\frac{\partial v}{\partial x}\right) + \frac{\partial}{\partial y}\left(\nu_T\frac{\partial v}{\partial y}\right) \tag{25}$$

$$u\frac{\partial w}{\partial x} + v\frac{\partial w}{\partial y} = -\frac{1}{\rho}\frac{\partial p}{\partial z} + \frac{\partial}{\partial x}\left(\nu_T\frac{\partial w}{\partial x}\right) + \frac{\partial}{\partial y}\left(\nu_T\frac{\partial w}{\partial y}\right) \tag{26}$$

and the equation of continuity becomes

$$\frac{\partial u}{\partial x} + \frac{\partial v}{\partial y} = 0 \tag{27}$$

The uniformity in the z-direction implies that the velocity w in the z-direction only influences the two other velocity components in virtue of its contribution to ν_T, which is calculated by the use of a k-ε turbulence model. The differential equations for the turbulent quantities k (the turbulent kinetic energy) and ε (the dissipation of turbulent kinetic energy) read (again assuming uniformity in the z-direction)

$$u\frac{\partial k}{\partial x} + v\frac{\partial k}{\partial y} = \frac{\partial}{\partial x}\left(\frac{\nu_T}{\sigma_k}\frac{\partial k}{\partial x}\right) + \frac{\partial}{\partial y}\left(\frac{\nu_T}{\sigma_k}\frac{\partial k}{\partial y}\right) + \nu_T\left(2\left(\frac{\partial u}{\partial x}\right)^2 + 2\left(\frac{\partial v}{\partial y}\right)^2 + \left(\frac{\partial u}{\partial y} + \frac{\partial v}{\partial x}\right)^2 + \left(\frac{\partial w}{\partial x}\right)^2 + \left(\frac{\partial w}{\partial y}\right)^2\right) - \varepsilon \tag{28}$$

$$u\frac{\partial \varepsilon}{\partial x}+v\frac{\partial \varepsilon}{\partial y}=\frac{\partial}{\partial x}\left(\frac{\nu_T}{\sigma_\varepsilon}\frac{\partial \varepsilon}{\partial x}\right)+\frac{\partial}{\partial y}\left(\frac{\nu_T}{\sigma_\varepsilon}\frac{\partial \varepsilon}{\partial y}\right)+C_{\varepsilon 1}C_\mu k\left(2\left(\frac{\partial u}{\partial x}\right)^2+2\left(\frac{\partial v}{\partial y}\right)^2+\left(\frac{\partial u}{\partial y}+\frac{\partial v}{\partial x}\right)^2+\left(\frac{\partial w}{\partial x}\right)^2+\left(\frac{\partial w}{\partial y}\right)^2\right)-C_{\varepsilon 2}\frac{\varepsilon^2}{k} \quad (29)$$

where

$$\nu_T=C_\mu\frac{k^2}{\varepsilon} \quad (30)$$

The set of model constants, C_μ, σ_k, σ_ε, $C_{\varepsilon 1}$, $C_{\varepsilon 2}$, is the standard choice originally proposed by Launder and Spalding (1974).

Boundary Conditions

At the water surface, the symmetry condition $\partial/\partial y = 0$ is imposed for all variables except for v, which has been set equal to zero. The flow model assumes that the Froude number ($=V/\sqrt{gD}$, where g = acceleration of gravity) is small; that is, the water surface is taken to be plane (rigid lid). At the bed, the no-slip condition is used for the velocities, whereas the k-equation uses the no-flux condition (i.e., $\partial k/\partial y = 0$ at the bed). A standard equilibrium condition—between production and dissipation of turbulent kinetic energy—is imposed at the bed for ε. At the lateral boundary far upstream of the channel, equilibrium profiles of u, v, w, k, and ε are imposed, whereas the lateral boundary downstream of the channel utilizes $\partial/\partial x = 0$ for the same parameters. The latter condition requires that the boundary is located sufficiently far downstream of the channel such that the profiles become fully developed.

Computational Details

In the 3D model, the equations are all transformed onto a general curvilinear coordinate system and subsequently solved with the finite-volume method [see Patankar (1980)]. This allows the grid to be smoothly conformed to the bed boundary. The continuity equation is replaced by an equation for the pressure, which is solved using the PISO-algorithm (velocity-pressure coupled solution algorithm). The fact that the z-dependency is eliminated from all equations (except for the $\partial p/\partial z$ constant) allows the numerical solution procedure to be considerably simplified. The set of equations, except for (26), along with the pressure equation, can be solved applying a 2D-model. The decoupled equation for w is treated separately as a simple transport equation.

Validation of 3D model

The performance of the numerical model has been compared with experimental results from the Hydraulics Research Station (HRS Wallingford 1973), in which velocities (speed and directions) across a channel for $\alpha_0 = 0°$, 10°, 20°, and 30° for several depth ratios were reported. The experimental data are well suited for verification of the numerical model, as velocities and flow angles were measured at different levels in the water column.

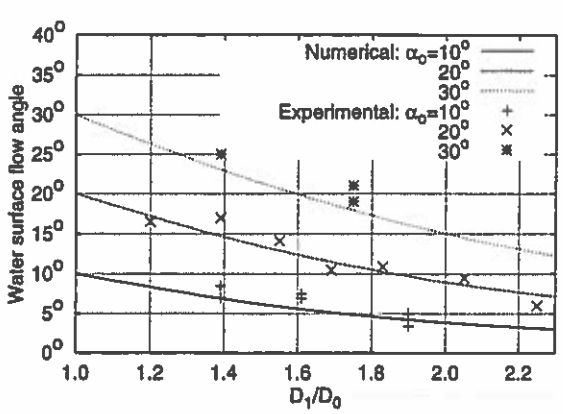

FIG. 6. Flow Angles at Water Surface Obtained Numerically and Experimentally

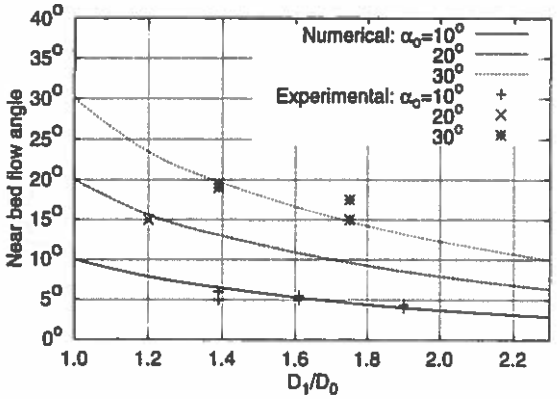

FIG. 7. Flow Angles near Bed Obtained Numerically and Experimentally

The comparisons between the simulated and measured direction of the surface and near-bed velocities are plotted in Figs. 6 and 7. The plotted angles are mean values across the plane part of the channel. It is seen that the measured and calculated flow angles agree quite well and that the 3D model captures the effect of increasing refraction toward the bed correctly.

Theoretical Results and Considerations

In Fig. 8(a) the flow across a channel inclined at 30° (left) and 60° (right) to the main flow direction is visualized using streamlines. Three streamlines are initiated upstream of the channel representing paths of three fluid particles. One is released just above the bed, one at middepth, and one near the water surface. The slope of the channel is relatively steep; thus a strong separation bubble will form. For this reason, a fourth streamline has been initiated within the separation zone. The fluid particles trapped within the separation bubble are carried downstream by the longitudinal velocity, and the resulting streamlines therefore acquire a flow pattern of a corkscrew eddy. It is seen that the corkscrew eddy is stretched in the longitudinal direction as the angle of the flow changes from $\alpha_0 = 60°$ (right) to 30° (left). In Fig. 8(c), the streamline of the depth-averaged flow is included. It is seen how a permanent horizontal deflection of streamlines initiated upstream is caused by the refraction. The near-bed streamline has the largest deflection compared with that of the depth-averaged streamline. Figs. 8(a) and 8(c) clearly illustrate that the current refraction varies strongly over the depth and that the near-bed particles experience the largest change of direction (similar to the helical flow in river bends).

Flow Entering Channel—Secondary Motion

Fig. 9 shows the outline of profiles of cross-channel horizontal velocities. It is seen how the fluid particles near the bed of the upstream slope are exposed to a larger relative deceleration than particles near the surface. The larger relative decelerations of near-bed particles are caused by the positive pressure gradient on the upstream slope affecting low inertia particles near the bed more strongly. As a result, the near-bed flow angle will be smaller than the depth-averaged flow angle. Conversely, a large negative $\partial p/\partial x$ (caused by the converging channel) is accelerating the flow on the downstream slope, where the near-bed flow angle may exceed the depth-averaged flow angle. The variation of the current refraction over the

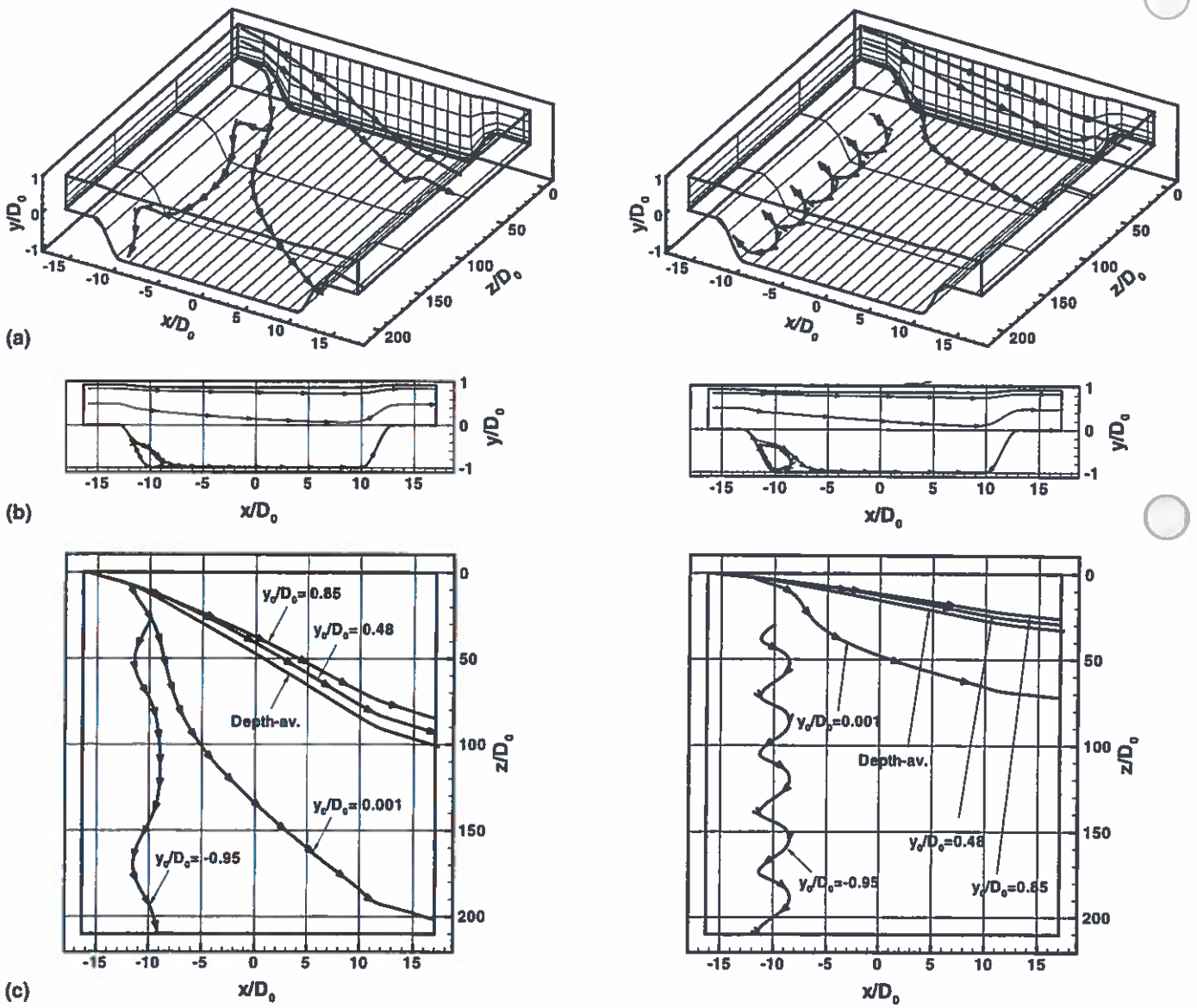

FIG. 8. (a) 3D Visualization of Refracted Streamlines; (b) Streamline Projection on (x, y)-Plane; (c) Streamline Projection on ( )-Plane. $D_1/D_0 = 2$, $W/D_0 = 23$, and $s_0 = \pi/6$. Left, $\alpha_0 = 30°$ and right, $\alpha_0 = 60°$

vertical may be considered as a secondary motion coexisting with the depth-averaged flow (Boer 1985).

Fig. 10 depicts the difference between the angle of the bed-shear stress and the depth-averaged flow angle found at the foot of the upstream slope as a function of the inlet angle. Curves of constant D_1/D_0 are shown.

The quantity $\Delta\alpha$ is a measure for the strength of the secondary motion, which is zero in the limiting cases of $\alpha_0 = 0°$ and 90°. If the inlet angle is gradually reduced, the flow will experience a more gentle slope, and the adverse pressure gradient confronting the flow will be reduced correspondingly. It is seen that the strongest secondary motion and therefore the largest deflections of streamlines occur for inlet angles in the range of $\alpha_0 = 60°–80°$ depending on the depth expansion.

The presence of the secondary motion was explained earlier by the nonequilibrium between the pressure gradient and the centrifugal forces in a refracted shear-layer flow. Because the magnitude of the centrifugal force is related to the curvature of horizontal streamlines, it can be expected that the strength of the secondary motion is related to the refraction of the depth-averaged flow.

The curvature of the streamline associated with the refraction of the depth-averaged flow can be assessed by considering the change in the depth-averaged flow angle occurring over the upstream slope $\Delta\alpha_{2DH}$. Using (17) $\Delta\alpha_{2DH}$ is estimated as

$$\Delta\alpha_{2DH} = \alpha_0 - \arctan\left(\frac{D_0}{D_1}\tan(\alpha_0)\right) \tag{31}$$

The point of maximum of (31) is seen to be located at increasing α_0 as the depth expansion is increased, which is the same behavior as seen in Fig. 10.

The effect of a change in depth expansion on $\Delta\alpha$ has been analyzed above for a fixed value of s_0. If, on the other hand, the slope is steepened and the expansion in depth is kept constant, then $\Delta\alpha$ will alter as well. In Table 1, the results of calculations with three different values of the steepness are summarized in terms of $\Delta\alpha$. It is seen that a steeper slope increases the strength of the secondary motion. This is in agreement with previous considerations that argue that the strength of the secondary motion increases as the distance over which the streamlines must bend is shortened (owing to a larger $\partial p/\partial x$ confronting the flow).

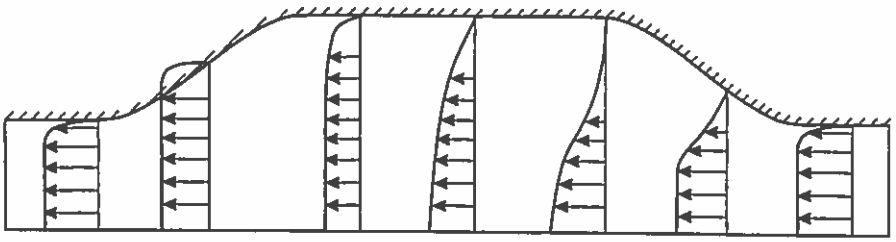

FIG. 9. Variation in Horizontal Velocity Profiles across Dredged Channel

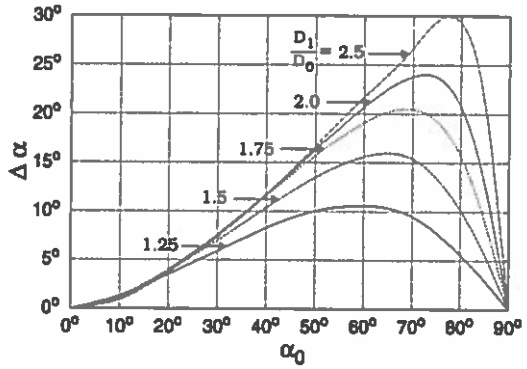

FIG. 10. Difference between Angles of Bed-Shear Stress and Depth-Averaged Flow Angle Just Downstream of Upstream Slope. $W/D_0 = 30$, $s_0 = \pi/20$, and $k_N/D_0 = 0.0001$

TABLE 1. Difference between Angle of Bed-Shear Stress and Depth-Averaged Flow Angle at Foot of Upstream Slope for Different Values of s_0

s_0 (1)	$\Delta\alpha$ (degrees) (2)
$\pi/10$	26
$\pi/20$	14
$\pi/40$	8.5

Note: $k_N/D_0 = 0.0001$, $\alpha_0 = 45°$, and $D_1/D_0 = 2$.

Development of Flow Crossing Channel

In Fig. 11, the flow angles near the bed and at the surface obtained with the 3D model are shown together with the angle of the depth-averaged velocity for two channel widths; $W/D_0 = 30$ and $W/D_0 = 110$. After the forcible refraction of the current on the upstream slope, the flow enters the plane bed section of the channel, where the deviation between the direction of the fluid particles over the vertical is gradually decreased by the work of the shear stress. At the downstream section of the channel, the bed flow angle has approached the depth-averaged flow angle. The flow is, however, not in equilibrium as the longitudinal acceleration continues, as previously discussed. In Fig. 11, this is also detectable on the depth-averaged flow angle, which continues to decrease across the channel.

In Fig. 12, the cross-channel development of the longitudinal depth-averaged flow calculated by the 2D analytical model and the 3D numerical model is shown for an infinitely wide channel. Along with the solution to the 3D model, solutions to (19) are included using $u_1/u_0 \tan(\alpha_0)$ and $\tan(\alpha_{eq})$ as estimates for $\tan(\alpha)$. Fig. 12 shows that the width of channels required to obtain fully developed flow conditions is much larger than the width used in Fig. 11. Furthermore, it is seen that the development of the longitudinal velocity component is well described by the analytical model.

The development of the depth-averaged total velocity across a channel is shown for various inlet angles in Fig. 13. The two extreme cases of $\alpha_0 = 0°$ and 90° are included. The change in the depth-averaged total velocity in the cross-channel direction $\partial V/\partial x$ is clearly seen to decrease as the inlet angle increases. This is caused by the following: (1) The contribution of the accelerating w-component to V is largest for small inlet angles; and (2) particles approaching the channel at small angles will be exposed to the longitudinal pressure gradient for a prolonged time compared with particles entering the channel

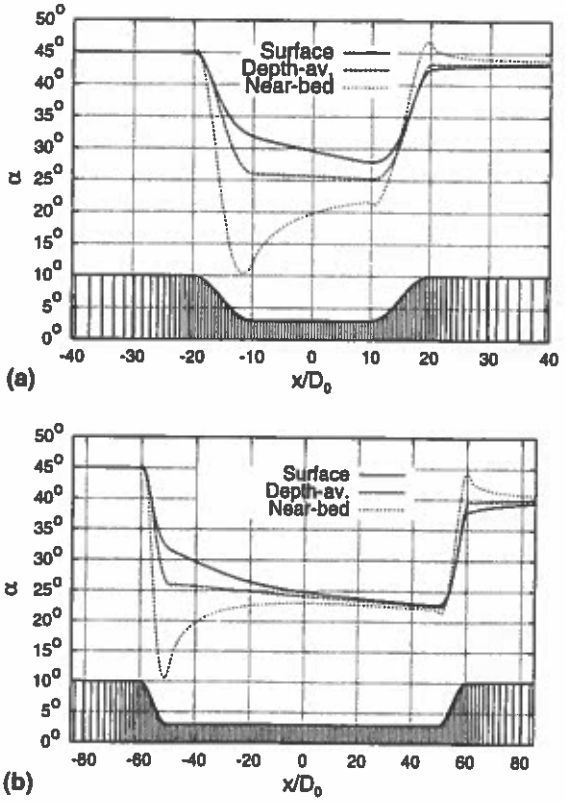

FIG. 11. Flow Angles across Channel near Bed, for Depth-Averaged Velocity, and at Surface, for: (a) $W/D_0 = 30$; (b) $W/D_0 = 110$. $\alpha_0 = 45°$, $D_1/D_0 = 2$, $s_0 = \pi/20$, and $k_N/D_0 = 0.0001$

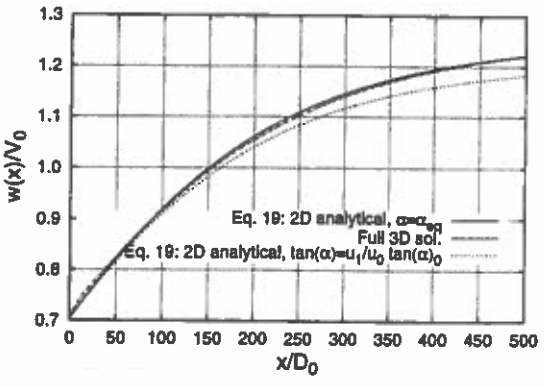

FIG. 12. Increase in Longitudinal Depth-Averaged Velocity for $\alpha_0 = 45°$, $k_N/D_0 = 0.001$, and $D_1/D_0 = 2$. Channel Step Is Located at $x/D_0 = 0$

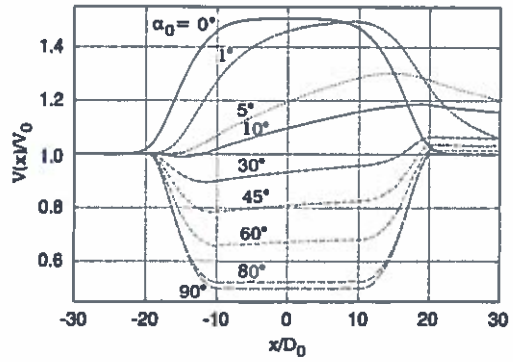

FIG. 13. Total Velocities across Channel for Different Inlet Angles. $W/D_0 = 30$, $s_0 = \pi/20$, $D_1/D_0 = 2$, and $k_N/D_0 = 0.0001$

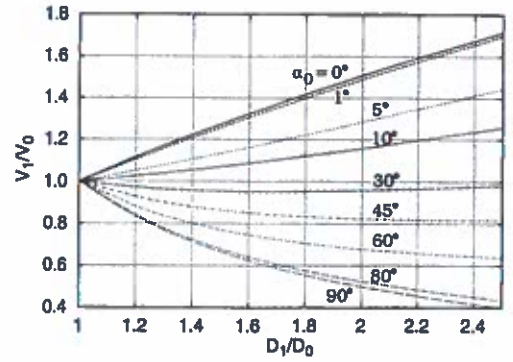

FIG. 14. Maximum Total Depth-Averaged Velocity within Channel Relative to V_0. $W/D_0 = 30$, $s_0 = \pi/20$, and $k_N/D_0 = 0.0001$

at larger angles of incidence. The ratio of the maximum total depth-averaged velocity within the channel to V_0 is plotted in Fig. 14. The tendency is the same as that seen in Fig. 5 for the 2D analysis, although the velocity in the channel of limited width is far smaller. To sum up on flow across channels, the direction of the depth-averaged flow can be determined by estimating u from the continuity constraint, whereas w is found from the analytical expression in (19). The near-bed fluid motions, and consequently the bed-shear stress, are more complicated and cannot be estimated from simple considerations.

CONCLUSIONS

A 3D mathematical model has been applied to study the flow pattern of a current crossing a dredged channel obliquely. The ability of the model to predict the complex 3D flow field has been verified by existing experimental data. It has been shown that the depth-averaged refraction of the flow toward the channel alignment was caused by (1) the continuity constraint on the cross-channel velocity component u; and (2) acceleration of the longitudinal velocity component w. The latter is shown to be a slowly developing process. A secondary flow coexisting with the depth-averaged flow is generated on the slopes of the channel. The near-bed flow is refracted more and the near-surface flow less than that of the depth-averaged flow. The strength of the secondary motion depends strongly on the angle of attack of the flow. The difference between the depth-averaged flow angle and the angle of the bed-shear stress reaches values up to 30°. The presence of the secondary motion gives rise to a permanent horizontal deflection of streamlines over the vertical. The bed-shear stress exceeds the flat bed value if the expansion in depth is large or the angle of attack is small.

ACKNOWLEDGMENTS

This work is jointly supported by Numerical and Experimental Fluid Mechanics and by Marine Technique all funded by the Danish Technical Research Council.

APPENDIX I. REFERENCES

Alfrink, B. J., and van Rijn, L. C. (1983). "Two-equation turbulence model for flow in trenches." *J. Hydr. Engrg.*, ASCE, 109(7), 941–958.

Basara, B., and Younis, B. A. (1995). "Prediction of turbulent flows in dredged trenches." *J. Hydr. Res.*, Delft, The Netherlands, 33(6), 813–824.

Bijker, E. W. (1980). "Sedimentation in channels and trenches." *Proc., 17th Coast. Engrg. Conf.*, Vol. II, ASCE, New York, 1708–1718.

Boer, S. (1985). "The flow across trenches at oblique angle to the main flow direction." *Rep. on Basic Research*, Waterloopkundig Laboratorium, Delft Hydraulics Laboratory, Delft, The Netherlands.

Engelund, F. (1974). "Flow and bed topography in channel bends." *J. Hydr. Div.*, ASCE, 100(11), 1631–1648.

Fredsøe, J. (1978). "Sedimentation of river navigation channels." *J. Hydr. Div.*, ASCE, 104(2), 223–236.

Fredsøe, J. (1979). "Natural backfilling of pipeline trenches." *J. Technol.*, 31, 1223–1230.

HRS Wallingford. (1973). "Laboratory studies of flow across dredged channels." *Rep. No. EX 618*, Wallingford, Berkshire, England.

Jensen, J. H., Madsen, E. Ø., and Fredsøe, J. (1999). "Oblique flow over dredged channels. II: Sediment transport and morphology." *J. Hydr. Engrg.*, ASCE, 125(11), 1190–1198.

Koutitis, C., and O'Connor, B. (1981). "Turbulence model for flow over dredged channels." *J. Hydr. Div.*, ASCE, 107(8), 989–1002.

Launder, B. E., and Spalding, D. B. (1974). "The numerical computation of turbulent flows." *Comput. Methods Appl. Mech. Engrg.*, 3, 269–289.

Patankar, S. V. (1980). *Numerical heat transfer and fluid flows*. Hemisphere, New York.

Rozovskii, I. L. (1961). *Flow of water in bends of open channels*. Israel Program for Scientific Translations, Jerusalem.

van Rijn, L. C. (1986). "Sedimentation of dredged channels by currents and waves." *Delft. Hydr. Communications No. 369*, Delft Hydraulic Laboratory, Delft, The Netherlands.

van Rijn, L. C. (1987). "Mathematical modelling of morphological processes in the case of suspended sediment." *Delft Hydr. Communications No. 382*, Delft Hydraulic Laboratory, Delft, The Netherlands.

APPENDIX II. NOTATION

The following symbols are used in this paper:

a, a_2, e = constants in analytical formula for $\bar{t} = f(\bar{w})$ and $\bar{w} = f(\bar{x})$;
b = distance between two horizontal streamlines;
C_f = friction formula coefficient;
C_μ, $C_{\varepsilon 1}$, $C_{\varepsilon 2}$ = k-ε model constants;
D = water depth ($\bar{D} = D/D_0$);
k = turbulent kinetic energy;
k_N = Nikuradse roughness;
p = pressure [$\bar{p} = p/(\rho V_0^2)$];
s_0 = maximum slope on channel slopes;
T_{xx}, T_{xz}, T_{zz} = depth-averaged horizontal shear stresses;
t = time ($\bar{t} = tV_0/D_0$);
u = velocity component in x-direction ($\bar{u} = u/V_0$);
V = total depth-averaged velocity;
V_{eq} = total depth-averaged velocity for fully developed flow;
V_f = friction velocity;
v = velocity component in y-direction;
W = width of channel;
w = velocity component in z-direction ($\bar{w} = w/V_0$);
x = coordinate perpendicular to channel alignment ($\bar{x} = x/D_0$);
y = vertical coordinate;
z = coordinate parallel to channel alignment ($\bar{z} = z/D_0$);

α = flow angle;
α_b = flow angle at bed;
α_{eq} = depth-averaged flow angle for fully developed flow;
ΔT = nondimensional time in analytical formula for $\bar{w}$;
$\Delta\alpha$ = difference between depth-averaged flow angle and bed flow angle at foot of upstream slope;
$\Delta\alpha_{2DH}$ = difference between inlet angle and depth-averaged flow angle at foot of upstream slope;
ε = dissipation of turbulent kinetic energy;
ν_T = eddy viscosity;
ρ = density of water;
σ_ε, σ_k = k-ε model constants;
τ_b = total bed-shear stress; and
τ_{bz}, τ_{bx} = bed-shear stress in longitudinal and cross-channel directions [$\bar{\tau}_{bz} = \tau_{bz}/(\rho V_0^2)$].

Subscripts

eq = equilibrium value;
x = transverse component;
z = longitudinal component;
0 = upstream channel value; and
1 = inside channel value.

OBLIQUE FLOW OVER DREDGED CHANNELS. II: SEDIMENT TRANSPORT AND MORPHOLOGY

By Jacob Hjelmager Jensen,[1] Erik Østergaard Madsen,[2] and Jørgen Fredsøe[3]

ABSTRACT: A 3D investigation of sediment transport processes across long, straight channels exposed to an oblique incoming current is presented. For this purpose a detailed mathematical flow and sediment transport model is applied. The governing flow and sediment transport equations are solved in a curvilinear coordinate system. The sediment transport model is composed of bed and suspended load, applying a convection-diffusion equation for the latter. As the flow crosses a channel obliquely, it is refracted toward the channel alignment. The effect of the current refraction on the sediment transport is studied using both 2D (depth-averaged) and 3D models. Shortcomings of models based on depth-averaged descriptions are underlined through comparison with the 3D model. A reliable description of the backfilling process requires a flow and sediment transport model capable of capturing the following aspects: (1) The direction and magnitude of the bed-shear stress; and (2) the adaptation of suspended sediment to local sediment transport capacities. Calculations of the morphological development of small-scale excavations (e.g., pipeline trenches) exposed to an oblique incoming current are presented.

INTRODUCTION

This paper is a continuation of Part I (Jensen et al. 1999). In Part I, flow approaching a long, straight channel obliquely was analyzed focusing on flow separation and the refraction of the flow. In this part the implications of these two items on the sediment transport processes are investigated. The channels considered are assumed to be long and straight, implying that the flow and sediment transport are uniform in the direction of the channel alignment (also termed the longitudinal direction).

If the flow is parallel to the alignment of the channel, the sediment transport capacity is larger within the channel than outside. Roughly, this can be explained by the fact that the longitudinal pressure gradient is constant across the channel. Therefore, as the driving force equals the local water depth times the pressure gradient, higher velocities occur at deeper sections. The longitudinal sediment transport, however, does not affect the morphology that is governed by the cross channel transport. Although the depth-averaged cross-channel velocity is zero, deposition within the channel occurs, mainly as a consequence of the action of gravity on bed load particles on the slopes [see, e.g., Fredsøe (1978)].

If the flow crosses a channel perpendicularly, the depth-averaged velocity will decrease within the channel, simply due to the continuity constraint on the flow. The lower velocities will produce less turbulent kinetic energy, causing the sediment transport capacity to decrease (Fredsøe 1979; van Rijn 1986, 1987). The settling of suspended sediment takes place as the sediment gradually adapts to the local capacity. The length scale of this process can be characterized by an adaptation length of suspended sediment [see, e.g., Fredsøe (1979)]. The direct use of an adaptation length is, however, associated with large uncertainties. This is due to the complexity of the turbulence structure, which is not included in an adaptation length model.

When the flow enters the channel obliquely, it is refracted toward the alignment of the channel. Current refraction takes place on the upstream slope owing to a reduction in the cross-channel velocity component. The refraction is amplified within the channel, where the longitudinal velocity component is gradually accelerated. On the side slopes of the channel a secondary motion coexisting with the refracted depth-averaged flow is generated as a consequence of the adverse pressure gradient acting on the vertically sheared oncoming flow.

Mayor-Mora et al. (1976), Fredsøe (1979), and Bijker (1980) proposed simple methods to assess backfilling of channels attacked obliquely by a current. In these studies, the effect of the obliqueness was only accounted for by an increase in the apparent channel width, thus neglecting the current refraction. van Rijn (1987) used a quasi-3D flow model and a 3D suspended sediment transport model to calculate the deposition. In this model, hydrostatic pressure distribution and logarithmic velocity profiles of horizontal flow were assumed. Vertical velocities were obtained through the equation of continuity.

In contrast to the simpler models mentioned earlier the quasi-3D models capture the effect of the depth-averaged flow refraction. Quasi-3D models are, nevertheless, built on the assumption that the horizontal velocities are unidirectional over the depth. Deviations between the direction of the bed-shear stress and the direction of the depth-averaged velocity are thus disregarded in quasi-3D models and associated sediment transport predictions.

PURPOSE OF PRESENT STUDY

In the present study a 3D flow and sediment transport model is applied. The model is capable of describing the variation in the flow direction over the depth. This is important as the direction of the bed-shear stress deviates from the direction of the depth-averaged flow. Only when the 3D flow behavior is captured are the magnitude and direction of the bed-shear stress correctly modeled.

The sedimentation pattern is investigated for both narrow and wide channels. In addition, the morphology of small channels (e.g., pipeline trenches) is presented.

MATHEMATICAL MODELING OF SEDIMENT TRANSPORT

In Part I, a 3D flow model was presented. The flow model solves the Reynolds-averaged Navier-Stokes equations em-

[1]PhD, Inst. of Hydrodynamics and Water Resour., Tech. Univ. of Denmark, DK-2800 Lyngby, Denmark; currently, Danish Hydr. Inst., Agern Allé 5, DK-2970 Hørsholm, Denmark.

[2]PhD Student, Inst. of Hydrodynamics and Water Resourc., Tech. Univ. of Denmark, DK-2800 Lyngby, Denmark.

[3]Prof., Inst. of Hydrodynamics and Water Resourc., Tech. Univ. of Denmark, DK-2800 Lyngby, Denmark.

Note. Discussion open until April 1, 2000. Separate discussions should be submitted for the individual papers in this symposium. To extend the closing date one month, a written request must be filed with the ASCE Manager of Journals. The manuscript for this paper was submitted for review and possible publication on September 9, 1998. This paper is part of the *Journal of Hydraulic Engineering*, Vol. 125, No. 11, November, 1999. ©ASCE, ISSN 0733-9429/99/0011-1190–1198/$8.00 + $.50 per page. Paper No. 19193.

ploying a standard k-ε model for turbulence closure in a curvilinear coordinate system. This model is the starting point of the sediment transport model described in the following. For the sake of simplicity the equations are presented in Cartesian coordinates.

The total transport of sediment, q (=$\{q_x, q_z\}$), is the sum of bed load, q_b (=$\{q_{bx}, q_{bz}\}$), and suspended load, q_s (=$\{q_{sx}, q_{sz}\}$). The same notation applies for the nondimensional transport components Φ.

Bed Load Transport

The bed load transport is calculated by using the Meyer-Peter and Müller formula expressed by the nondimensional quantity Φ_b

$$\Phi_b = \frac{q_b}{\sqrt{(s-1)gd^3}} = 8(\theta - \theta_c)^{3/2} \tag{1}$$

where s (=2.65) = relative density of the sand; g = acceleration of gravity; d = mean grain diameter; and θ = nondimensional bed-shear stress—the Shields parameter—defined by

$$\theta = \frac{\tau_b}{\rho(s-1)gd} \tag{2}$$

where τ_b = bed-shear stress; and ρ = density of water. Furthermore, θ_c is the critical Shields parameter for the initiation of sediment movement. In the case of a sloping bed θ_c is modified according to Engelund and Fredsøe (1982) to include the action of gravity on the bed load particles

$$\theta_c = \theta_{co}\cos(\beta)\left(\frac{\sin(\alpha_b)\tan(\beta)}{\mu_s} + \sqrt{1 - \left(\frac{\cos(\alpha_b)\tan(\beta)}{\mu_s}\right)^2}\right) \tag{3}$$

where β = slope of the bed; α_b = angle between the bed-shear stress and the channel alignment (z-direction); μ_s = static friction coefficient; and θ_{co} (=0.05) = critical Shields parameter on a horizontal bed.

On a sloping bed the direction of the bed load particles deviates from the direction of the bed-shear stress by the angle ψ. Engelund and Fredsøe (1982) derived an expression for ψ, here modified with the local near-bed angle [i.e., $\cos(\alpha_b)$]

$$\tan(\psi) = \frac{\tan(\beta)}{1.6\sqrt{\theta}}\cos(\alpha_b) \tag{4}$$

Suspended Sediment Transport

The distribution of sediment in suspension is determined by using the convection-diffusion equation of the concentration of suspended sediment c. The mixing coefficient is taken to be equal to the eddy viscosity ν_T. If the condition of uniformity in the longitudinal direction is enforced, the equation of concentration of suspended sediment reads

$$u\frac{\partial c}{\partial x} + v\frac{\partial c}{\partial y} = w_s\frac{\partial c}{\partial y} + \frac{\partial}{\partial x}\left(\nu_T\frac{\partial c}{\partial x}\right) + \frac{\partial}{\partial y}\left(\nu_T\frac{\partial c}{\partial y}\right) \tag{5}$$

where w_s = fall velocity of the mean grain diameter in suspension; y = vertical coordinate; and u and v = velocity components in the transverse and vertical directions, respectively. Variations in the z-direction are neglected (as in Part I).

Regarding the boundary conditions, a no flux of sediment through the water surface is employed

$$w_s c + \nu_T\frac{\partial c}{\partial y} = 0 \quad \text{at} \quad y = D \tag{6}$$

where D = local water depth. The bed condition proposed by Engelund and Fredsøe (1976) is adopted, specifying the value of the concentration directly at $y = 2d$. This model for the bed concentration does not deviate significantly from the formula by Zyserman and Fredsøe (1994), which is based on experimental data. The suspended fluxes in the two horizontal directions are found by integration of concentration times velocity over the depth.

Morphological Model

The morphology is obtained by using the equation of continuity for sediment (the Exner equation)

$$\frac{\partial h}{\partial t} + \frac{1}{1-r}\frac{\partial q_x}{\partial x} = 0 \tag{7}$$

where h = bed elevation; t = time; and r = porosity of the bed material. In (7) the uniformity in the longitudinal direction has once again been utilized. For this reason, only the cross-channel component of the sediment flux contributes to the morphological development. The numerical treatment of (7) can be found in Appendix I.

THEORETICAL RESULTS

The shape of the excavated channel and the definition of parameters are identical to those defined in Part I. The main parameters are shown in Fig. 1.

It is not straightforward to define the rate of sedimentation. If the rate of sedimentation is defined by $\Delta\Phi_x = \Phi_{x3} - \Phi_{x1}$ [e.g., as Bijker (1980)], where Cross Sections 1 and 3 are defined in Fig. 2, then the local redistribution of sediment on the upstream slope (see the dashed line in Fig. 2 at Cross Section 2) is disregarded. The local redistribution of sediment is often included in definitions of backfilling [see, e.g., Fredsøe (1978)]. Another possibility could be to define the sedimentation as $\Delta\Phi_x = \Phi_{x4} - \Phi_{x2}$ (i.e., the difference between the transports at the centers of the two slopes). However, this measure will not account for the deposition between Cross Sections 2 and 3 and the erosion between Cross Sections 3 and 4, which mainly will result in downstream migration of the dredged channel. Migration of the channel is, however, also of large engineering importance. A very good integrated measure of the sedimentation is the change with time of the distance between the center of gravity of the channel and the level outside the excavated region. This measure, denoted CG, will be applied in a later section. In this section the sedimentation is defined in the following way:

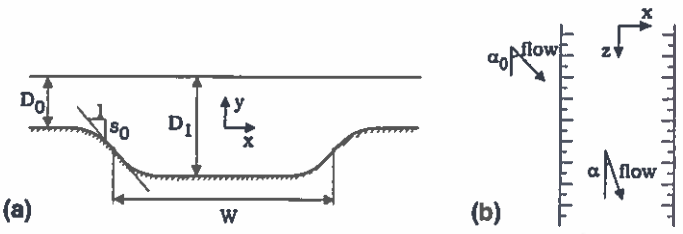

FIG. 1. Definition Sketch of Channel Parameters: (a) Cross Section; (b) Top View and Definition of Flow Angle

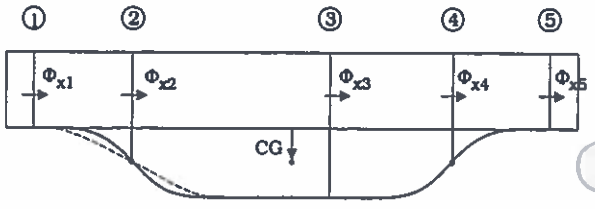

FIG. 2. Possible Locations of Boundaries of Control Box Used to Define Sedimentation

$$\Delta = \frac{\Phi_{x0} - \Phi_x}{\Phi_{x0}} \tag{8}$$

where Φ_{x0} = sediment transport in the transverse direction far upstream; and Φ_x = equivalent at a location on the horizontal part of the bed within the channel (e.g., Cross Section 3).

Infinitely Wide Channel

To evaluate the effect of a fully developed current refraction (see Part I) on the sediment transport capacity, an infinitely wide channel will be considered first. Here the significance of the adaptation length of suspended sediment and the presence of a separation zone is eliminated. The latter features, important in relation to trenches and channels of limited width, are treated subsequently.

Whether the inside channel capacity of sediment transport exceeds the inlet value or not depends on the approaching angle of the flow α_0, the expansion in depth defined by D_1/D_0, the width of the channel W, and the upstream Shields parameter (i.e., outside of the channel) denoted θ_0.

Sediment Transport Pattern

Figs. 3(a and b) show the variation of the Shields parameter θ and of the cross-channel sediment transport for flow entering an infinitely wide channel at flow angles of 30° and 60° along with $D_1/D_0 = 2$, $\theta_0 = 0.5$, and $k_N/D_0 = 0.0001$. The Nikuradse bed roughness k_N is taken to be $2.5d$ (Engelund and Hansen 1972). It is seen that the cross-channel sediment transport Φ_x drops in the separation zone located immediately after the depth expansion. However, further downstream the acceleration of the flow in the direction of the channel alignment increases the sediment transport capacity, which gives an increase in cross-channel sediment flux. In Part I the timescale associated with the longitudinal acceleration of the flow was investigated. Obviously, the very large timescales for the flow development will affect the sediment transport development as well.

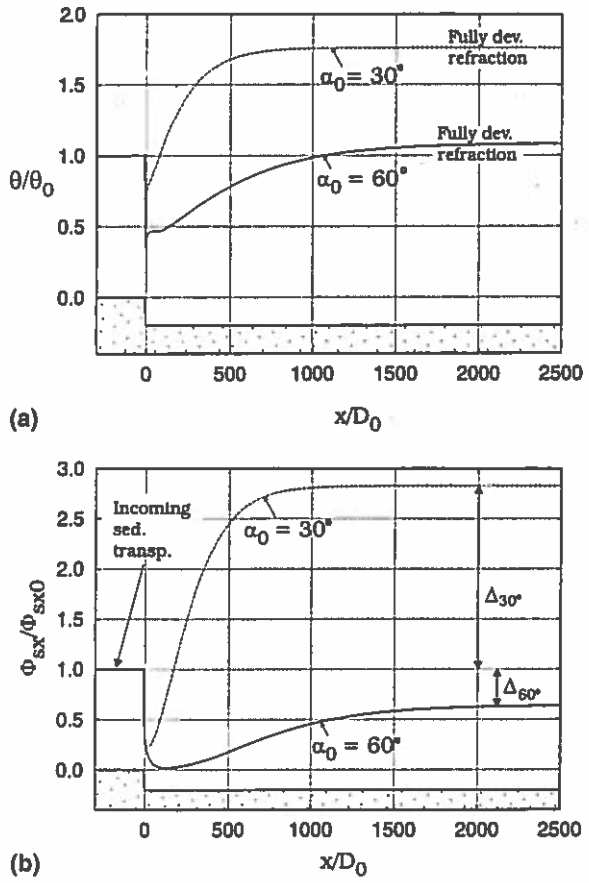

FIG. 3. For $\alpha_0 = 30°$ and 60° over Infinitely Wide Channel: (a) Variation of Shields Parameter; (b) Cross-Channel Sediment Transport. Remaining Parameters Are $D_1/D_0 = 2$, $s_0 = \pi/20$, $\theta_0 = 0.5$, and $k_N/D_0 = 0.0001$. Δ Is Defined in Eq. (8)

For $\alpha_0 = 60°$ the Shields parameter far downstream of the depth expansion is only slightly increased compared with θ_0. This implies that the increase in the longitudinal velocity component counterbalances the loss in the cross-channel velocity component. Although the deviation between the Shields parameters upstream (i.e., θ_0) and far downstream (inside the channel) is small, the cross-channel components of the sediment transport differ significantly. The increase in the level of turbulent kinetic energy due to the accelerated longitudinal velocity does not fully compensate for the reduction in the cross-channel velocity. For $\alpha_0 = 30°$, however, the accelerated longitudinal velocity and the corresponding level in turbulent kinetic energy increase the sediment transport capacity to such a degree that a net increase in the cross-channel sediment transport occurs. In the latter case, the cross-channel suspended sediment transport Φ_{sx} is influenced by the strong nonlinear behavior of the sediment transport to levels in turbulent kinetic energy far more than by the reduced cross-channel velocity.

Sedimentation

For sufficiently wide channels the flow and sediment transport will attain equilibrium conditions of uniform flow (Fig. 3). In the following, Δ_{eq} corresponds to the value of Δ for a control box for which the downstream boundary (Cross Section 3) is located at $x \to \infty$ (i.e., the deposition in an infinitely wide channel). A solution for the deposition Δ_{eq} can be obtained analytically. Details of the derivation of the equilibrium sediment transport values are given in Appendix II. In Fig. 4, Δ_{eq} is shown (solid lines) as a function of the inlet angle for four different combinations of θ_0 and D_1/D_0. The solid curves in Fig. 4 reflect the dependency of the sedimentation on the fully refracted flow. As explained earlier, the nonlinear behavior of the sediment transport due to levels in turbulent kinetic energy may lead to an erosion between Cross Sections 1 and 3. In Fig. 4(d) it is seen that an infinitely wide channel with $D_1/D_0 = 3$ and $\theta_0 = 0.5$ experiences a net erosion for inlet angles smaller than ~34°. For $D_1/D_0 = 1.2$ and $\theta_0 = 0.5$ [Fig. 4(a)] the erosion occurs for inlet angles smaller than ~23°. It is seen that larger expansions in depth amplifies both the erosion (small inlet angles) and the deposition (large inlet angles). An increase in the Shields parameter from $\theta_0 = 0.5$ to 1.0 [Figs. 4(b and c)] increases the maximum erosion as well.

The deposition curve corresponding to $\Delta = \Delta_{2D} \sin(\alpha_0)$ has been included in Fig. 4 (dashed lines) where Δ_{2D} = deposition caused by a current approaching perpendicularly (i.e., Δ_{eq} for $\alpha_0 = 90°$). The obliquity of the flow is in this manner only accounted for by the amount of incoming sediment. This approach therefore excludes the effects of the refraction of the flow, as in the simple models mentioned earlier (Mayor-Mora et al. 1976; Fredsøe 1979; Bijker 1980). Consequently, the difference between the two curves in each graph of Fig. 4 indicates the effect of the fully refracted flow. Obviously, the curves coincide for $\alpha_0 = 90°$.

Channels of Limited Width

For channels of limited width in which the flow and sediment transport conditions are not fully developed, a more detailed description than the analytical solution presented in Appendix II is needed. As compared with channels of infinite width, at least three additional processes influencing the sediment transport pattern are introduced. These are as follows:

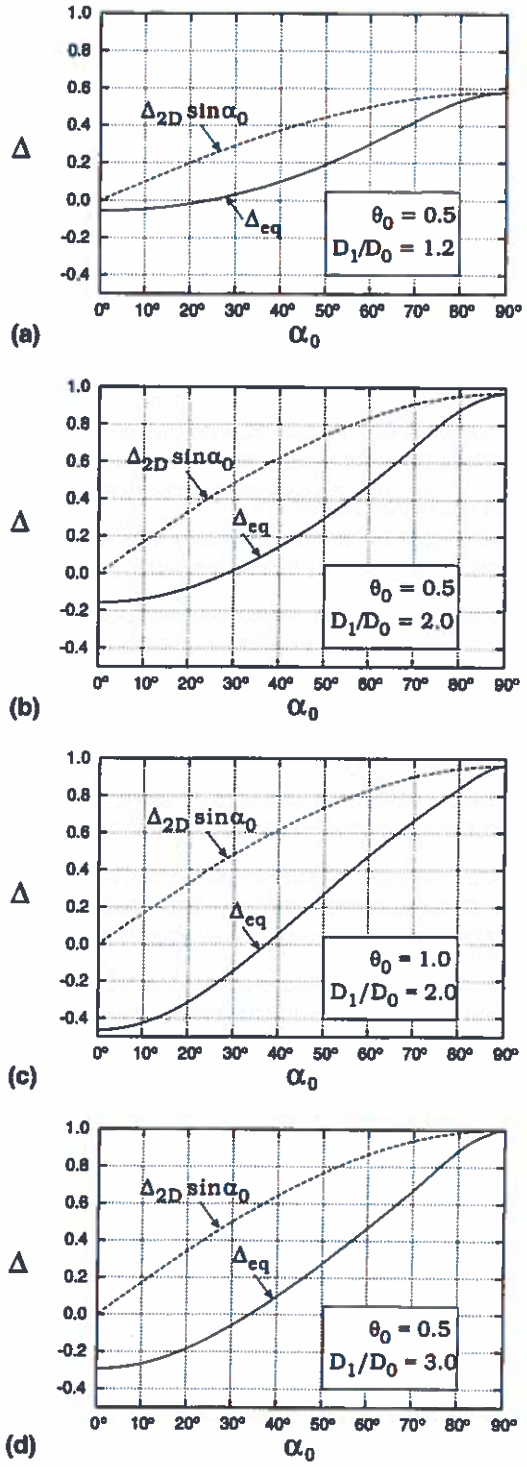

FIG. 4. Deposition of Sediment as Function of Inlet Angle for Various Expansions in Depth and Shields Parameters. Sediment Transport Is Considered to Be in Local Equilibrium. ——, Fully Refracted Flow; – – –, Refraction Excluded. $k_N/D_0 = 0.001$

1. The acceleration of the longitudinal velocity component across the channel.
2. The strongly varying flow direction over the vertical.
3. The gradual adaptation of suspended sediment to the local sediment transport capacities within the channel.

The influence of the first item has been discussed in the previous section. The latter two items are discussed in the following.

Sediment Transport Pattern

The transverse and longitudinal components of the suspended sediment transport across a channel are shown in Fig. 5 for two different width-to-depth ratios. The increase in the longitudinal suspended sediment transport on the upstream slope is caused by two processes: (1) High levels in turbulent kinetic energy generated by the strong vertical free shear layer characteristic of flow over a diverging channel; and (2) the distance between a particular fluid particle and the bed level increases as the flow crosses the slope. This brings the sediment particles to levels above the bed with higher longitudinal velocities. Across the channel the suspended sediment transport in the longitudinal direction decreases as the sediment adapts through settling. On the downstream slope, Process (2) is reversed as the distance between the fluid particle considered above and the bed level decreases. On the downstream slope near the adjoining flat bed, the level of turbulent kinetic energy increases leading to an increasing sediment transport. Even though the level of turbulent kinetic energy on the upstream slope increases, the cross-channel suspended sediment flux decreases at this location. This is associated with a deceleration of the cross-channel velocities, which is most pronounced near the bed. Across the horizontal part of the channel, the near-bed fluid particles gain cross-channel momentum, mainly through turbulent mixing. This causes the transverse velocity profile to redevelop. The suspended sediment continues nevertheless to settle, adapting to the lower level of turbulent kinetic energy.

In the case of a wider channel, $W/D_0 = 110$, the increase in the longitudinal velocity across the channel becomes more advanced. The corresponding increase in the level of turbulent kinetic energy is, however, not yet sufficiently strong to prevent the sediment in the overloaded concentration profile to continue settling. As in the case with wider channels, smaller

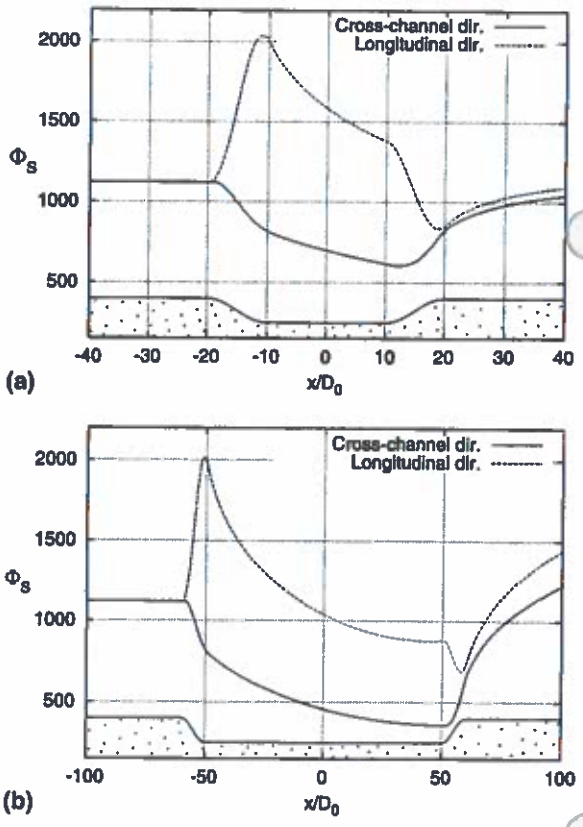

FIG. 5. Transverse and Longitudinal Components of Suspended Sediment Transport across Channel for: (a) $W/D_0 = 30$; (b) $W/D_0 = 110$. $\theta_0 = 1$, $\alpha_0 = 45°$, $D_1/D_0 = 2$, $s_0 = \pi/20$, and $k_N/D_0 = 0.0001$

inlet angles will give a more advanced acceleration of the longitudinal velocity across the channel. The distribution of suspended sediment across the channel for $\alpha_0 = 5°$ is compared with 90° in Fig. 6. The channel width is $W/D_0 = 30$, and the remaining parameters are as in Fig. 5. The suspended sediment concentration for $\alpha_0 = 5°$ is influenced by the longitudinal acceleration and the corresponding level of turbulent kinetic energy to such an extent that sediment is brought into suspension continuously across the channel stretch as opposed to the monotonous precipitation that take place in the 90° case.

Sedimentation

The initial deposition of sediment in a channel similar to the one considered in Fig. 5(a) with $W/D_0 = 30$ is investigated. The deposition of sediment can be nondimensionalized by using either the total sediment transport upstream of the channel or its cross-channel component. The latter is equal to Δ [see (8)] and the former equal to $\Delta \sin(\alpha_0)$.

In Fig. 7 the two approaches [i.e., $\Delta \sin(\alpha_0)$ and Δ] are depicted as a function of the expansion in depth, calculating Φ_x in (8) at the vertical section adjoining the plane part of the channel and the downstream slope (Cross Section 3). In Fig. 7(a) it is seen that the amount of sediment that is deposited increases with the inlet angle. Recall that the total sediment transport upstream of the channel does not depend on the inlet angle. If the deposition is depicted relative to the cross-channel component of the sediment flux upstream of the channel, the effect of an increased sediment transport capacity is accentuated. In Fig. 7(b), it is seen that the deposition curves (curves of constant α_0) are similar for inlet angles in the range of $\alpha_0 = 20°–90°$. Therefore, for this particular width of the channel

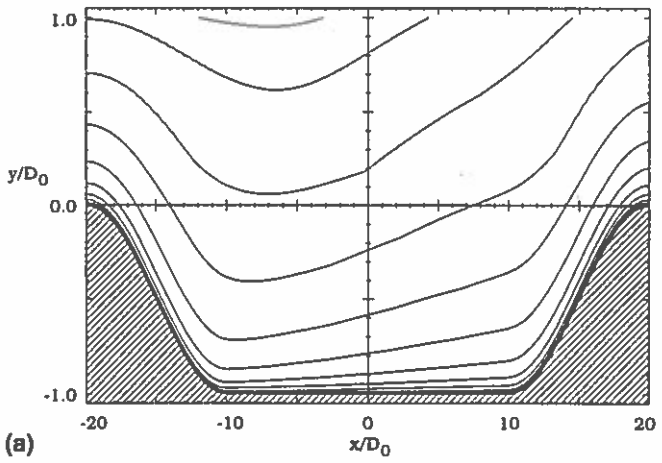

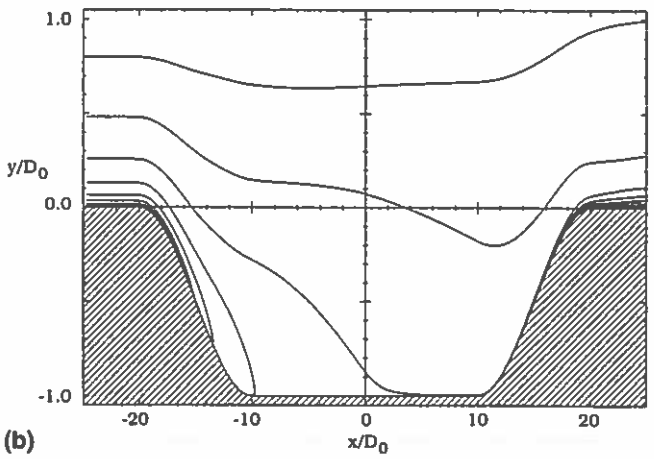

FIG. 6. Contours of Suspended Sediment Concentration for: (a) $\alpha_0 = 5°$; (b) 90°. Other Parameters as in Fig. 5(a)

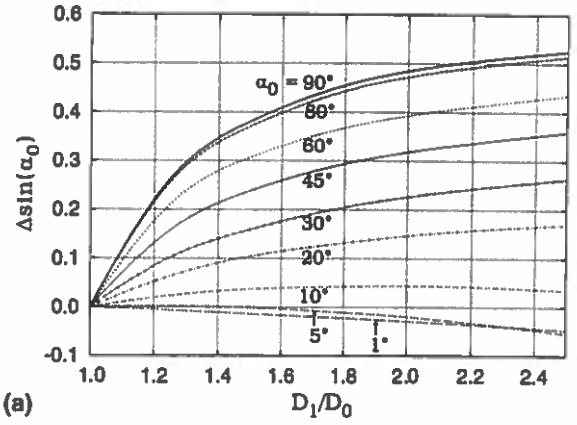

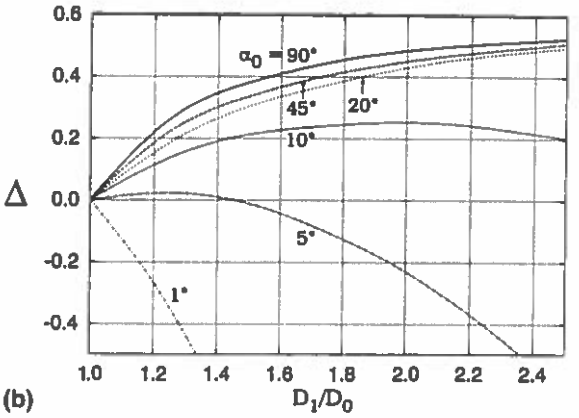

FIG. 7. For Various Inlet Angles and Expansions in Depth, Deposition Compared with: (a) Total Upstream Transport; (b) Upstream Transverse Transport Component. Parameters as in Fig. 5(a)

the flow will deposit nearly the same fraction of the incoming sediment for larger inlet angles whereas the effect of the increased level of turbulent kinetic energy inside the channel will affect the sediment transport pattern for small inlet angles [note that the backfilling due to slope effects is not detectable in the results shown in Figs. 7(a and b), as the control sections are located on horizontal parts of the bed].

Comparison between Full 3D Model and Simpler Models

In this section the full 3D model is compared with two simpler models. To study the entire region influenced by the expansion in depth a very wide channel excavation is considered. The first of the simpler models, referred to as the quasi-3D model, is composed of the analytical flow description presented in Part I combined with a numerical solution to the equation of concentration of suspended sediment [(5)]. The horizontal velocity profiles are assumed logarithmic, and the vertical velocities are found from the equation of continuity. The eddy viscosity is taken to be parabolic corresponding to the local bed-shear stress. The second model used for comparison is that of Mayor-Mora et al. (1976). This model uses the equilibrium values of suspended sediment at depths D_0 and D_1 and describes the adaptation process by using an exponential decay. Oblique attack of the current is treated by replacing the transverse coordinate x with $x/\cos(\alpha_0)$.

In Fig. 8 the cross-channel sediment transport over the channel is shown by using the three models mentioned above with $\alpha_0 = 60°$. Fig. 8(a) shows the transverse bed load transport Φ_{bx} in a region in the proximity of the upstream channel slope. Fig. 8(b) is the equivalent for the transverse suspended sediment transport Φ_{sx}. Fig. 8(c) shows Φ_{sz} in the region from

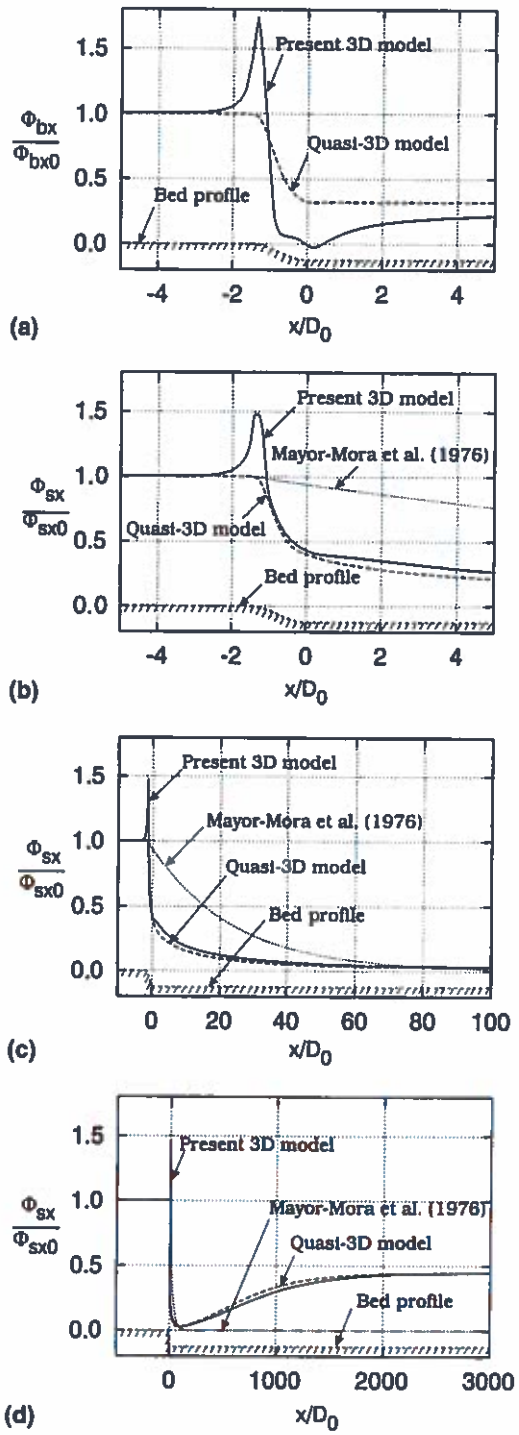

FIG. 8. (a) Variations in Φ_{bx} Predicted by 3D Model and Quasi-3D Model in Proximity of Slope; (b), (c), and (d) Variations in Φ_{sx} Predicted by 3D Model, Quasi-3D Model, and that of Mayor-Mora et al. (1976). $D_i/D_0 = 1.5$, $s_0 = \pi/6$, $\theta_0 = 0.35$, $k_N/D_0 = 0.0001$, and $\alpha_0 = 60°$

$x/D_0 = -10$ to $x/D_0 = 100$, whereas Fig. 8(d) shows the equivalent in the entire region influenced by the channel expansion.

The full 3D model predicts an increase in the bed-shear stress immediately upstream the slope. This is due to an imbalance between the centrifugal force and the pressure gradient normal to the streamlines. The centrifugal force of the low-velocity fluid near the bed is very small but increases rapidly (with the velocity squared) away from the bed. The pressure gradient required to bend the streamlines some distance above the bed is thus much larger than the outwardly directed centrifugal force on the fluid very close to the bed. This imbalance will cause the streamlines to converge near the bed and therefore increase the bed-shear stress. In Fig. 8(a) it is seen that the increase in the bed-shear stress immediately upstream the slope increases Φ_{bx} significantly (~80%). The amplification in the bed-shear stress is relatively high in this case, as the curvature is large. On the part of the slope where the corkscrew eddy is present, the bed-shear stress decreases and becomes negative. Consequently, the bed load approaches zero, and on a small stretch becomes negative. Note that the gravity effect on the longitudinal bed load transport contributes to a positive transverse bed load transport, and the transverse bed load can therefore become positive although the transverse bed-shear stress is negative. Immediately downstream the slope, still within the separation bubble, the transverse bed-shear stress is negative and the bed is plane, which results in predicted negative Φ_{bx}. The quasi-3D model predicts values of Φ_{bx} corresponding to the local velocity and depth, which results in less variation in Φ_{bx}. The predicted sedimentation due to bed load is thus larger in the full 3D model.

If the transverse suspended sediment transport predicted by the 3D model is compared with that of the quasi-3D model, two features important for the sedimentation are observed. The first feature is that of the increase in the transport in front of the channel. As a consequence, local erosion of the bed in front of the channel and an increase in the supply of sediment to the channel are predicted. The second feature is the larger sedimentation on the upstream slope. The pronounced decrease in the suspended load is associated with the presence of a separation zone in which sediment is trapped. Fig. 8(c) shows that the sediment transport predicted by the quasi-3D model and the full 3D model approaches the same value. This happens when the flow properties of the 3D model recover from the depth expansion and when the additional sediment picked up at the entry of the channel has settled. The small deviation between these two models found further downstream [Fig. 8(d)] is due to the analytical flow solution slightly overestimating the bed-shear stress (see Part I). Eventually, however, the two models predict an equal sediment transport value.

Two drawbacks of the simple model of Mayor-Mora et al. (1976) are revealed in Figs. 8(b–d). First, the length of the adaptation process is overestimated, and second, the model disregards the longitudinal acceleration.

MORPHOLOGY OF TRENCHES

In this section, the morphology of small sinusoidally shaped channels or pipeline trenches, where $W/D_0 = 1$, is investigated. When $W/D_0 \approx 1$, the acceleration of the longitudinal velocity component, discussed in Part I, is of no practical importance. As the excavated depth of pipeline trenches is often only a fraction of the water depth, a detailed model is required for a reliable sediment transport description. The use of a quasi-3D flow model may introduce errors much larger than those illustrated in the preceding section. This can be explained by the following example. Consider a pipeline trench with an excavated depth of 1/10 of the water depth. The presence of the trench will change the flow structure in its vicinity. Depending on the steepness of the slopes this may lead to flow separation —captured by the 3D model—and a pronounced deposition. In a quasi-3D flow model, however, the sediment transport is only slightly modified, as the velocity is reduced corresponding to the depth increase (10% for perpendicularly attacking flow).

Streamlines projected onto the vertical/transverse plane and the distribution of the concentration of suspended sediment over a trench are shown for $\alpha_0 = 90°$ in Figs. 9(a and b) and for $\alpha_0 = 30°$ in Figs. 9(c and d). The transverse sectional view of the streamlines in Figs. 9(a and c) for $\alpha_0 = 90°$ and 30°, respectively, shows that the flow separates from the bed as it

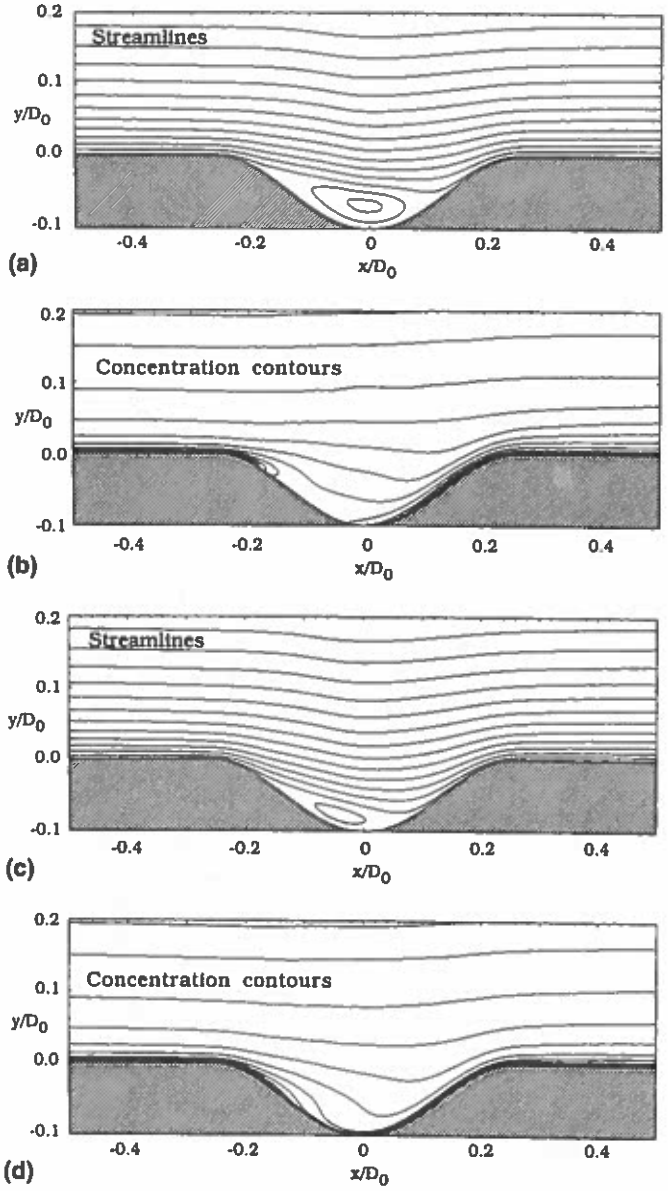

FIG. 9. Streamlines for: (a) $\alpha_0 = 90°$; (c) $\alpha_0 = 30°$. Contours of Concentration of Suspended Sediment for: (b) $\alpha_0 = 90°$; (d) $\alpha_0 = 30°$. Other Parameters Are $D_1/D_0 = 1.1$, $W/D_0 = 0.25$, $s_0 = \pi/5$, $\theta_0 = 0.3$, and $k_N/D_0 = 0.000025$

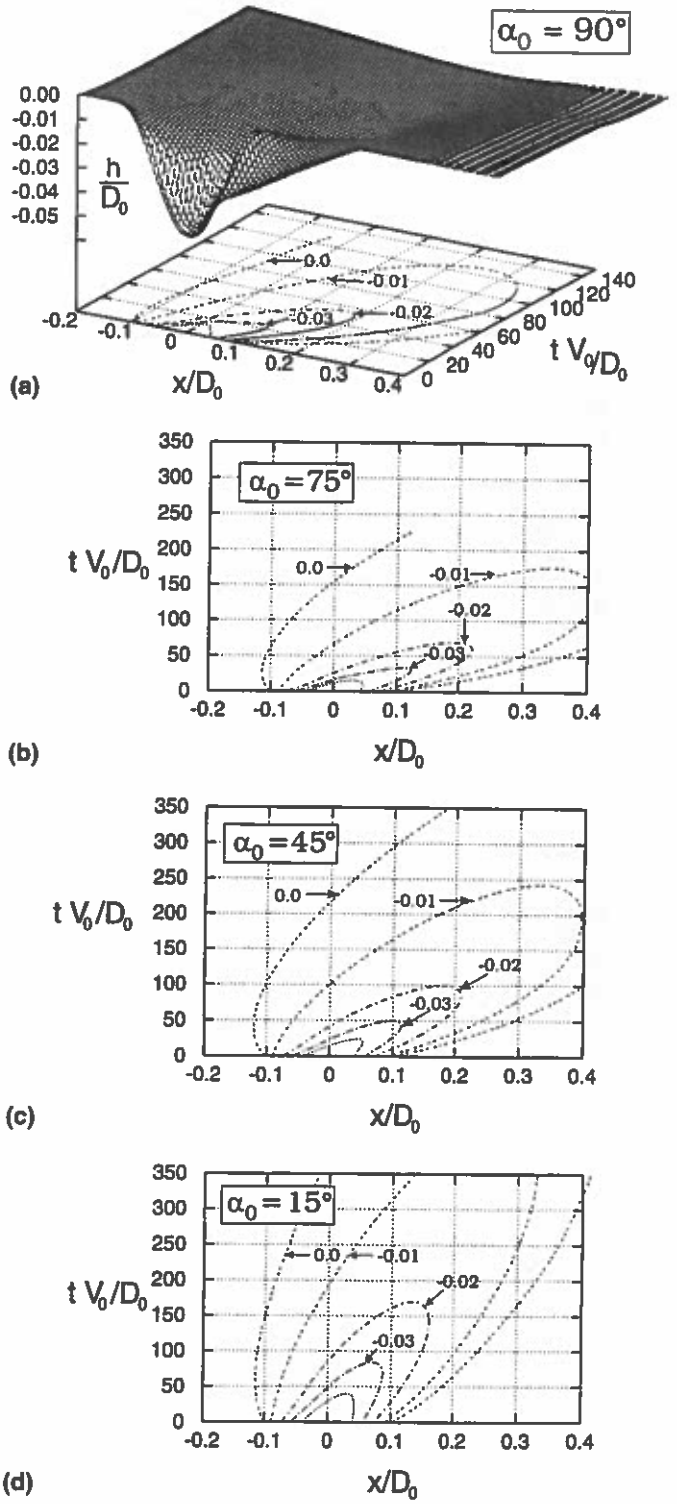

FIG. 10. Morphological Development of Trench Attacked by Current at: (a) $\alpha_0 = 90°$; (b) $\alpha_0 = 75°$; (c) $\alpha_0 = 45°$; (d) $\alpha_0 = 15°$. Other Parameters Are $D_1/D_0 = 1.05$, $W/D_0 = 0.125$, $s_0 = \pi/5$, $\theta_0 = 1$, and $k_N/D_0 = 0.000025$

enters the trench and reattaches subsequently on the downstream slope. The separation bubble is seen to be relatively strong when $\alpha_0 = 90°$ and becomes weaker when $\alpha_0 = 30°$. The weakening of the separation bubble in the latter case is due to less transverse momentum yet equivalent level of turbulent kinetic energy (from the constant total velocity). The turbulent mixing of the transverse momentum will therefore reduce the size of the separation bubble. From the contours of concentration, which are the paths along which suspended particles travel by advection and diffusion, it is observed that sediment located near the bed is trapped inside the separation bubble. Due to the extent of the separation bubble, the trapping is less effective on the upstream slope when $\alpha_0 = 30°$ compared with $\alpha_0 = 90°$.

Figs. 10(a–d) show the morphological development of a trench attacked by a current at four different inlet angles. The $\alpha_0 = 90°$ case is visualized with a time-space surface plot of the bed level and projected contours on the horizontal plane in Fig. 10(a). Figs. 10(b–d) contain the calculated contours of bed levels for $\alpha_0 = 75°$, 45°, and 15°. The sediment transport is dominated by the suspended part. In Fig. 10 the timescale for the backfilling is seen to increase as the flow becomes more oblique (smaller α_0). In fact, the inlet angle influences the morphological development in four distinctive ways. First, the supply of sediment to the trench decreases with obliquity. Second, sediment transport capacity across the trench becomes more uniform with obliquity as the contribution to the total velocity from that of the longitudinal velocity increases. Furthermore, the above-mentioned strength of the separation bubble and the time the flow is detained within the trench (increasing with decreasing inlet angle) influences the morpho-

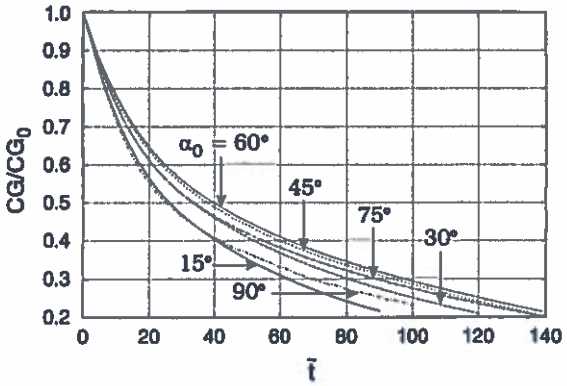

FIG. 11. Backfilling as Function of Normalized Time [Eq. (9)] of Trench Exposed to Current. Other Parameters as in Fig. 10

logical development. The latter is important regarding the settling process and is the only mechanism of those mentioned above that will enhance the rate of sedimentation when α_0 is decreased. In the following, a timescale normalized with the inlet angle is introduced

$$\bar{t} = t \frac{V_0}{D_0} \sin(\alpha_0) \tag{9}$$

where V_0 = total depth-averaged velocity upstream of the channel. This timescale $\bar{t}$ will eliminate the dependency of the supply of sediment with the inlet angle; that is, for a given $\bar{t}$ an equal amount of sediment will have approached the trench regardless of the inlet angle. The use of (9) will thus accentuate the remaining governing mechanisms, as the relative disposition is studied.

In Fig. 11 the process of backfilling is shown by using the center of gravity of the trench, CG/CG_0, as a function of normalized time (CG_0 is the center of gravity at $\bar{t} = 0$). CG is defined by

$$CG = \frac{\int_{-\infty}^{\infty} h^2\, dx}{\int_{-\infty}^{\infty} h\, dx} \tag{10}$$

(see also Fig. 2). It is seen that an inlet angle equal to $\alpha_0 = 60°$ causes the slowest backfilling.

For $\alpha_0 = 90°$ and 15° the normalized timescale of the backfilling is seen to be relatively fast. The fast backfilling for the flow attacking perpendicularly is caused mainly by a more effective trapping of sediment in suspension [Fig. 9(b)]. The fast backfilling for the flow being nearly parallel with the alignment of the channel stems partly from the prolonged time the flow is detained within the trench region (enhancing the adaptation process) and partly from the effect of gravity on bed load particles [(4) and (3)]. The backfilling rate for $\alpha_0 = 90°$ is seen to be approximately 30% higher than that for $\alpha_0 = 60°$ with the normalized timescale.

CONCLUSIONS

Sediment transport over navigation channels and pipeline trenches exposed to an obliquely incoming current has been investigated. It was found that current refraction influences the sedimentation pattern and that a 3D description of the flow is important. The sediment transport predicted by the full 3D model was compared with that of two simpler models to highlight the importance of a 3D flow description. The full 3D model predicted much higher rates of sedimentation near the upstream slope. For very wide navigation channels it was demonstrated that the gradual acceleration of the longitudinal velocity component should be taken into account in sediment transport calculations. The latter feature is captured by 2D horizontal models as well as full 3D models. Finally, examples of morphological calculations of pipeline trenches were presented.

APPENDIX I. MORPHOLOGICAL SCHEME

A numerical solution to (7) will introduce numerical errors compared with an exact solution. As the backfilling process is diffusive, the numerical diffusion must be minimized to such a degree that the physical diffusion dominates. For this reason a second-order scheme of the leapfrog type where both derivatives of (7) are discretized with central differences is chosen [see Abbott and Basco (1989) for a stability analysis and a general discussion of the qualities and drawbacks of the leapfrog scheme]. This reads

$$\frac{h_i^{m+1} - h_i^{m-1}}{2\Delta t} + \frac{1}{1-r} \frac{q_{i+1/2}^m - q_{i-1/2}^m}{\Delta x} = 0 \tag{11}$$

where Δt = morphological time step; Δx = spatial step; and m = integers such that $t = m\Delta t$ and $x = i\Delta x$. In (11) it has been utilized that variables found with the finite-volume method [see, e.g., Patankar (1980)] are cell-centered allowing the sediment fluxes to be calculated between two adjacent grid points—see second term of (11). The bed form at the time level $m + 1$ is found explicitly.

One drawback of using the standard leapfrog scheme is the possibility that two decoupled solutions may emerge with respect to time and space (known as the checkerboard syndrome). Spacewise, this is avoided with the present version of the leapfrog scheme. With respect to time, the problem is treated by adding a stabilizer (i.e., a diffusion term $K\partial^2 h/\partial t^2$) to (7) where the diffusion coefficient K is of the order $O(\Delta t^2)$ or smaller ensuring that the numerical diffusion remains small. The methodology is reported in Roache (1972).

The use of a complex turbulent flow model will nevertheless cause all length scales of the bed to amplify owing to the phase lag between the bed-shear stress and the bed form. Consequently, the numerical solution will become unstable to unresolved length scales (i.e., length scales being of the order of the grid size). This calls for a smoothing algorithm, which should only be effective on disturbances of the order of the grid size. Such a smoothing algorithm has been developed: the bed form h at time level $m + 1$, is filtered by a standard filtering operator

$$\tilde{f}_i := 0.5 f_i + 0.25(f_{i+1} + f_{i-1}) \tag{12}$$

The resulting filtered bed form $\tilde{h}$ is then subtracted from the unfiltered bed form h and denoted Δh. Subsequently, Δh is filtered using (12) and added to $\tilde{h}$. This is repeated N times.

The algorithm is shown in the pseudocode below:

- Filtering of h with (12) $\rightarrow \tilde{h}$
- Do 1 . . . N
  - —$\Delta h = h - \tilde{h}$
  - —Filtering of Δh with (12) $\rightarrow \Delta\tilde{h}$
  - —$\tilde{h} = \tilde{h} + \Delta\tilde{h}$
- Enddo

The effect of this filtering process is that only disturbances in the bed of the order of the grid size Δx are smoothed.

APPENDIX II. EQUILIBRIUM SEDIMENT TRANSPORT

If a linear eddy viscosity profile ($\nu_T = \kappa V_f y$) is employed, a solution to the steady uniform equation of concentration [see (5)] is obtained

$$c(y) = c_b \left(\frac{y}{2d}\right)^{-Z} \tag{13}$$

where $Z = w_s/(\kappa V_f)$ = Rouse parameter; κ (=0.4) = von Kármán constant; c_b = bed concentration; and V_f = friction velocity defined by $V_f = \sqrt{|\tau_b|/\rho}$. Furthermore, if the velocity profile $V(y)$ is unidirectional and logarithmic, the suspended sediment transport in the direction of the flow can be found

$$\Phi_s = \int_{2d}^{D} \frac{V(y)c(y)}{\sqrt{(s-1)gd^3}}\,dy = \frac{2c_b\sqrt{\theta}}{\kappa(1-Z)^2}\left\{\left(\frac{D}{2d}\right)^{1-Z} \cdot\left((1-Z)\log\left(12\frac{D}{d}\right)-1\right)-\left((1-Z)\log(24)-1\right)\right\} \tag{14}$$

The bed load transport Φ_b can be found directly from (1) taking $\theta_c = \theta_{co}$. It is seen that the values of the Shields parameter, the Rouse parameter, and the angle of the flow (for the x-projection of the sediment transport) are required for the cross-channel flux of sediment [i.e., Φ_s and Φ_{s0} in (8)] to be determined.

By means of (2) the equilibrium Shields parameter within the channel can be related to the upstream value

$$\theta_{eq} = \theta_0 \left(\frac{V_{feq}}{V_{f0}}\right)^2 \tag{15}$$

Adopting the Colebrook-White friction formula for the friction velocity

$$\frac{1}{C_f} = \frac{V_f}{V} = \frac{1}{6.1 - 2.5\log\left(\frac{k_N}{D}\right)} \tag{16}$$

where C_f = friction formula coefficient, (15) becomes

$$\theta_{eq} = \theta_0 \left(\frac{V_{eq}}{V_0}\frac{C_{f0}}{C_{feq}}\right)^2 \tag{17}$$

The Rouse parameter is scaled with the friction velocity as well

$$Z_{eq} = Z_0 \frac{V_{f0}}{V_{feq}} = Z_0 \frac{V_0}{V_{eq}}\frac{C_{feq}}{C_{f0}} \tag{18}$$

where $Z_0 = w_s/(\kappa V_{f0})$.

In Part I, analytical expressions for the total fully developed depth-averaged velocity inside the channel V_{eq}/V_0 and for the corresponding flow angle α_{eq} were derived [see (11) and (12) of the companion paper (Jensen et al. 1999)]. Therefore, if the sediment flux is projected onto the transverse direction, the deposition in the fully developed case (i.e., Δ_{eq}) can be found analytically if the upstream Shields parameter, the inlet angle, the expansion in depth, and the grain diameter are prespecified.

ACKNOWLEDGMENTS

This work is jointly supported by Numerical and Experimental Fluid Mechanics, and by Marine Technique all funded by the Danish Technical Research Council.

APPENDIX III. REFERENCES

Abbott, M. B., and Basco, D. R. (1989). *Computational fluid dynamics*. Wiley, New York.

Bijker, E. W. (1980). "Sedimentation in channels and trenches." *Proc., 17th Coast. Engrg. Conf.*, Vol. II, ASCE, New York, 1708–1718.

Engelund, F., and Fredsøe, J. (1976). "A sediment transport model for straight alluvial channels." *Nord. Hydrol.*, Copenhagen, Denmark, 7, 293–306.

Engelund, F., and Fredsøe, J. (1982). "Hydraulic theory of alluvial rivers." *Advances in Hydroscience*, 13, 187–215.

Engelund, F., and Hansen, E. (1972). *A monograph on sediment transport in alluvial streams*, 3rd Ed., Technical Press, Copenhagen.

Fredsøe, J. (1978). "Sedimentation of river navigation channels." *J. Hydr. Div.*, ASCE, 104(2), 223–236.

Fredsøe, J. (1979). "Natural backfilling of pipeline trenches." *J. Pet. Technol.*, 31, 1223–1230.

Jensen, J. H., Madsen, E. Ø., and Fredsøe, J. (1999). "Oblique flow over dredged channels. I: Flow description." *J. Hydr. Engrg.*, ASCE, 125(11), 1181–1189.

Mayor-Mora, R., Mortensen, P., and Fredsøe, J. (1976). "Sedimentation studies of the Niger river delta." *Proc., 15th Coast. Engrg. Conf.*, Vol. II, ASCE, New York, 2151–2169.

Roache, J. P. (1972). *Computational fluid dynamics*. Hermosa Publisher, Albuquerque, N.M.

van Rijn, L. C. (1986). "Sedimentation of dredged channels by currents and waves." *Delft Hydr. Communications No. 369*, Delft Hydraulics Laboratory, Delft, The Netherlands.

van Rijn, L. C. (1987). "Mathematical modelling of morphological processes in the case of suspended sediment." *Delft Hydr. Communications No. 382*, Delft Hydraulics Laboratory, Delft, The Netherlands.

Zyserman, J. A., and Fredsøe, J. (1994). "Data analysis of bed concentration of suspended sediment." *J. Hydr. Engrg.*, ASCE, 120(9), 1021–1042.

APPENDIX IV. NOTATION

The following symbols are used in this paper:

C_f = friction formula coefficient;
CG = center of gravity of trench with respect to $y = 0$;
c = concentration of suspended sediment;
c_b = bed concentration;
D = local water depth;
d = mean grain diameter;
g = acceleration of gravity;
h = bed elevation;
k_N = Nikuradse roughness;
q = sediment transport;
q_b = bed load;
q_s = suspended sediment transport;
r = porosity of bed material;
s = relative density of sand;
s_0 = maximum slope on channel slopes;
t = time [$\bar{t} = tV_0/D_0 \sin(\alpha_0)$];
u = velocity component in x-direction;
V = depth-averaged total velocity;
$V(y)$ = velocity profile of total velocity;
V_f = friction velocity;
v = velocity component in y-direction;
W = width of channel;
w_s = fall velocity of mean grain diameter in suspension;
x = coordinate perpendicular to channel alignment;
y = vertical coordinate;
Z = Rouse number;
z = coordinate parallel with channel alignment;
α = angle of flow with respect to channel alignment;
α_b = angle of flow at bed;
β = bed slope;
Δ = deposition;
θ = Shields parameter;
θ_c = critical Shields parameter on sloping bed;
θ_{co} = critical Shields parameter on plane bed;
κ = von Kármán constant;
μ_s = static friction coefficient;
ν_T = eddy viscosity;
ρ = density of water;
τ_b = bed-shear stress;
Φ_b = nondimensional bed load;
Φ_s = nondimensional suspended sediment transport; and
ψ = angle between path of bed load particles and direction of bed-shear stress.

Subscripts

eq = equilibrium value;
x = transverse component;
z = longitudinal component;
0 = upstream channel value; and
1 = inside channel value.